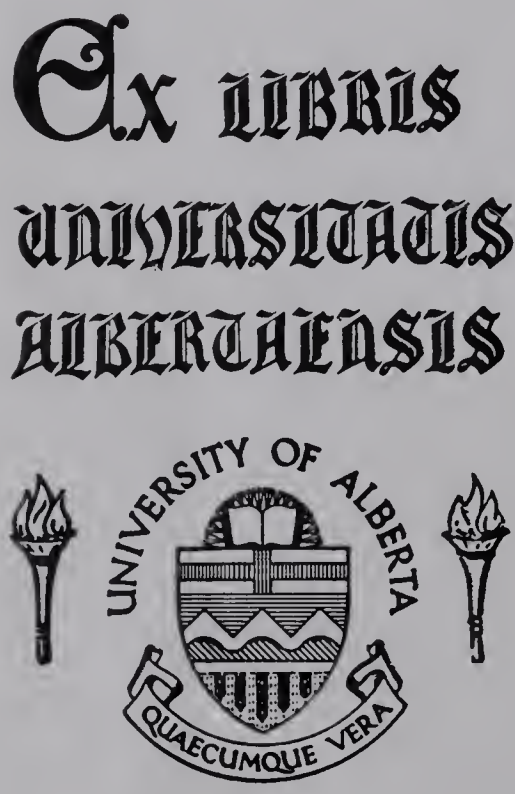

University of Alberta
Printing Department

THE UNIVERSITY OF ALBERTA

HYDRAULICS OF B-JUMPS AT ABRUPT DROPS

by

NESTOR VICENTE ORTIZ

A THESIS

SUBMITTED TO THE FACULTY OF GRADUATE

STUDIES IN PARTIAL FULFILMENT OF THE

REQUIREMENTS FOR THE DEGREE OF

MASTER OF SCIENCE

DEPARTMENT OF CIVIL ENGINEERING

EDMONTON, ALBERTA

December, 1966

UNIVERSITY OF ALBERTA

FACULTY OF GRADUATE STUDIES

The undersigned certify that they have read, and recommend to the Faculty of Graduate Studies for acceptance, a thesis entitled HYDRAULICS OF B-JUMPS AT ABRUPT DROPS submitted by NESTOR VICENTE ORTIZ in partial fulfilment of the requirements for the degree of Master of Science.

ABSTRACT

An extensive experimental study has been made on the maximum B-Jump at abrupt drops in a smooth rectangular channel. This jump is considered as a phenomenon in which the supercritical turbulent stream undergoes diffusion; firstly as a curved free jet and later as a reattached wall jet under adverse pressure gradient. The different portions were analysed separately with a view to understand the mechanics of this phenomenon. The wall jet portion was split into a free mixing region and a boundary layer region. It was found that the velocity distribution in the free mixing region is "similar" and in the boundary layer portion, the velocity distribution followed the $\frac{1}{8.5}$ power law. A generalised bed shear stress distribution has been developed. An analysis was also made of the velocity distribution in the symmetrical region of the free jet. For predicting the maximum velocity at any section a curve has been developed. Also a generalised distribution has been established for the junction velocity. Some observations have also been made on the length characteristics as well as on the pressure distribution on the face of the drop.

ACKNOWLEDGMENTS

The author is grateful to Dr. N. Rajaratnam for his valuable guidance and encouragement throughout the course of this program.

Grateful acknowledgment is made to Dr. T. Blench for his valuable comments and to Prof. A.W. Peterson for his help in setting up the experimental arrangement.

Thanks are due to the staff of the Hydraulic Laboratory for their help in various phases of the work.

The author is thankful to the Government of Venezuela for the fellowship awarded during the period of work.

This study was supported by a grant from the National Research Council of Canada to whom the author is grateful.

TABLE OF CONTENTS

LIST OF TABLES

LIST OF FIGURES

LIST OF FIGURES (con't.)

LIST OF FIGURES (con't.)

NOMENCLATURE

b	width of flume
d	external diameter of Preston tube
F_1	supercritical Froude number
g	acceleration due to gravity
h	height of drop
h'	piezometric head
L_e	length of standing eddy
L_j	length of jump
L_{rj}	length of surface roller
p	total pressure on Preston tube
p_o	static pressure at any point
u	(turbulent mean) velocity at any point
u_j	junction plane velocity
u_{jm}	maximum velocity in junction plane
u_m	maximum mean velocity at any section
U_t	mean velocity at the end of jump
U_o	initial mean velocity at efflux section
U_1	mean velocity of supercritical stream
u_*	shear velocity

NOMENCLATURE (con't.)

x	longitudinal distance from efflux section
x_m	distance of section of U_{jm} from the face of the drop
x_o	distance of section of τ_{om} from the face of the drop
x_1	longitudinal distance from the face of the drop
x_2	longitudinal distance measured from the end of eddy
x_3	longitudinal distance from the section at which $\tau_o = \tau_{om}$
x_4	longitudinal distance from the beginning of jump
x_5	longitudinal distance from the section at which $u_j = u_{jm}$
y	normal distance from boundary
y_r	depth of flow at the end of roller
y_t	tailwater depth
$\bar{y}$	depth of maximum velocity filament below the surface of the supercritical stream
y_o	depth of slot
y_1	supercritical stream depth
y_2	subcritical sequent depth of the classical jump
z	height above downstream bed
θ	longitudinal distance between the sections at which u_j is respectively equal to u_{jm} and $\frac{u_{jm}}{2}$
δ	boundary layer thickness
δ_1	length scale for wall jet

NOMENCLATURE (con't.)

η, η'	non-dimensional ordinates
ν	kinematic viscosity of the fluid
ρ	mass density of the fluid
τ_o	bed shear stress
τ_{om}	maximum shear stress on the bed
λ	longitudinal distance between the sections at which τ_o is respectively equal to τ_{om} and $\frac{\tau_{om}}{2}$

CHAPTER I

INTRODUCTION

Hydraulic jump is the transition phenomenon from supercritical to subcritical open channel flow. The jump formed in a level, wide and smooth rectangular channel is known as the classical jump. For a classical jump if y_1 is the supercritical depth and if F_1 is the supercritical Froude number, defined as

$$F_1 = \frac{U_1}{\sqrt{gy_1}} \qquad (1\text{-}01)$$

where U_1 is the supercritical mean velocity and g is the acceleration due to gravity, the subcritical sequent depth y_2 is given by the well-known Belanger equation

$$\frac{y_2}{y_1} = \frac{1}{2}\left[\sqrt{1 + 8F_1^2} - 1\right] \qquad (1\text{-}02)$$

Fig. 1-1 is a schematic representation of the classical jump. In Fig. 1-1 L_j is the length of the jump, L_{rj} is the length of the surface roller and y_r is the depth of flow at the end of the roller. The jump is specified completely by the supercritical depth y_1 and the Froude number F_1.

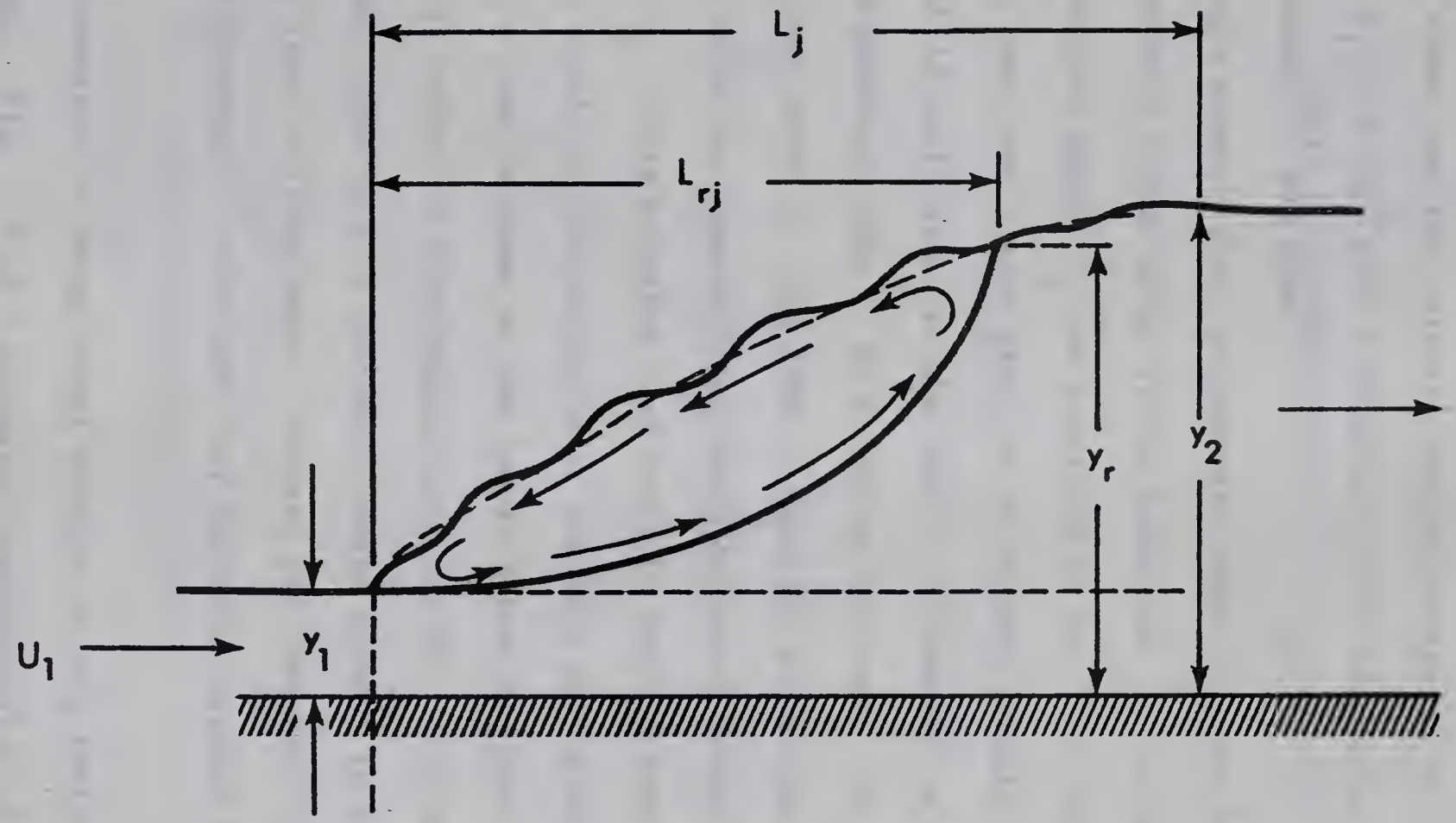

FIG. 1-1 The Classical Jump

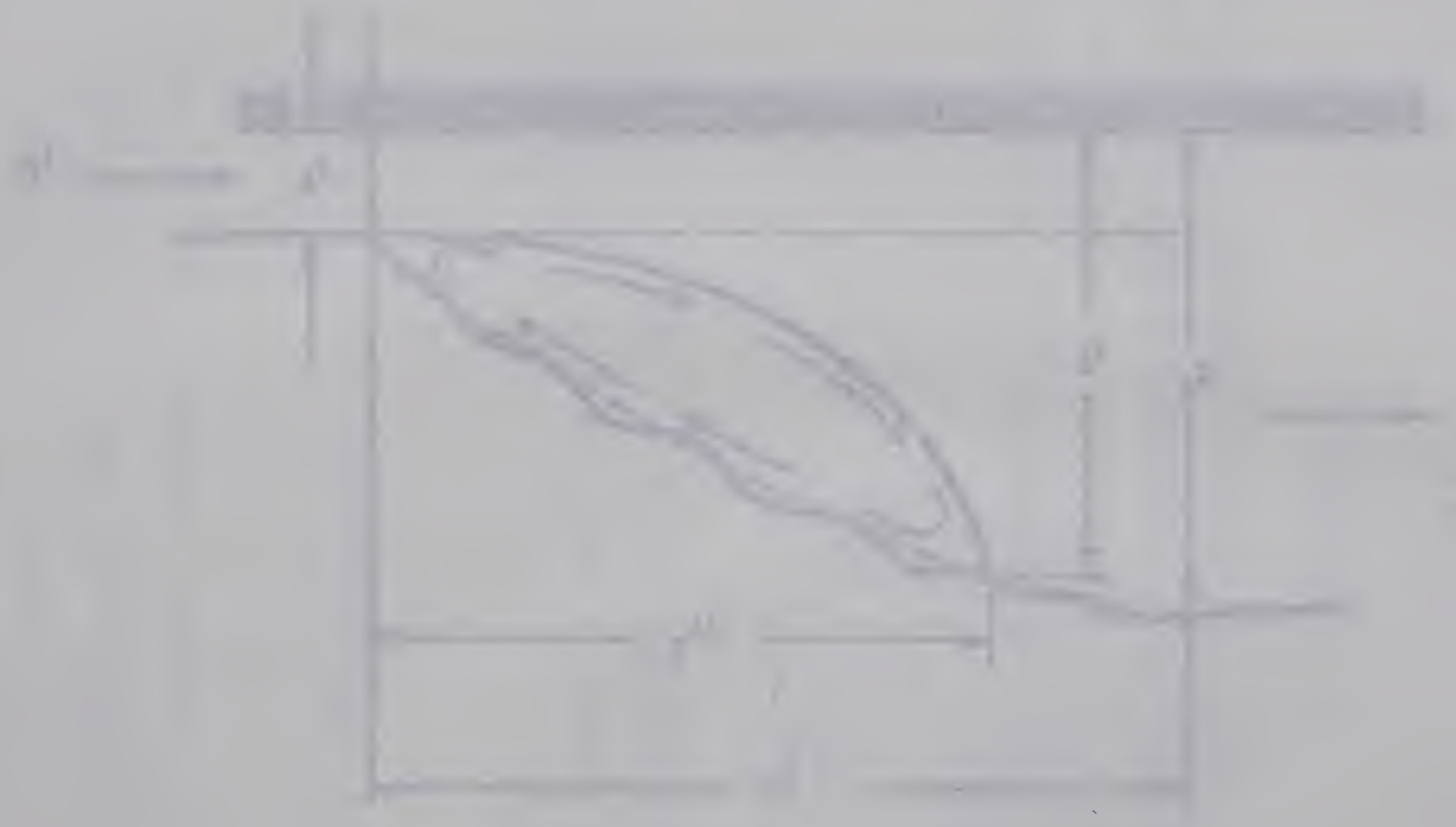

In the jump a large portion of the mean energy of the supercritical stream is converted into turbulence and later dissipated through viscous shear. It could be shown that the relative energy dissipated in a jump is a function of only F_1 . A very full discussion of the hydraulic jump has been given by Elevatorski[1] and Chow[2].

Considering a supercritical stream with depth y_1 and Froude number F_1 coming under a sluice gate, if the tailwater y_t is equal to the subcritical sequent depth y_2 as predicted by Eq. 1-02, then the jump is formed right under the sluice gate (or to be more precise, at the vena contracta, which is quite close to the gate). If however y_t is greater than y_2 , a submerged jump[3] is formed at the gate. If, on the other hand, y_t is less than y_2 the jump is repelled downstream and occurs at a section where the supercritical depth of the retarding stream becomes sequent to y_t . This repelled jump could be made to move upstream and form at the gate itself by the provision of suitable baffle walls or baffle blocks. Such a jump is known as the forced hydraulic jump.

A very large amount of experimental work has been done on the forced hydraulic jump, since this is the basic design element in the well-known hydraulic jump type stilling basin. Forster and Skrinde[4] , Bradley and Peterka[5] and Rajaratnam[6] have made very extensive studies of the forced jump.

The jump formation at abrupt drops belongs to this family of forced hydraulic jumps. Fig. 1-2 is a schematic representation of the three possible jump types that are formed at an abrupt drop. (The width of the channel above the drop is the same as that below the drop and hence

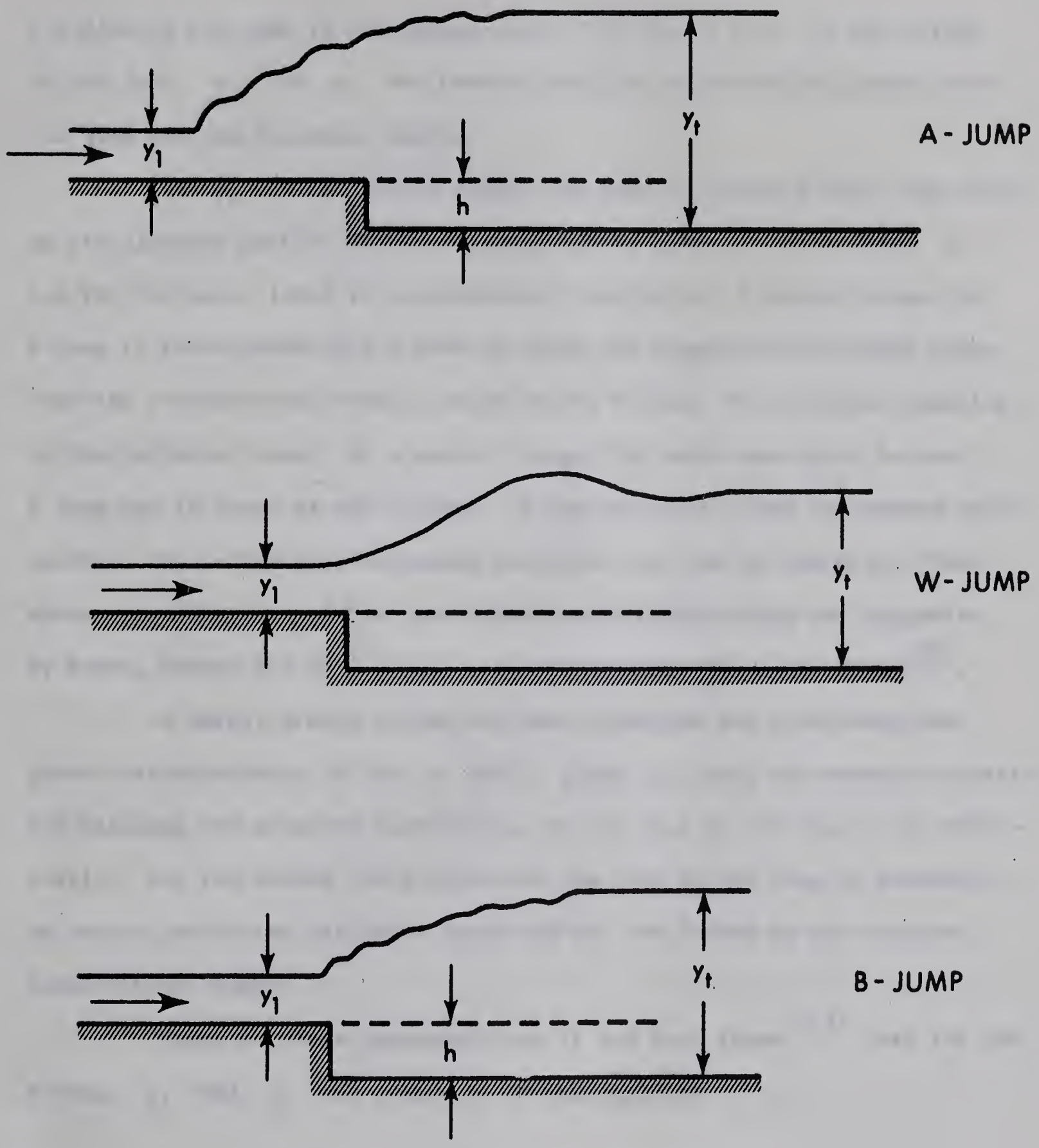

FIG. 1-2 Jump Formation at Abrupt Drops

the flow in the jump is two dimensional). In Fig. 1-2 h is the height of the drop, y_1 and y_t are respectively the supercritical depth before the jump and the tailwater depth.

If y_t is relatively large, the jump is formed almost completely on the elevated portion of the channel, and is known as the A-Jump. If now the tailwater level is progressively lowered, at a certain stage the A-Jump is transformed into a wave in which the supercritical stream rides over the tailwater and this is known as the W-Jump. With further lowering of the tailwater level, at a certain stage, the wave once again becomes a jump and is known as the B-Jump. If the tailwater level is lowered still further, the B-Jump will be pushed away from the foot of the drop. The above classification of the jump formation at abrupt drops was suggested by Rouse, Bhoota and Hsu[7] and later finalized by Moore and Morgan[8].

A fairly simple method has been developed for predicting the gross characteristics of the A and B jumps, by using the momentum equation and assuming the pressure distribution on the face of the drop to be hydrostatic. For the A-Jump the pressure on the face of the drop is assumed to be controlled by the tailwater depth and for the B-Jump by the upstream supercritical depth.

Based on these considerations it has been shown[7,8] that for the A-Jump, y_1 and y_t are connected by the equation

$$F_1^2 = \frac{\left(\frac{y_t}{y_1} - \frac{h}{y_1}\right)^2 - 1}{2\left(1 - \frac{y_1}{y_t}\right)} \qquad (1\text{-}03)$$

and for the B-Jump by the equation

$$F_1^2 = \frac{\left(\frac{y_t}{y_1}\right)^2 - \left(1 + \frac{h}{y_1}\right)^2}{2\left(1 - \frac{y_1}{y_t}\right)} \qquad (1\text{-}04)$$

These equations have been experimentally verified fairly well by Rouse et al[7] and by Moore and Morgan[8]. The range of their data is given in TABLE I-1.

Based on their fairly extensive work, Moore and Morgan have given a design chart for predicting the type of jump formed for given conditions and it is reproduced in Fig. 1-3. It has also been observed that the direction of change of the tailwater level affects the limiting depths for various types of jumps. Some exploratory experiments have also been carried out by Ingram, Ottman and Tracy[9] in 1956 and McPherson and Dittig[10] in 1957.

In the present work the B-Jump that is formed just at the lower end of the wave is termed the maximum B-Jump and is considered in great detail with a view of understanding the detailed processes that take place inside.

TABLE I-1(a)

Data Range of Rouse, Bhoota and Hsu[7]

h (in)	h/y_1	F_1
2.0	1.0	3 to 10
2.0	2.0	
2.0	3.0	
2.0	4.0	

TABLE I-1(b)

Data Range of Moore and Morgan[8]

Test No.	h (ft)	y_1 (ft)	$\frac{h}{y_1}$	F_1
1	0.400	0.100	4	2,4,6,8
2	0.400	0.133	3	2,4
3	0.200	0.067	3	6,8
4	0.200	0.100	2	2,4,6

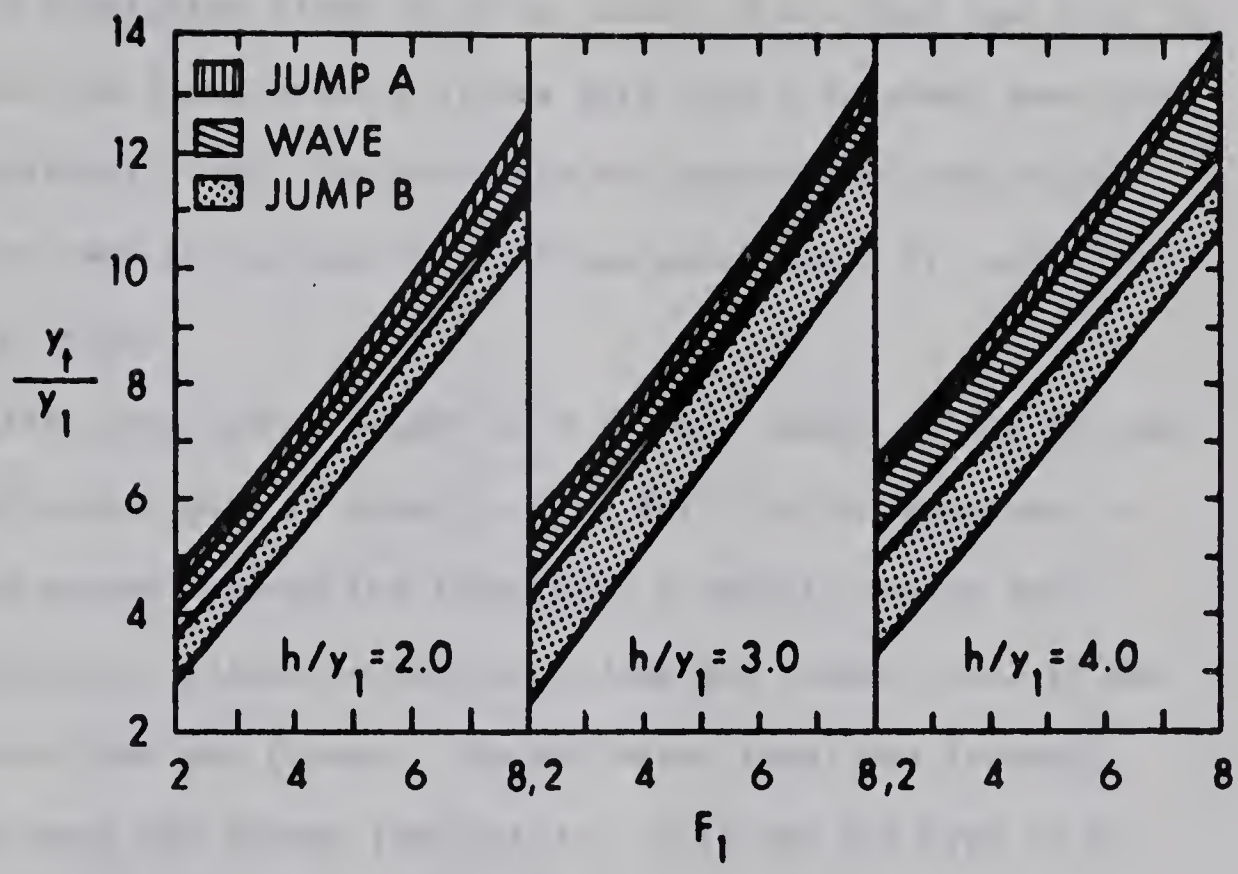

FIG. 1-3 Chart for A, W and B Jumps

CHAPTER II

EXPERIMENTS

The experimental arrangement is shown in Fig. 2-1. The experiments were conducted in a plexiglass flume 16.25 in. wide, 13 in. high and 31.67 ft. long. Water entered the flume under a sluice gate from a constant head tank, supplied by a centrifugal pump. The discharge was measured volumetrically using the collection tank at the end of the flume which was 6 ft. wide, 10 ft. long and 3.5 ft. high.

A plexiglass step with a height of 3 in. and length of 6.5 ft. was installed under the sluice gate as shown in Fig. 2-1. In an experiment a fixed discharge was passed through the flume with a certain sluice gate opening. The tailgate was raised so that an A-Jump was formed; then it was lowered so that the W-Jump was formed. The tailwater level was lowered further and stopped when the B-Jump just set in. This was the type of B-Jump on which all the measurements were made.

After this maximum B-Jump was properly positioned, the mean surface profile of the jump was measured along the centerline of the flume using a point gage of least count of 0.001 ft. Fig. 2-2 to 2-15 show the surface profiles for all the 14 runs. For each run the beginning of the jump, the end of the jump, and the end of the surface roller were found and the length of the jump L_j and the length of the roller L_{rj} were calculated.

Just below the drop a standing eddy is formed and its length L_e was measured in the early stages using the air bubbles that were present

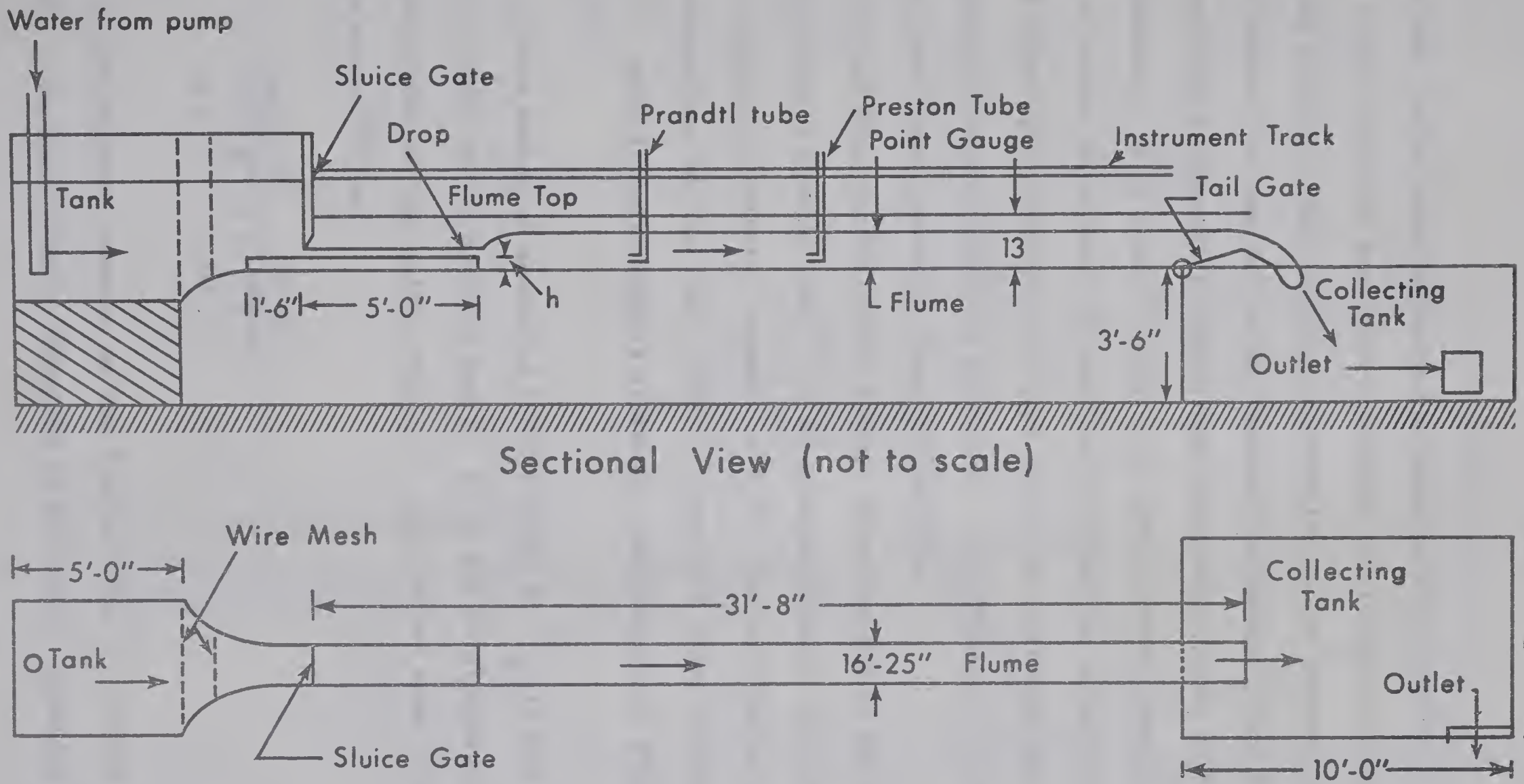

FIG. 2-1 Details of Experimental Arrangement

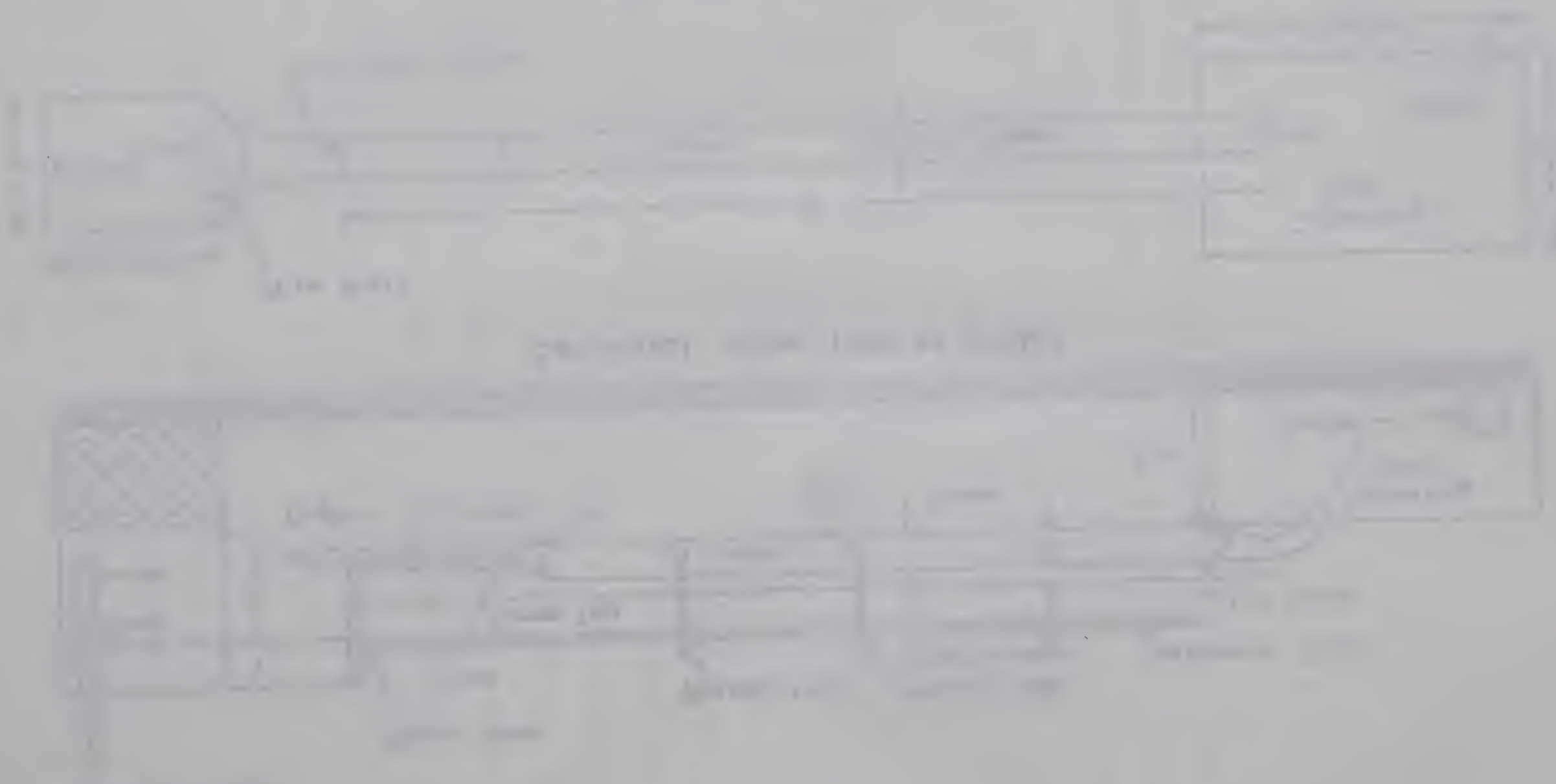

in the jump and, in the later experiments, using colour injection. It was found that colour injection gave more consistent and reliable results.

The turbulent mean velocity distribution in the supercritical stream just before the jump and in the forward flow region of the B-Jump was measured using a commercial Prandtl-type pitot-static tube of 3 mm external diameter. It is known[11] that this tube is very insensitive to the angle of attack up to about 15° and that it gives the velocity vector, which was assumed to be horizontal in this work. No correction was made to the velocities for the effect of turbulence. The velocity distribution measurements are shown plotted in Figs. 2-2 to 2-15.

The bed shear stress in the B-Jump, after the end of the eddy, was measured using a Preston tube[12] 3 mm external diameter and having a ratio of internal to external diameter of 0.67. The calibration curve used for calculating the bed shear stress τ_o was that given recently by Patel[13], which is only slightly different from that given originally by Preston[12].

In this method of measuring shear stress, if p_o is the static pressure at a point on the boundary and if p is the total pressure given by the Preston tube at that point, and if τ_o is the bed shear stress, it has been shown[12] that

$$\frac{(p-p_o)\,d^2}{4\rho\nu} = f\left(\frac{\tau_o\,d^2}{4\rho\nu}\right) \qquad (2\text{-}01)$$

where d is the external diameter of the Preston tube, ρ is the mass density and ν is the kinematic viscosity of the fluid. Equation 2-01

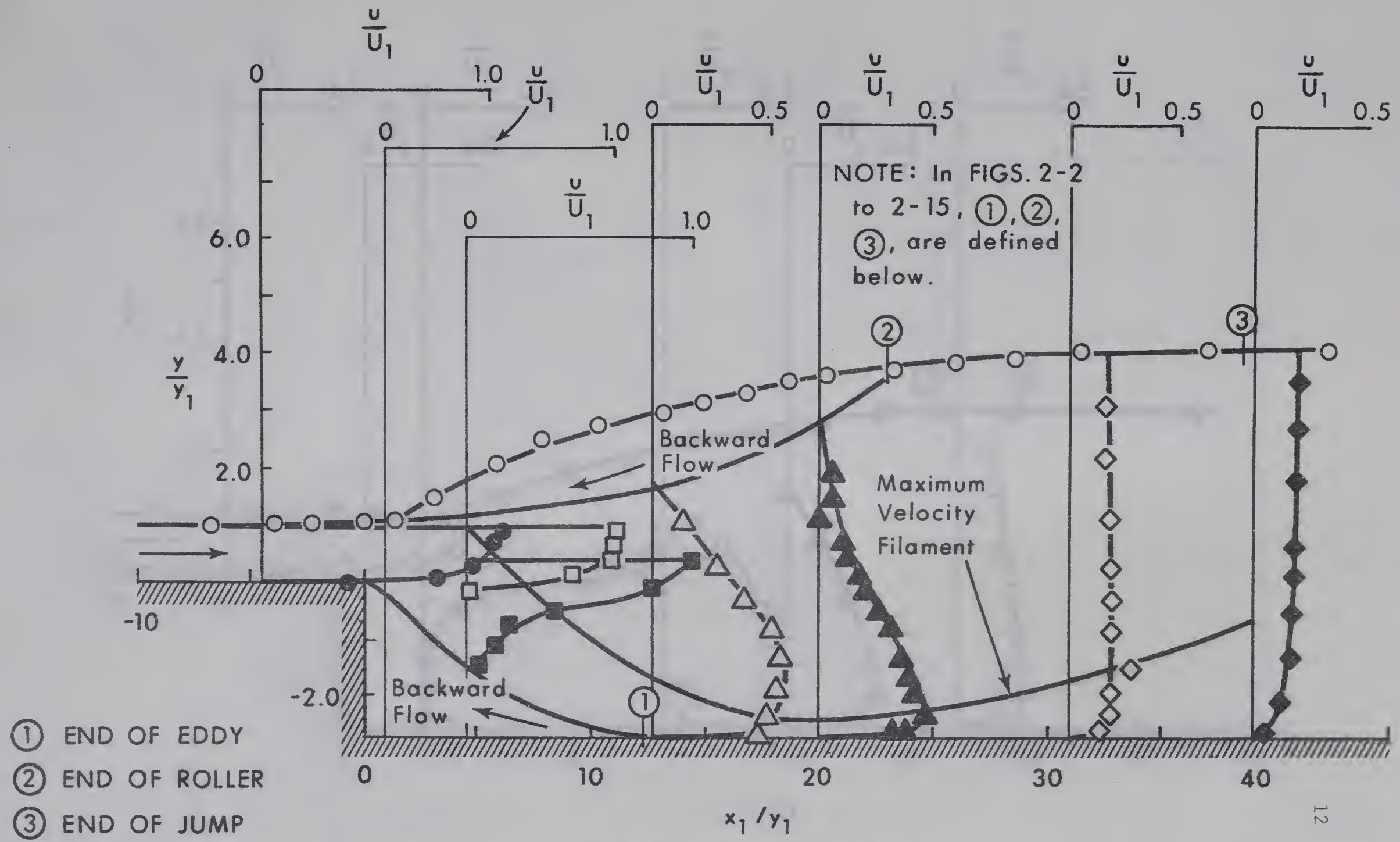

FIG. 2-2 Experimental Results (Run 1-A)

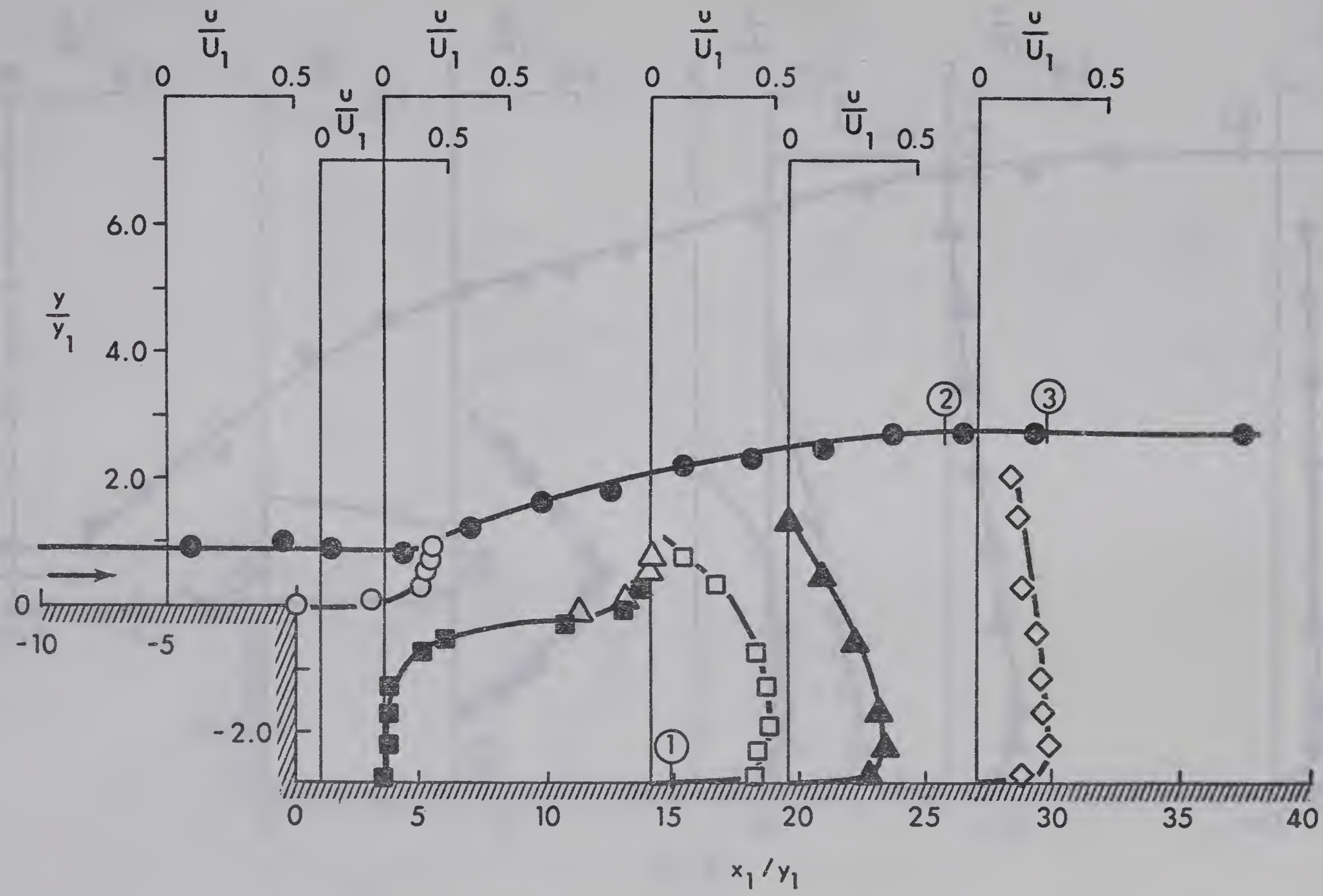

FIG. 2-3 Experimental Results (Run I-B)

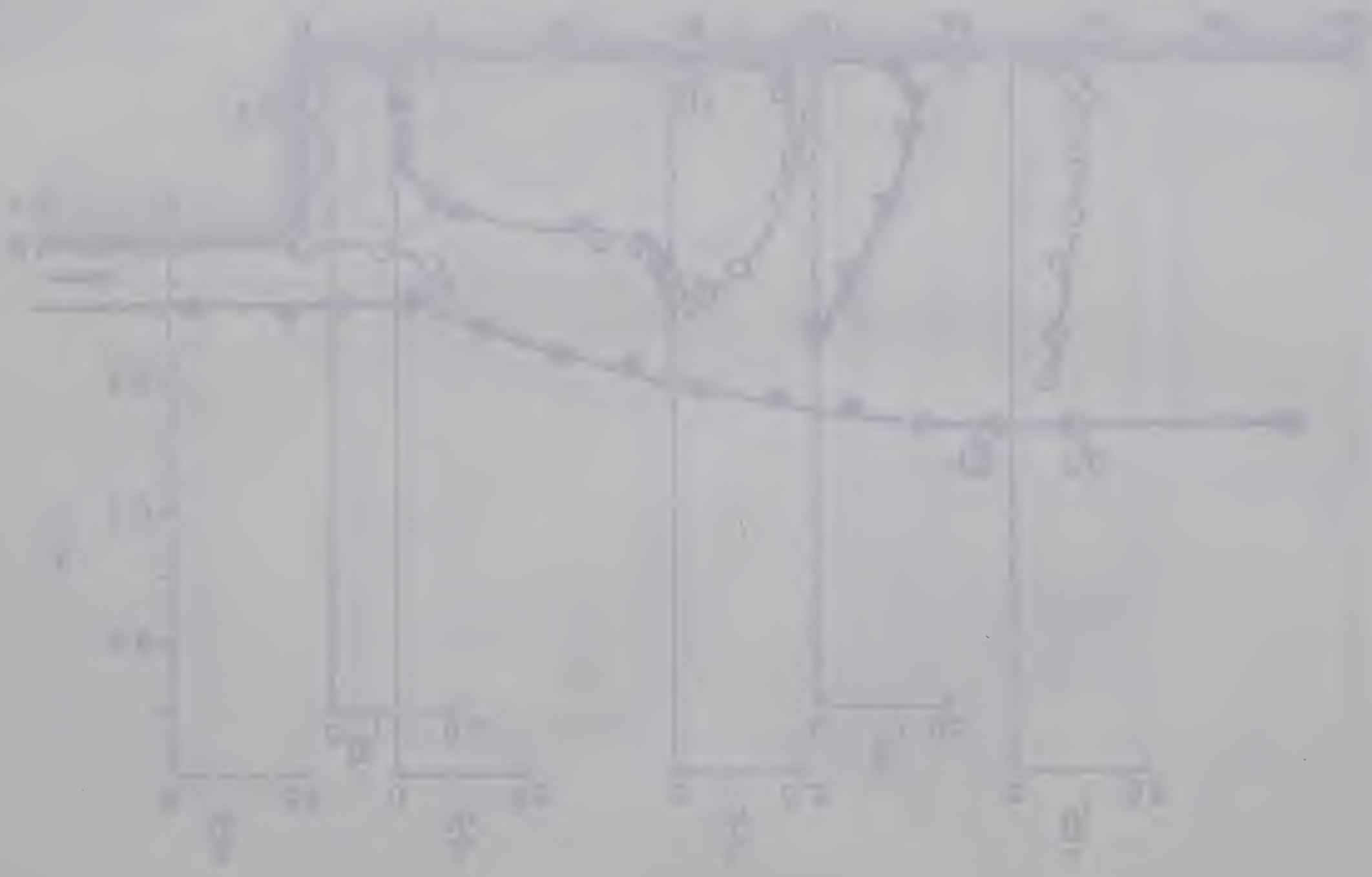

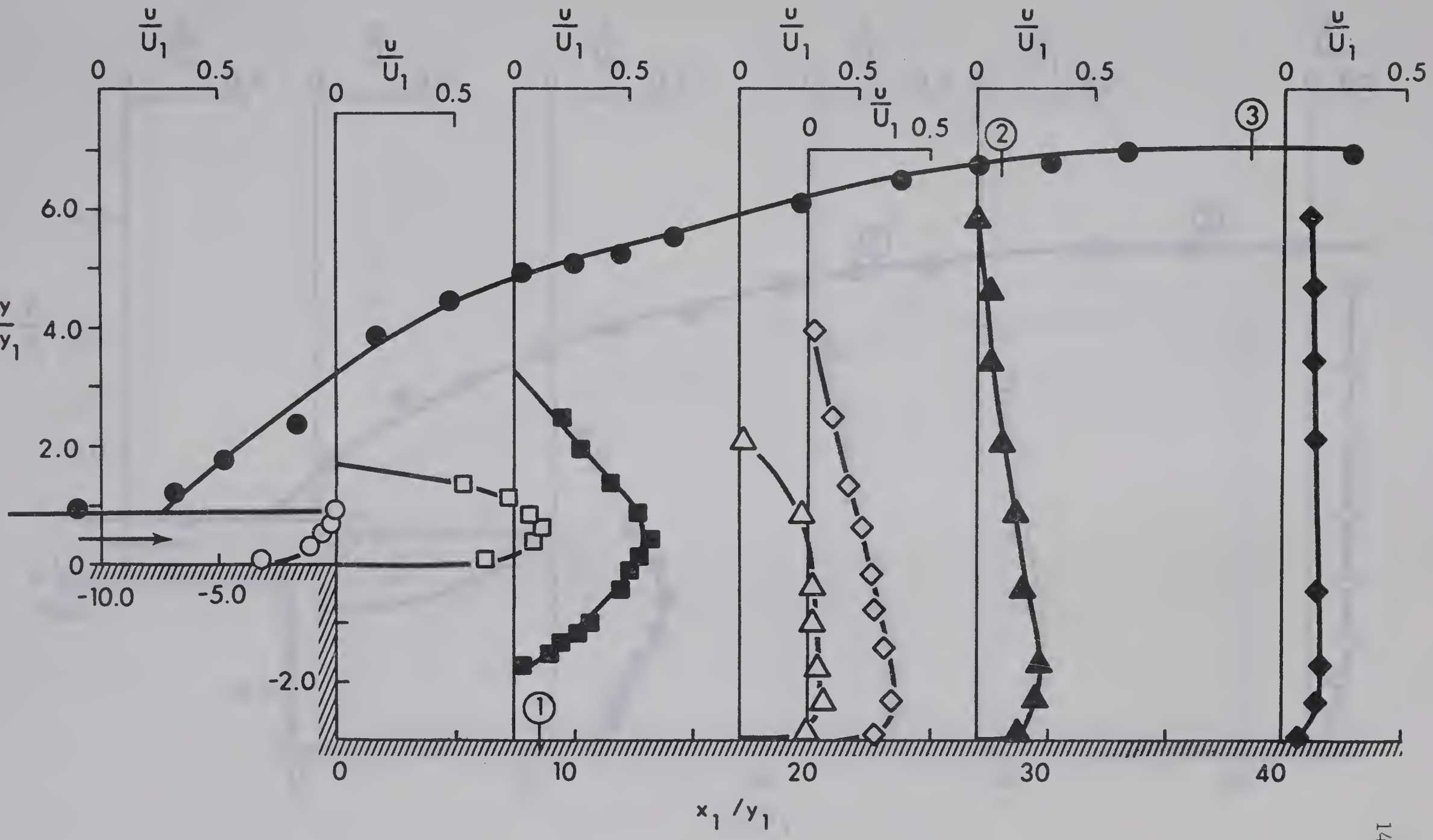

FIG. 2-4 Experimental Results (Run I-C)

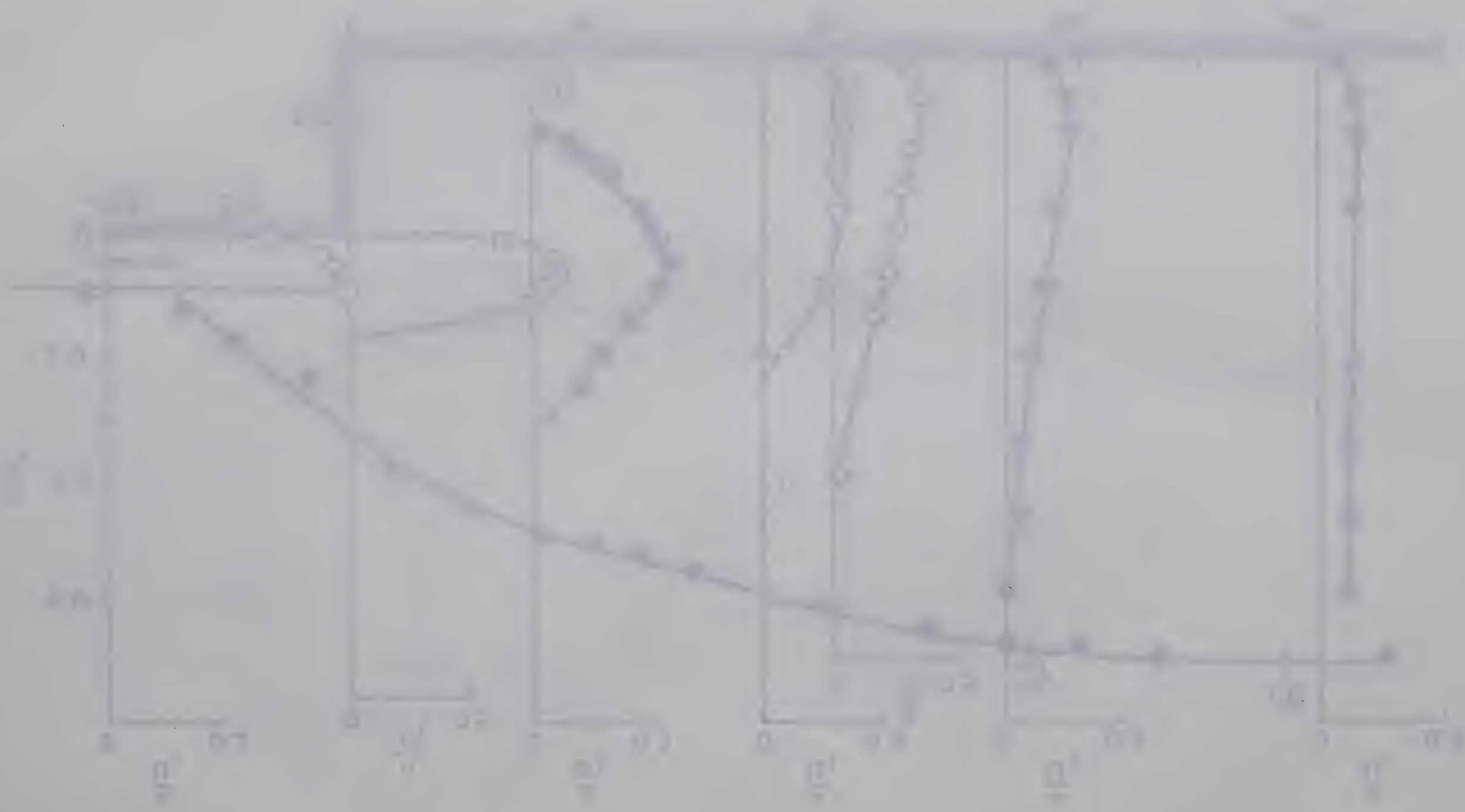

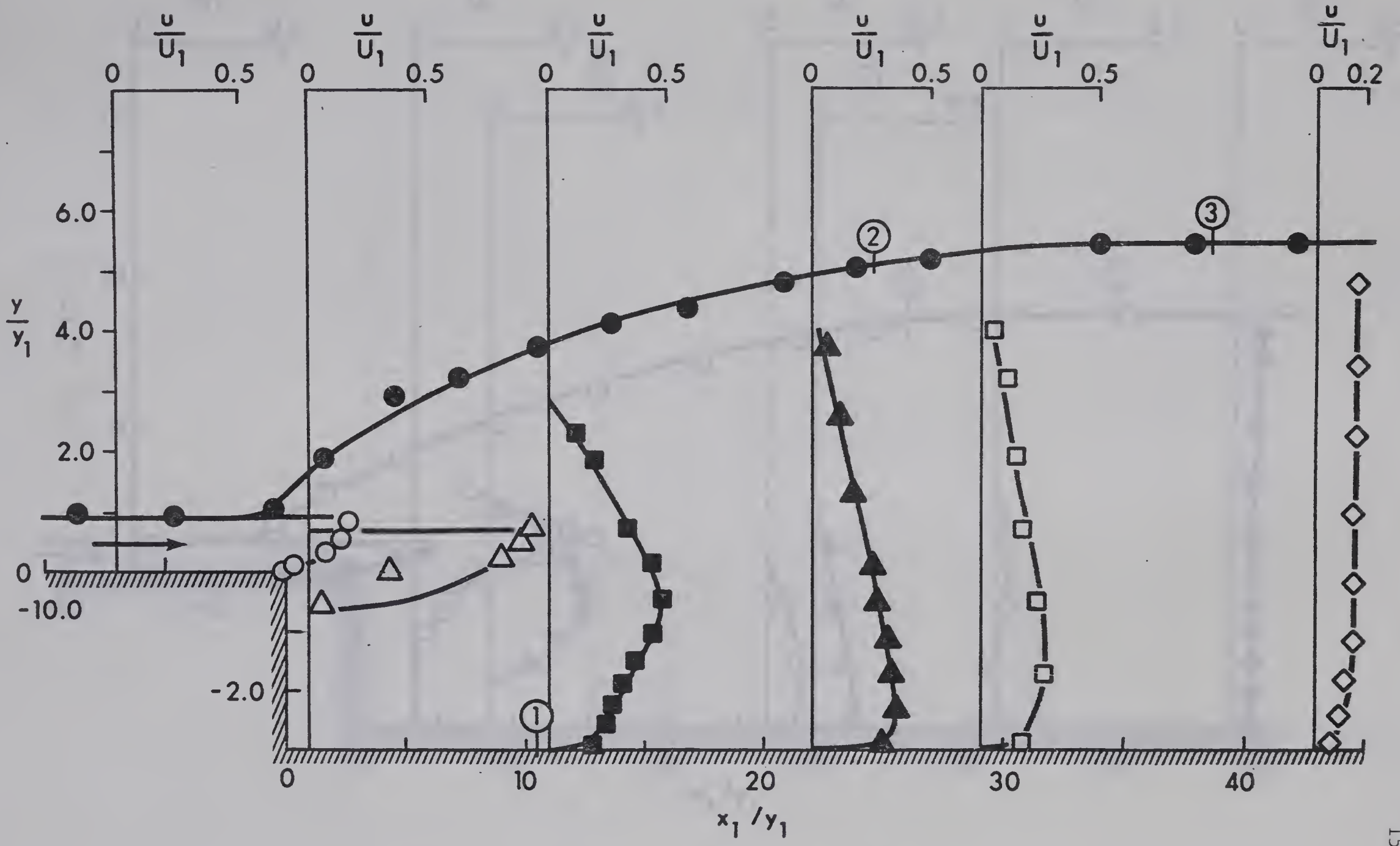

FIG. 2-5 Experimental Results (Run I-D)

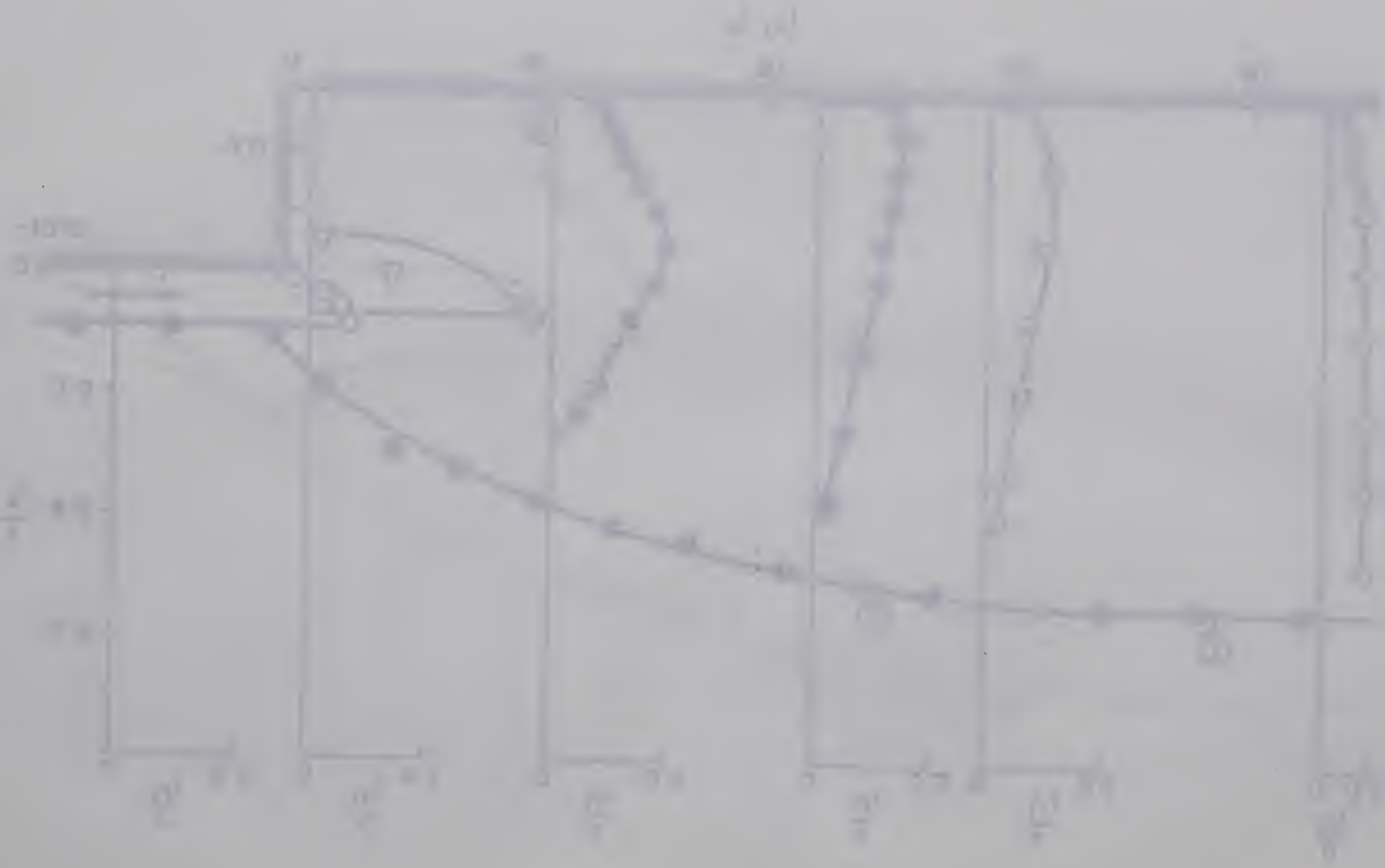

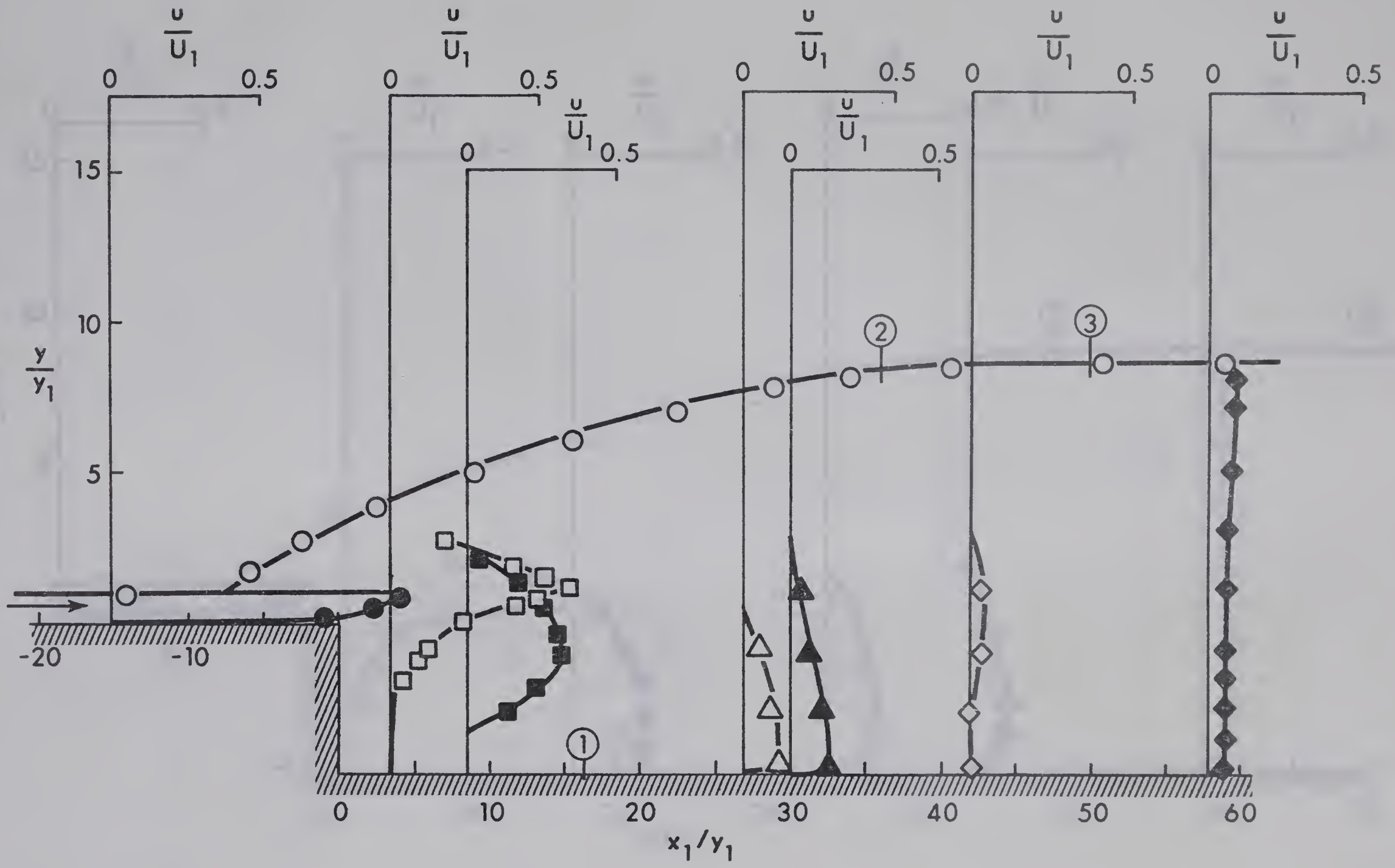

FIG. 2-6 Experimental Results (Run 2-A)

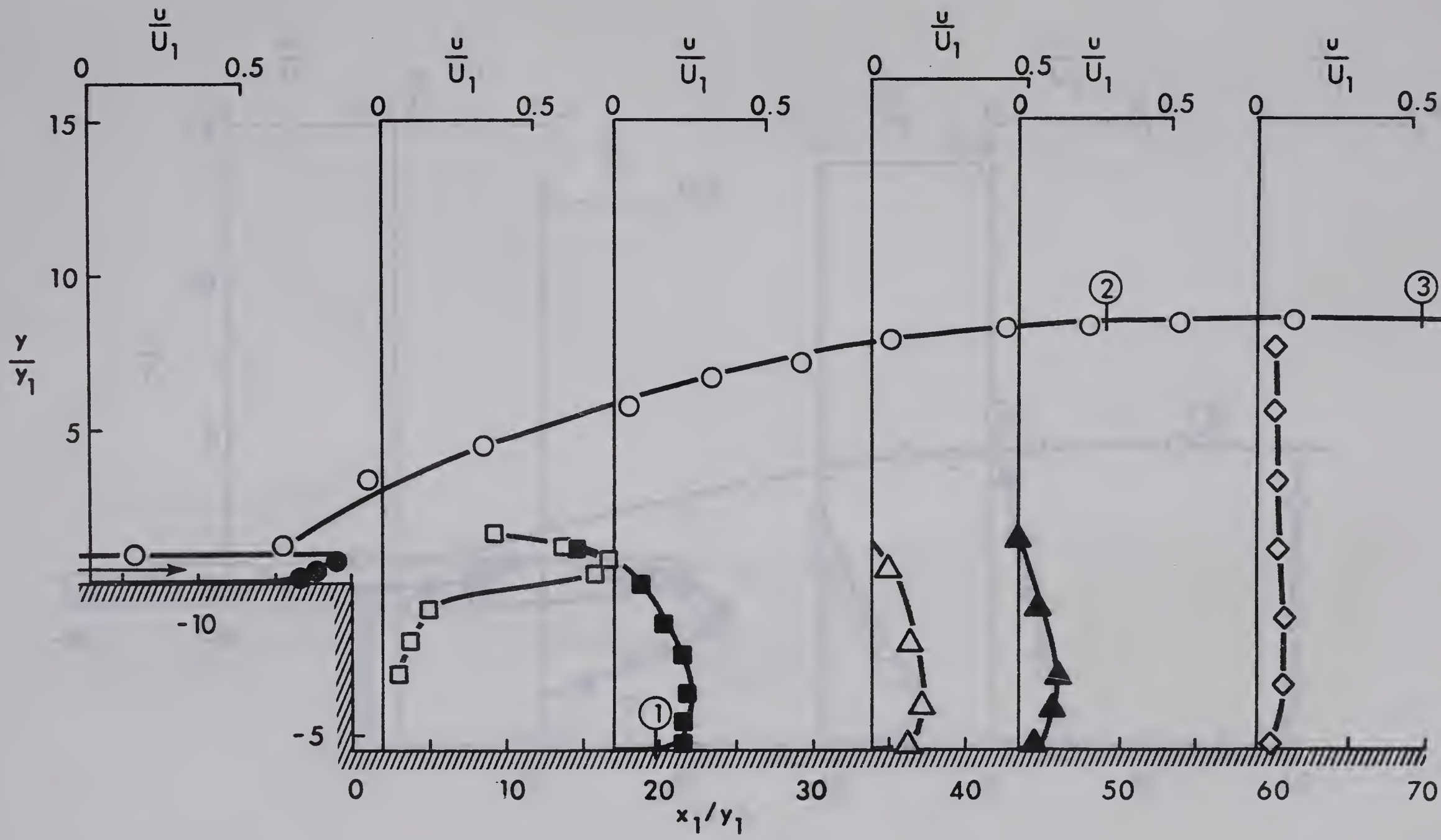

FIG. 2-7 Experimental Results (Run 2-B)

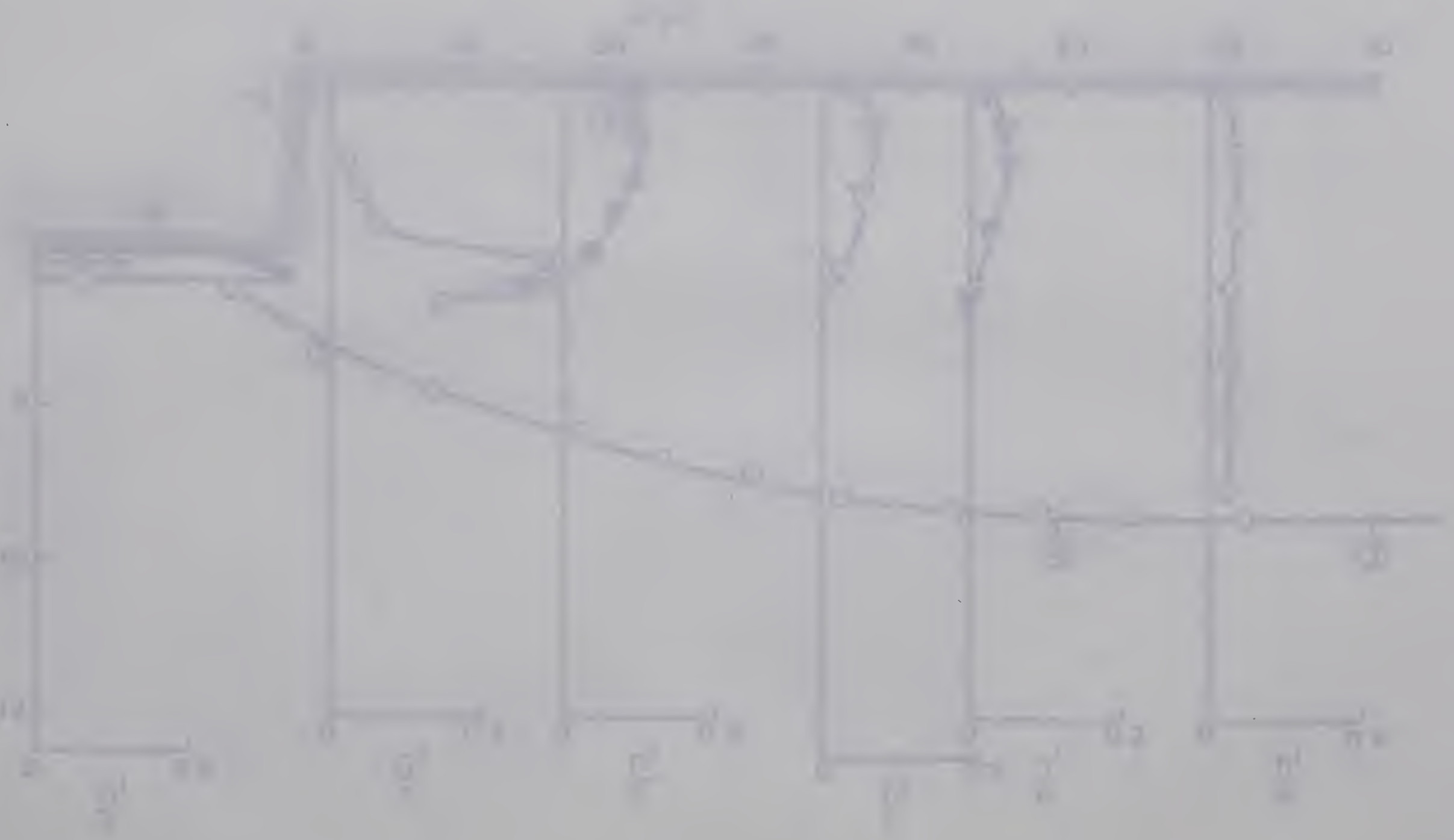

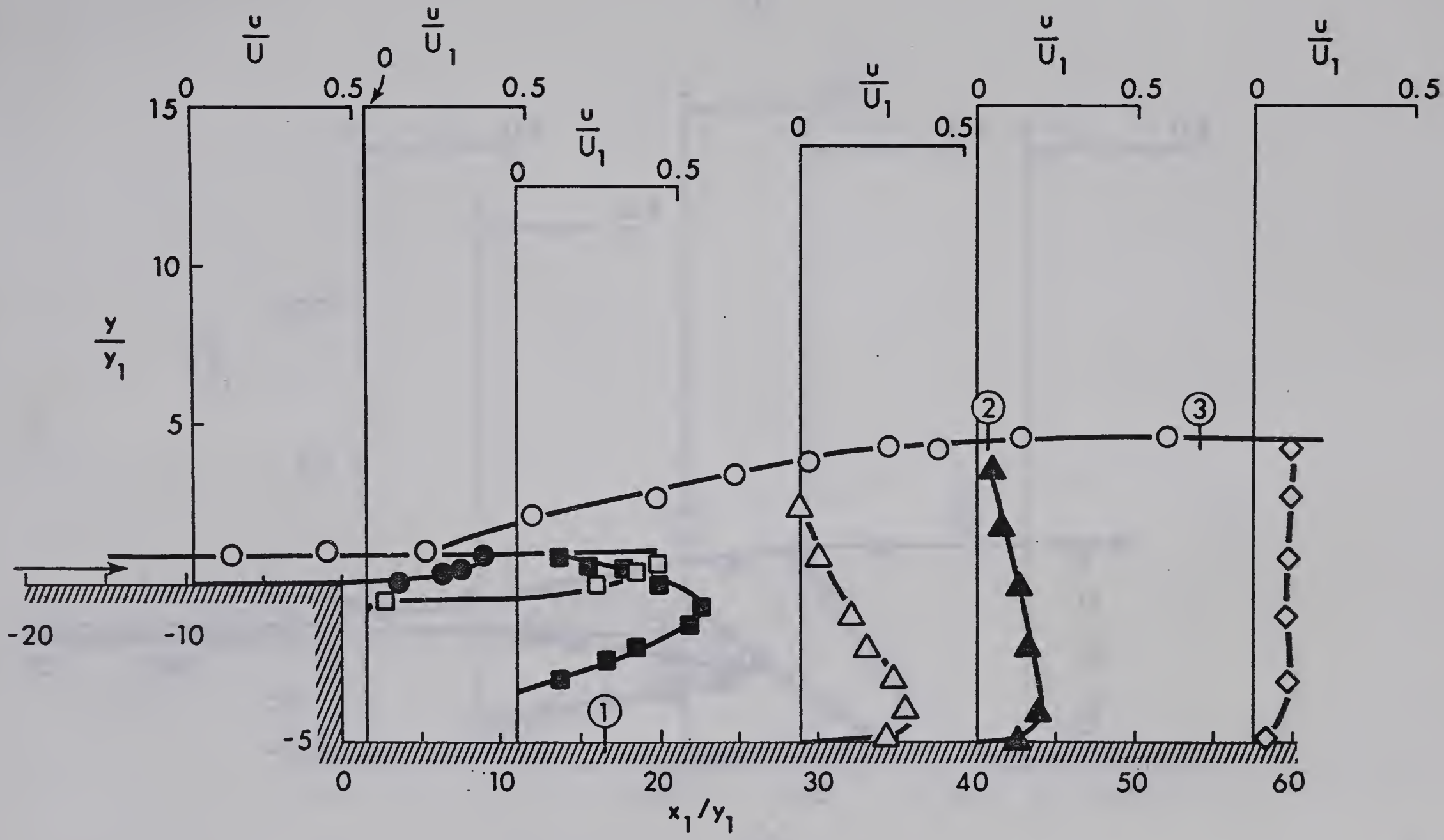

FIG. 2-8 Experimental Results. (Run 2-C)

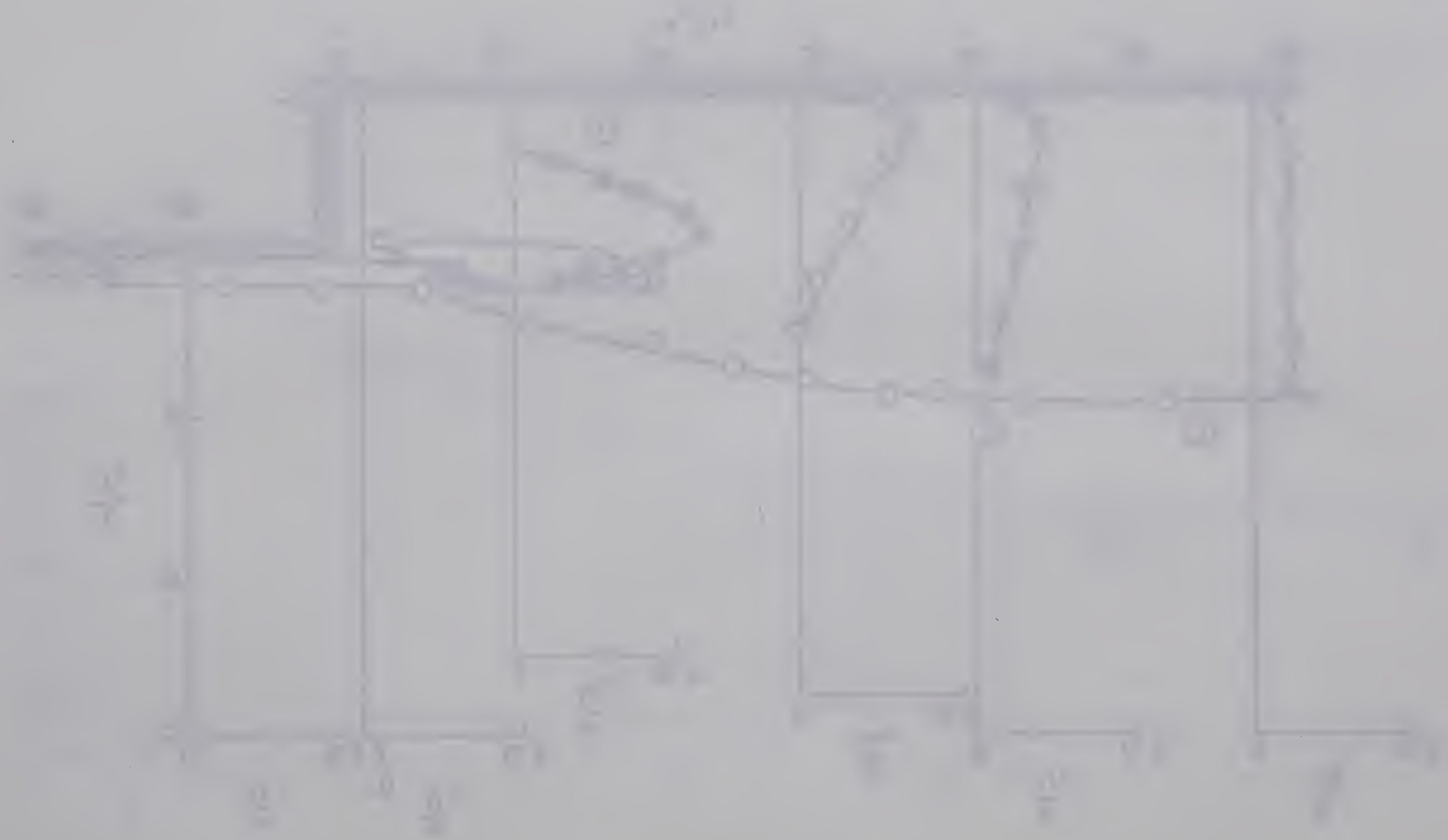

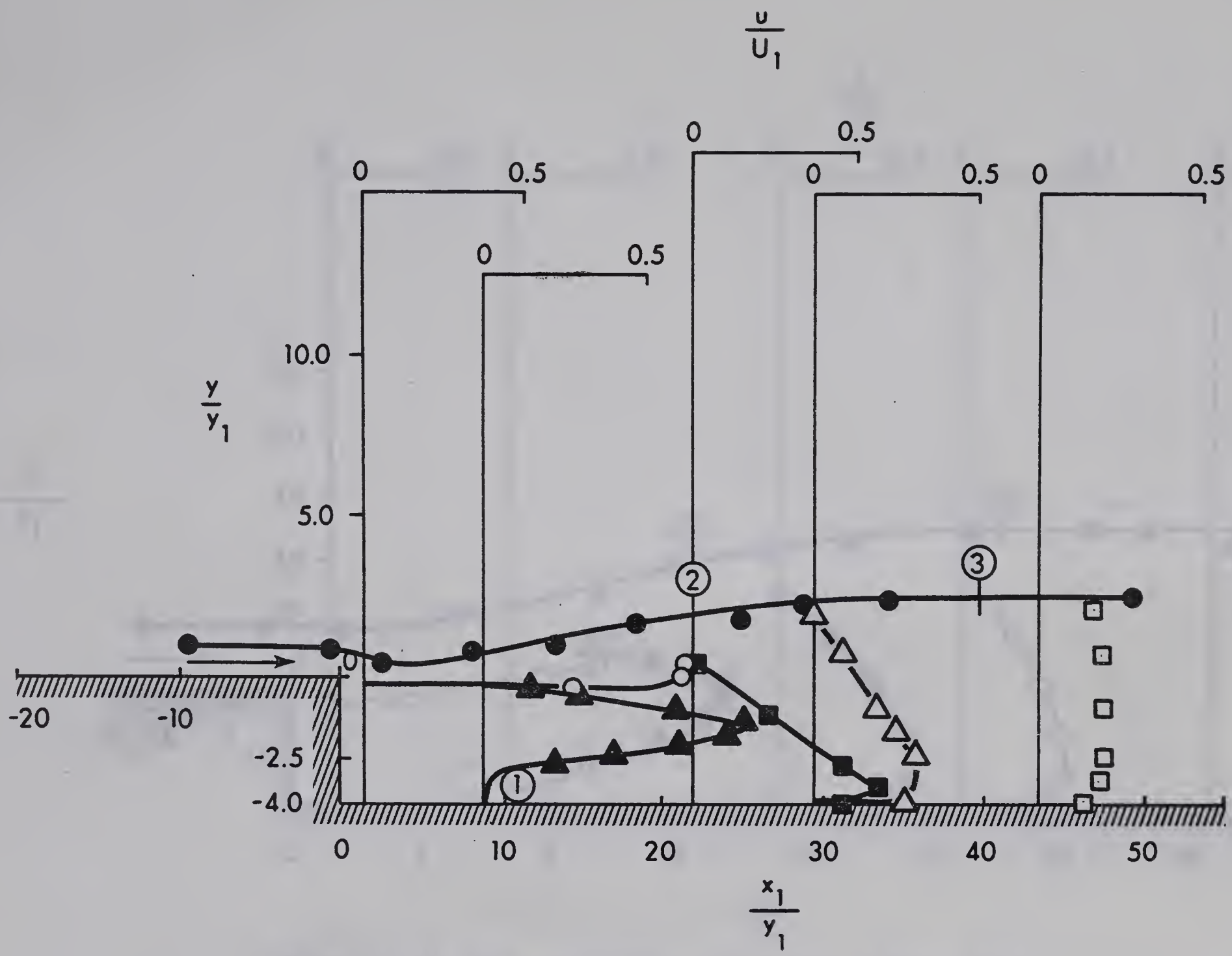

FIG. 2-9 Experimenal Results (Run 2-D)

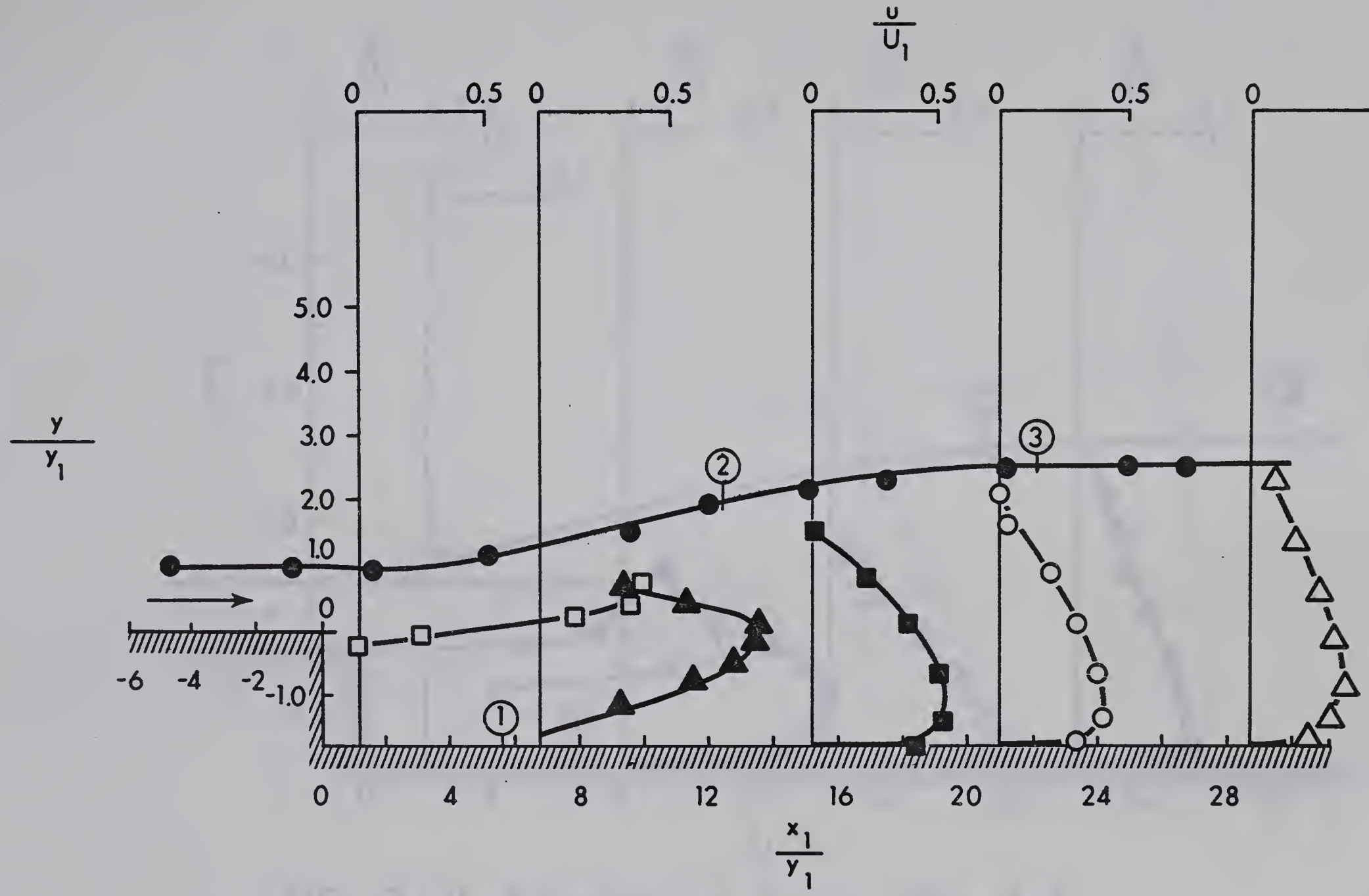

FIG. 2-10 Experimental Results (Run 3-A)

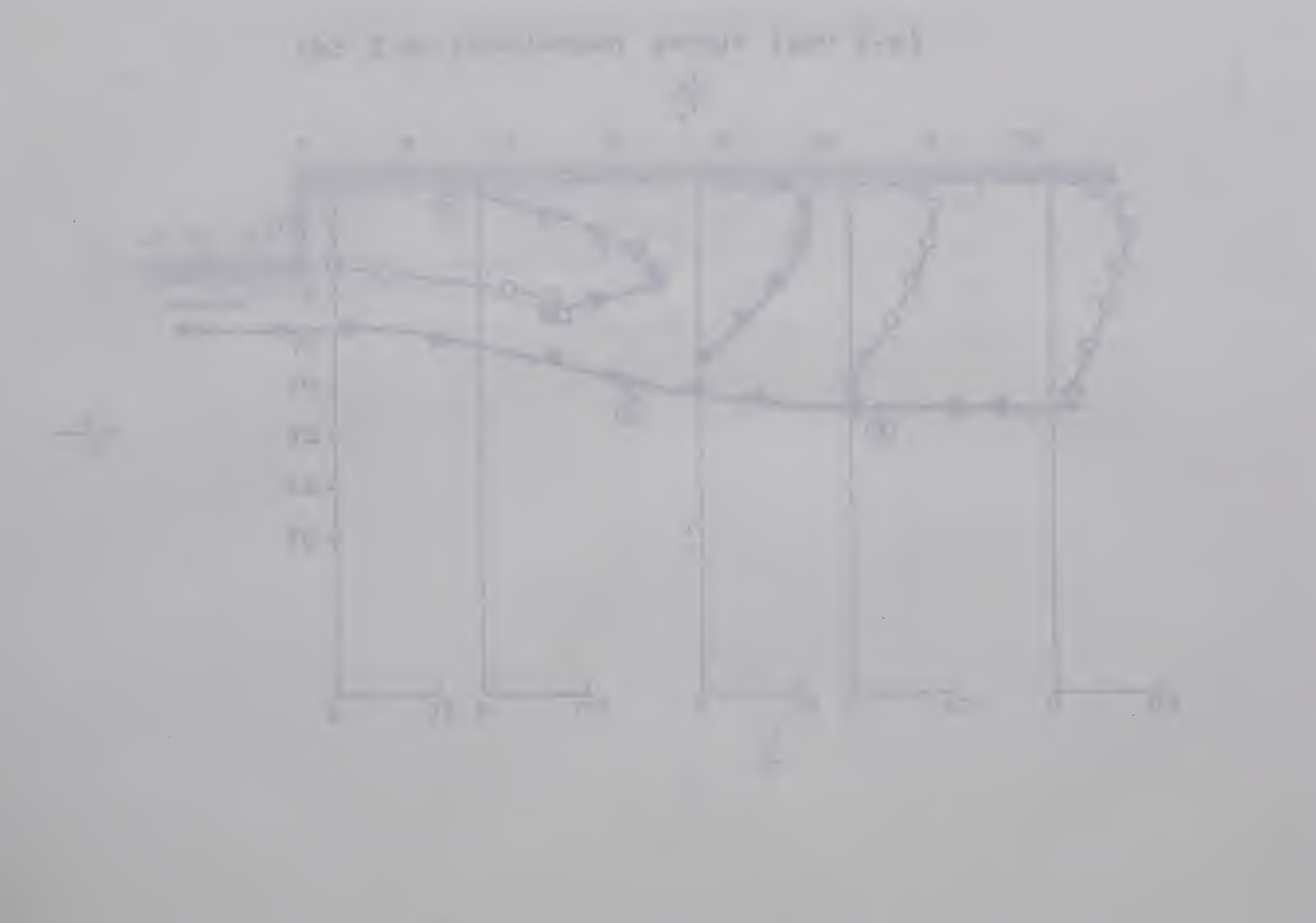

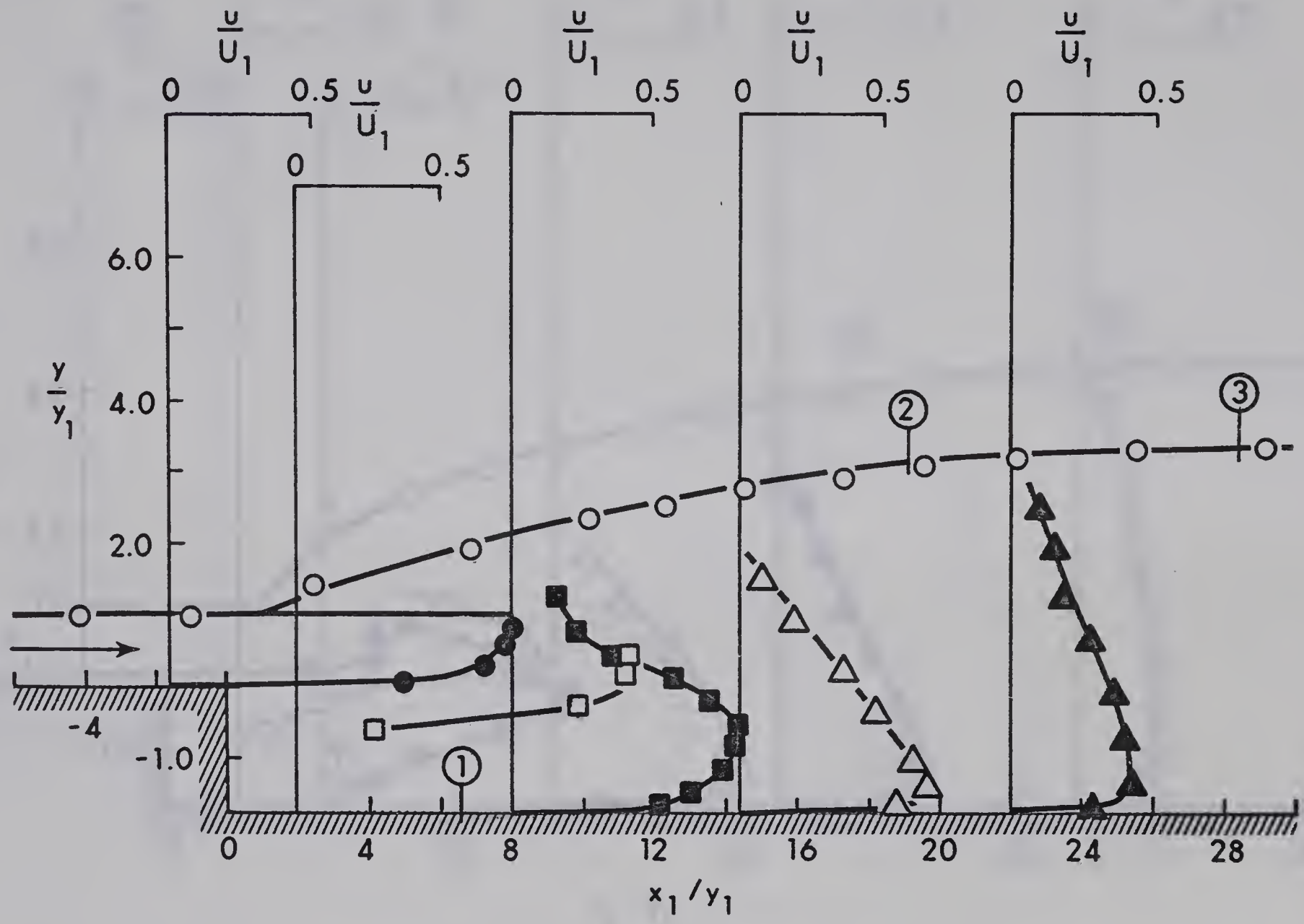

FIG. 2 - 11 Experimental Results (Run 3-B)

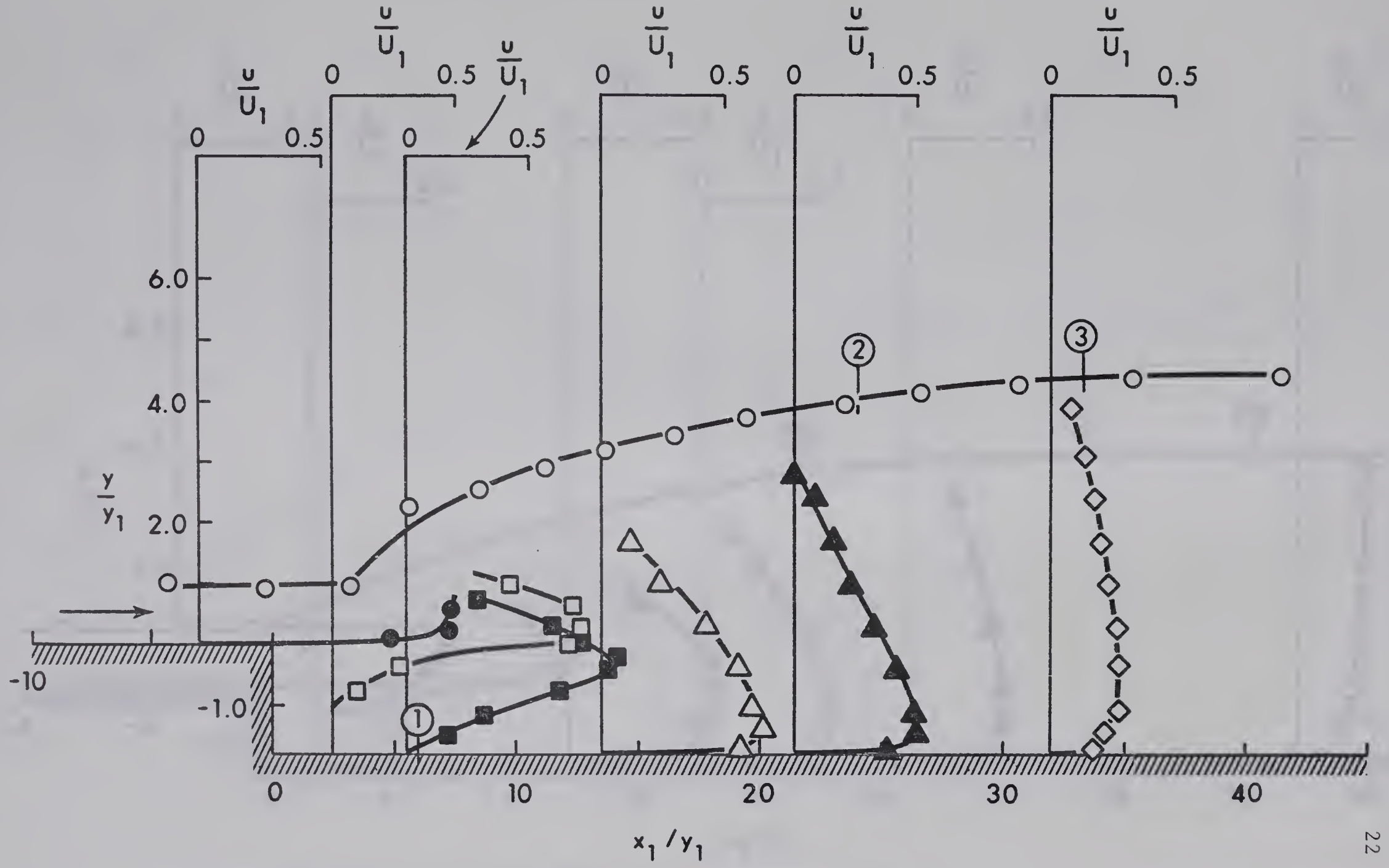

FIG. 2-12 Experimental Results (Run 3-C)

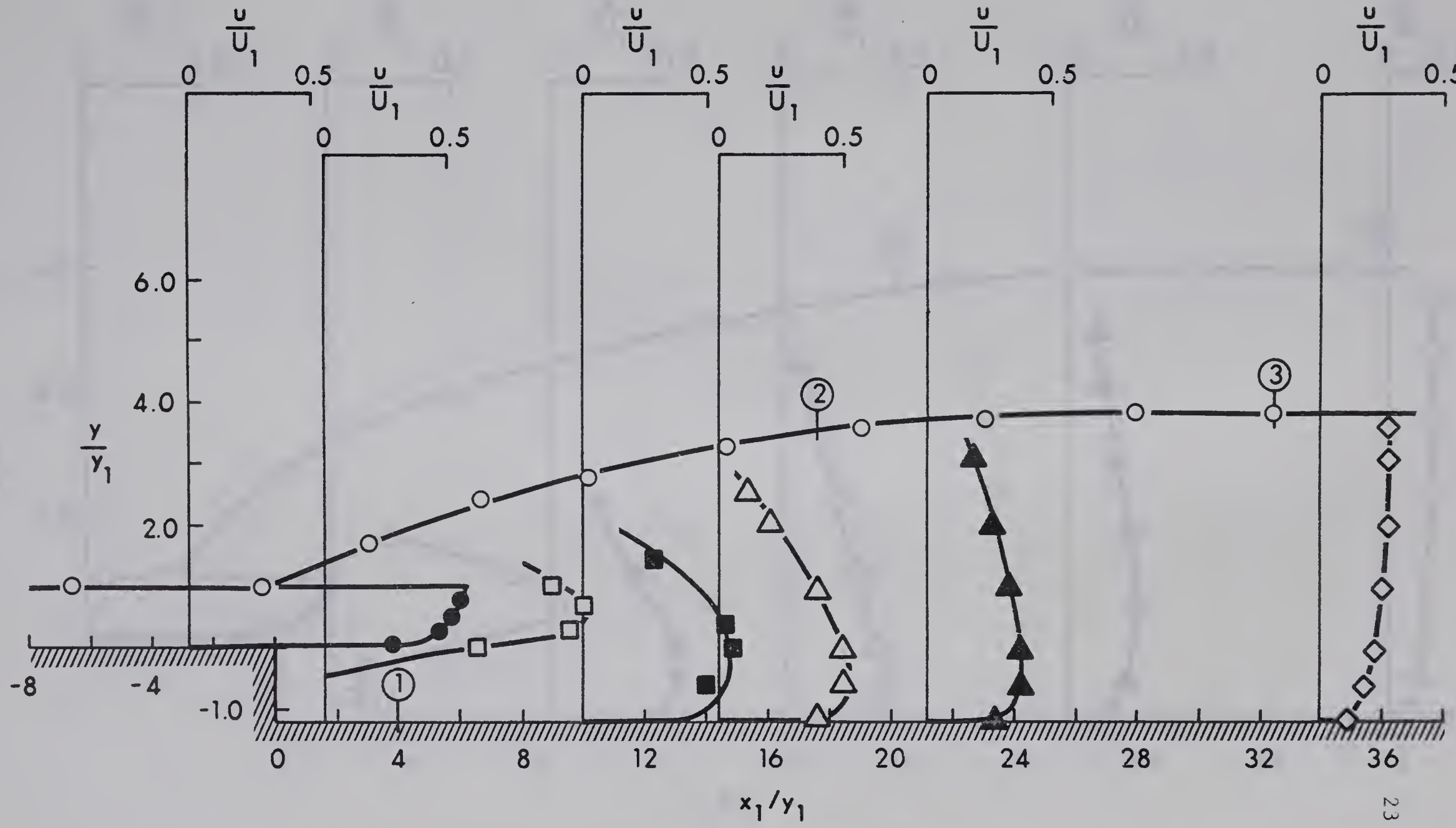

FIG. 2-13 Experimental Results (Run 4-A)

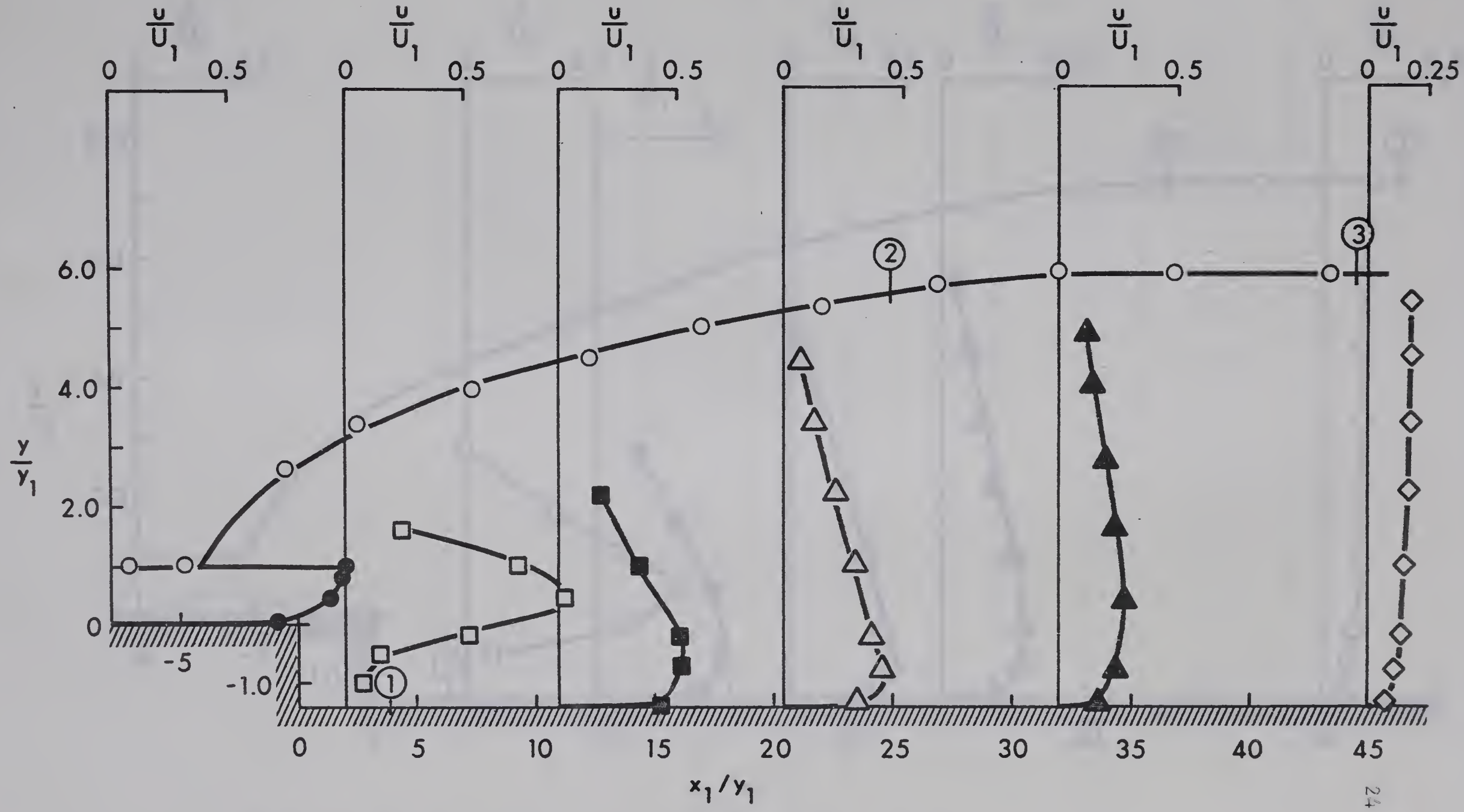

FIG. 2-14 Experimental Results (Run 4-B)

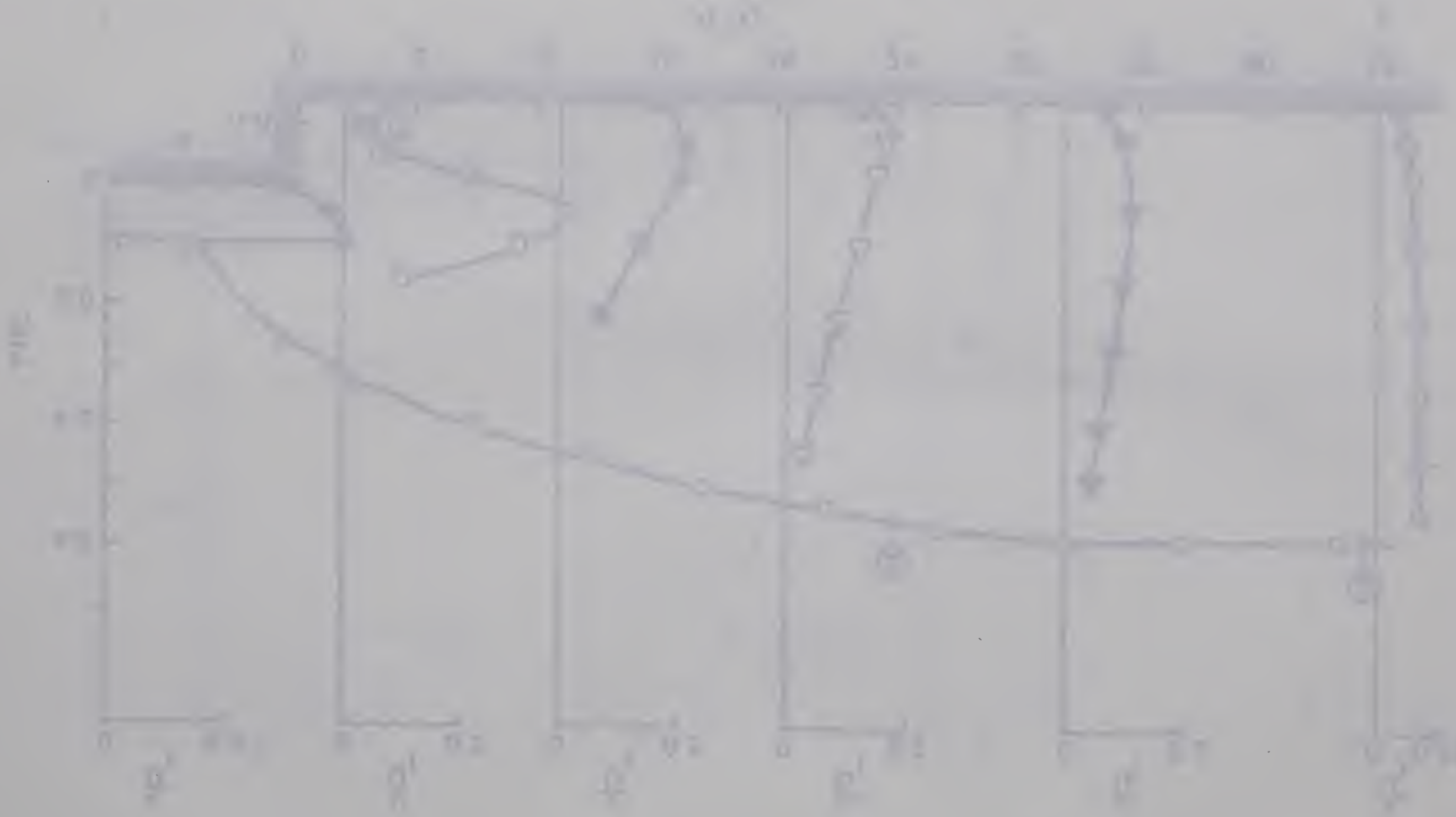

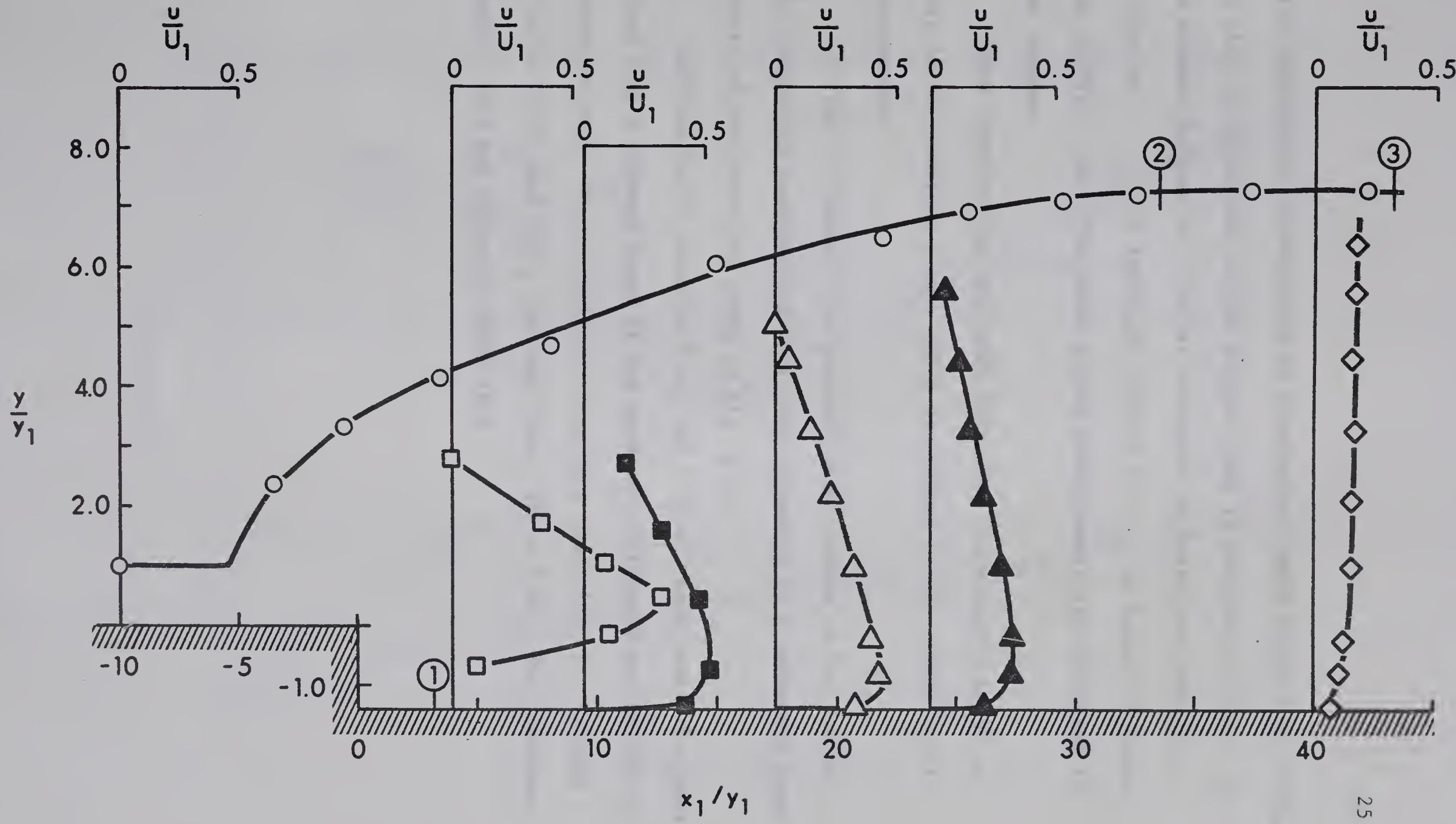

FIG. 2-15 Experimental Results (Run 4-C)

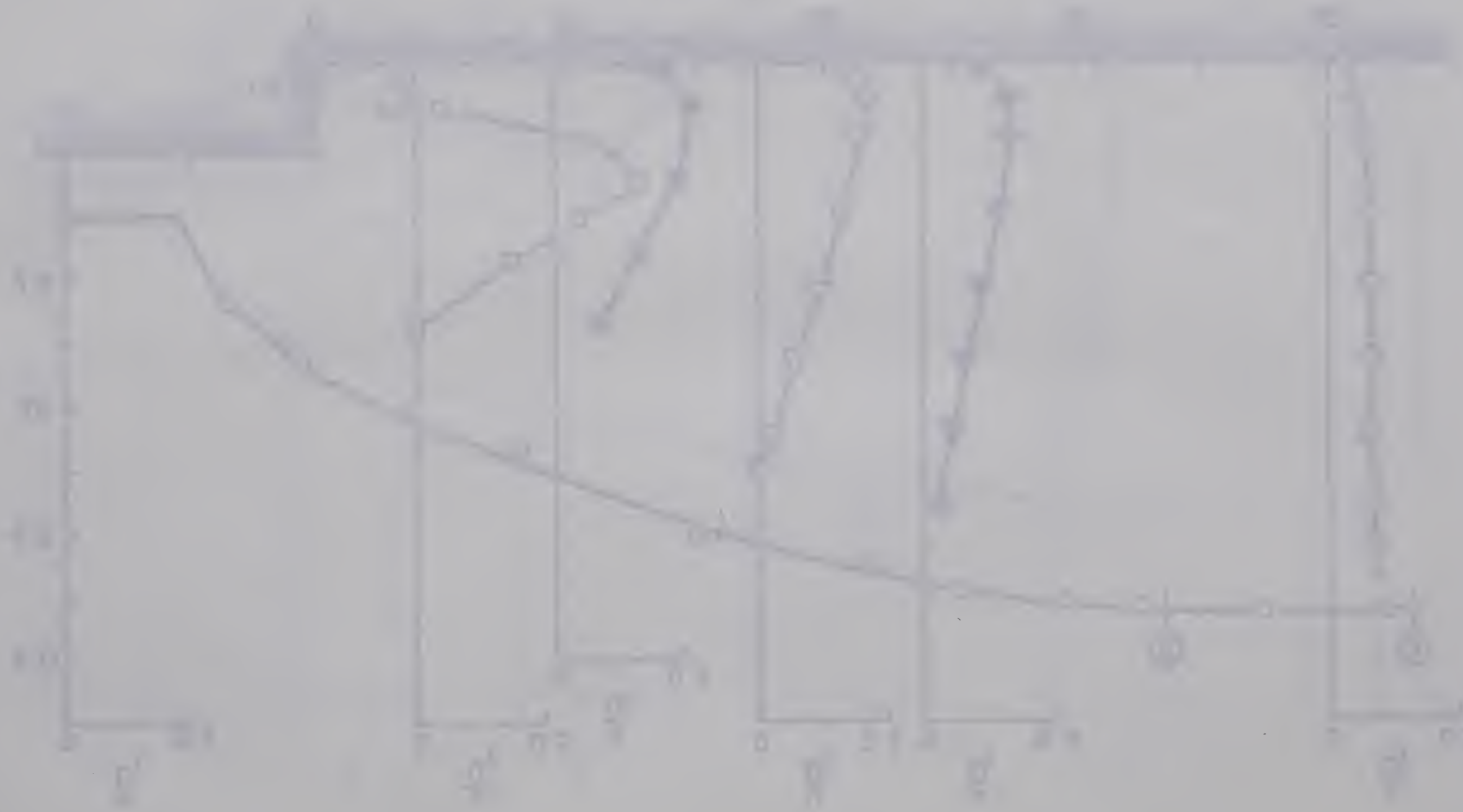

was first experimentally evaluated by Preston and later studied by others. (A full list of references on the Preston tube is available in Ref. 13). For the present purpose Eq. 2-01 as evaluated by Patel was reduced to a simple plot of τ_o in lbs/sq.ft. versus $p - p_o$ in inches of water, as shown in Fig. 2-16. The shear stress measurements are discussed in the next chapter.

Some observations were made regarding the velocity build up and decay on the junction plane, which is defined as the extension of the upstream bed.

In order to measure the pressure distribution on the face of the drop, ten holes were drilled in it and connected to a manometer board. The details of the holes are shown in Fig. 2-17.

Two heights of drops of 3 in. and 1.58 in. were used. To obtain the second drop a plywood board of the necessary thickness was bolted to the downstream bed. On the whole, 14 runs were made with F_1 varying from 3.14 to 10.55, and h/y_1 varying from 1.26 to 5.68. The pertinent experimental data are given in TABLE II-1.

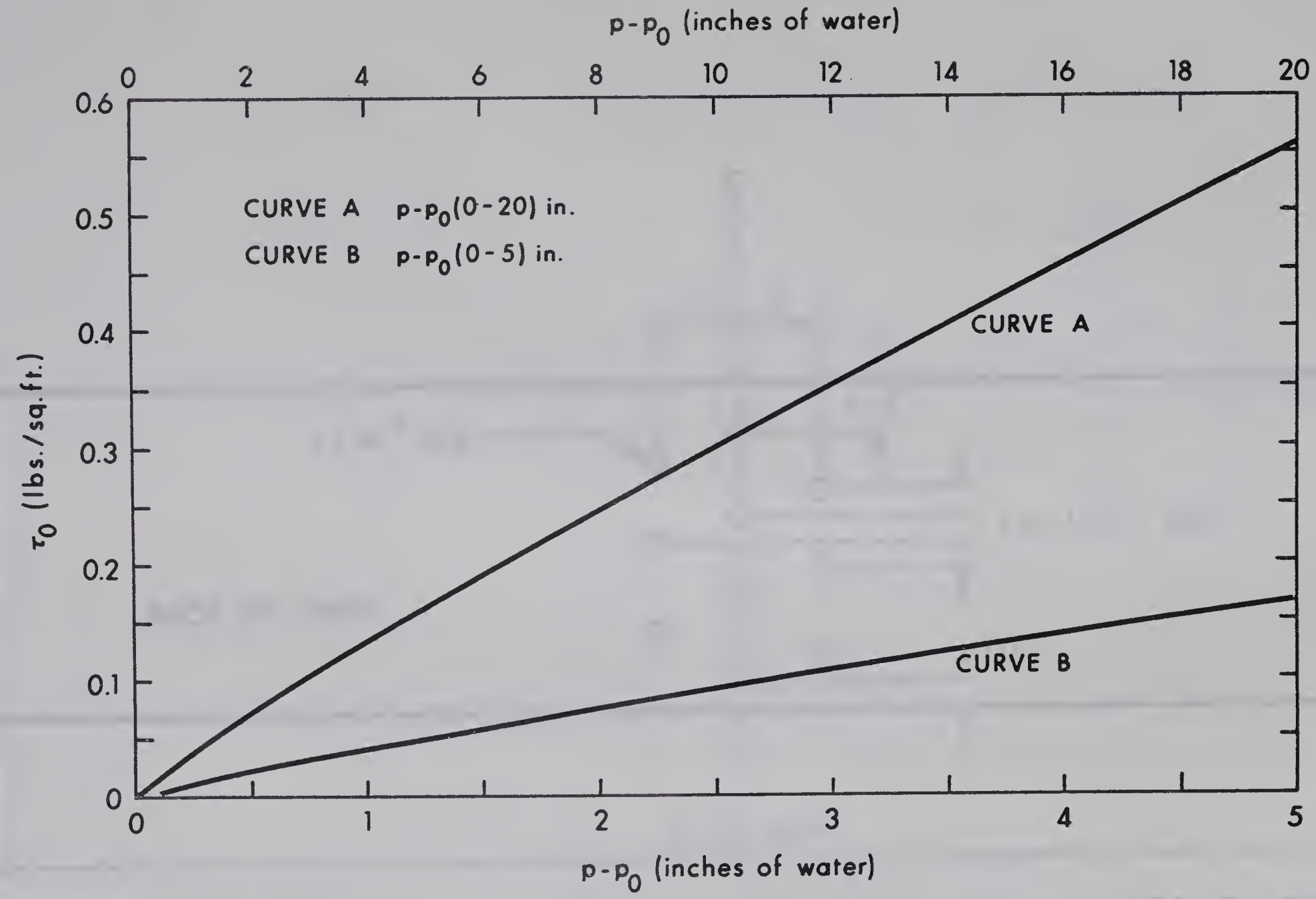

FIG. 2-16 Simplified Calibration Curve for the Preston Tube

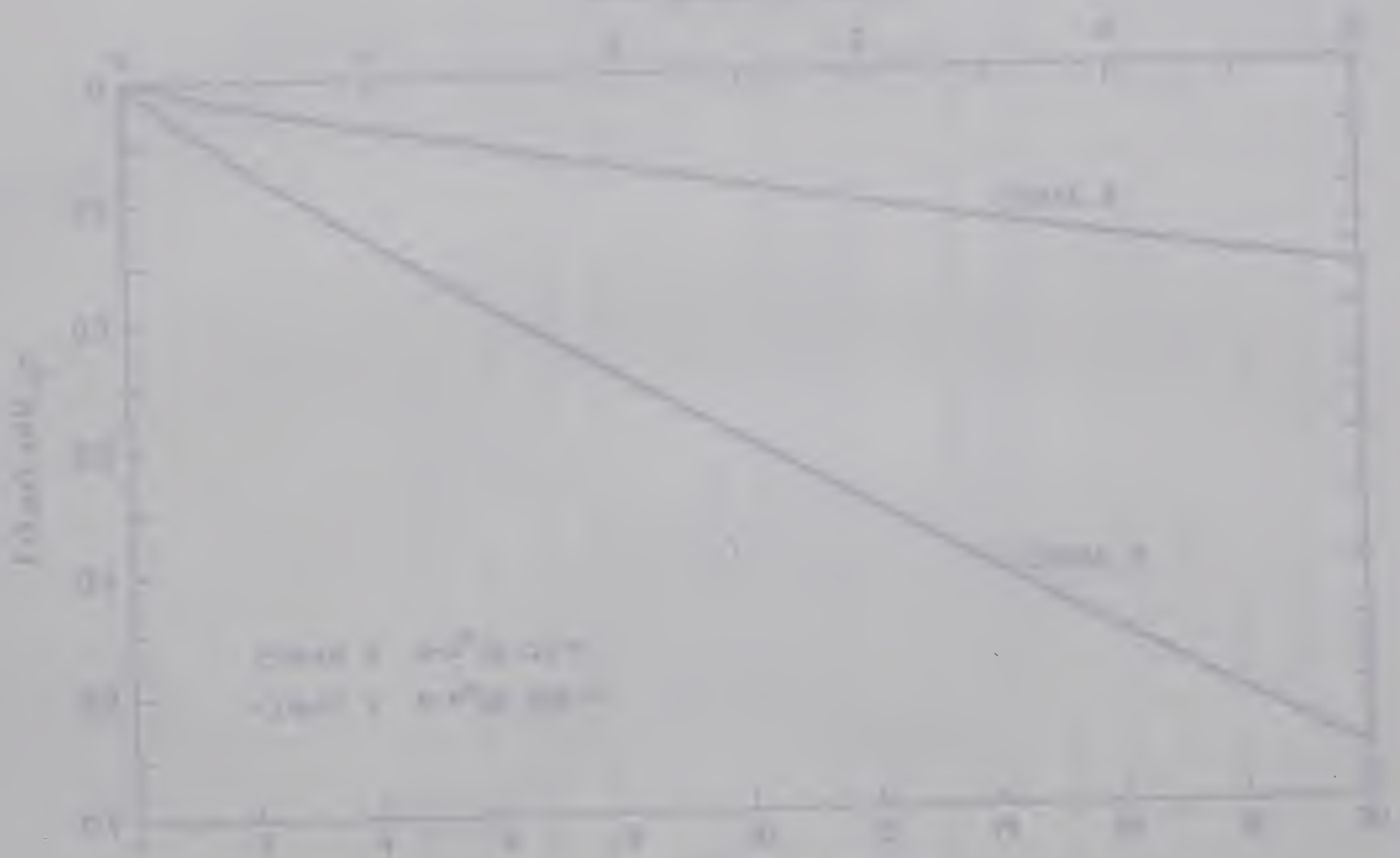

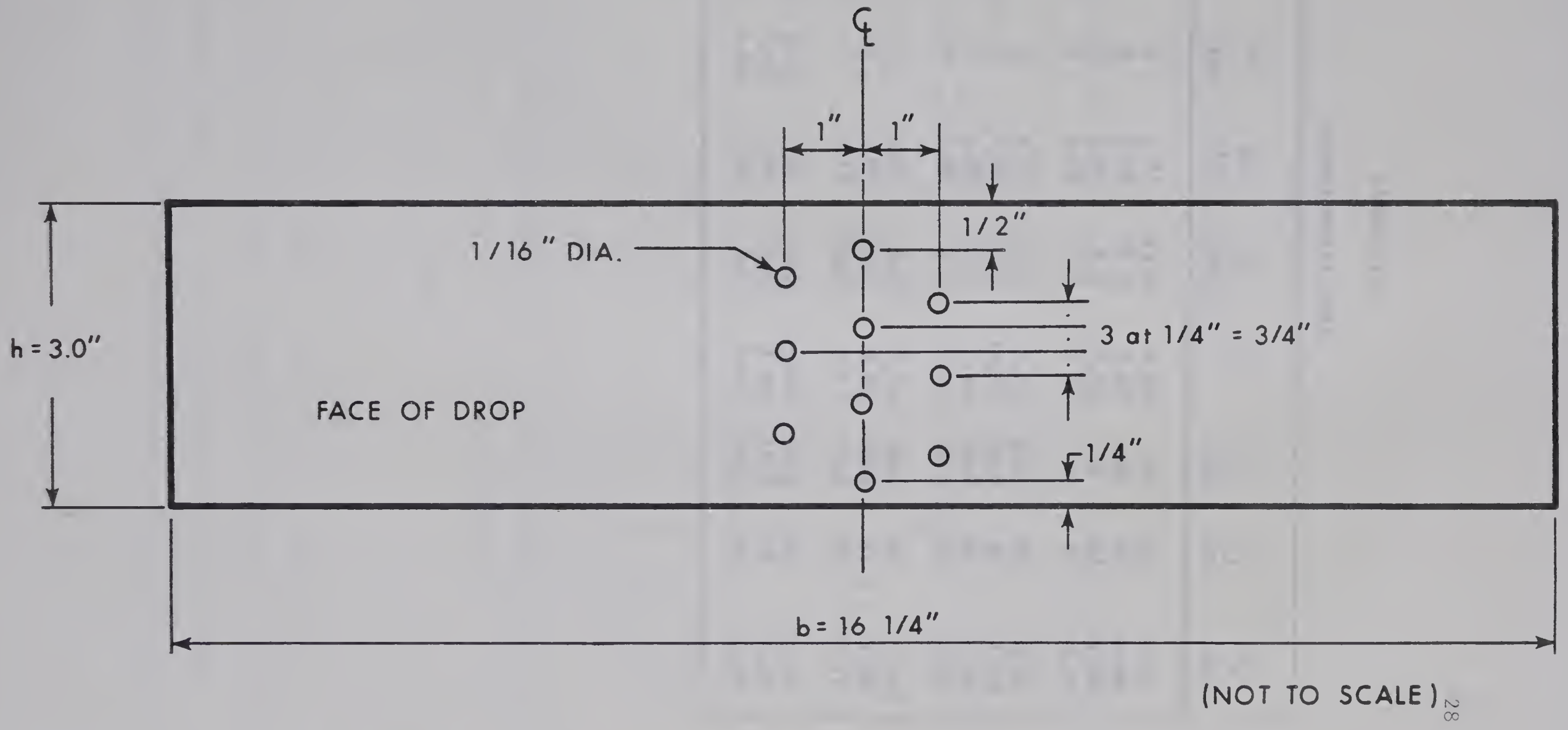

FIG. 2-17 Details of Piezometer Holes on Face of Drop.

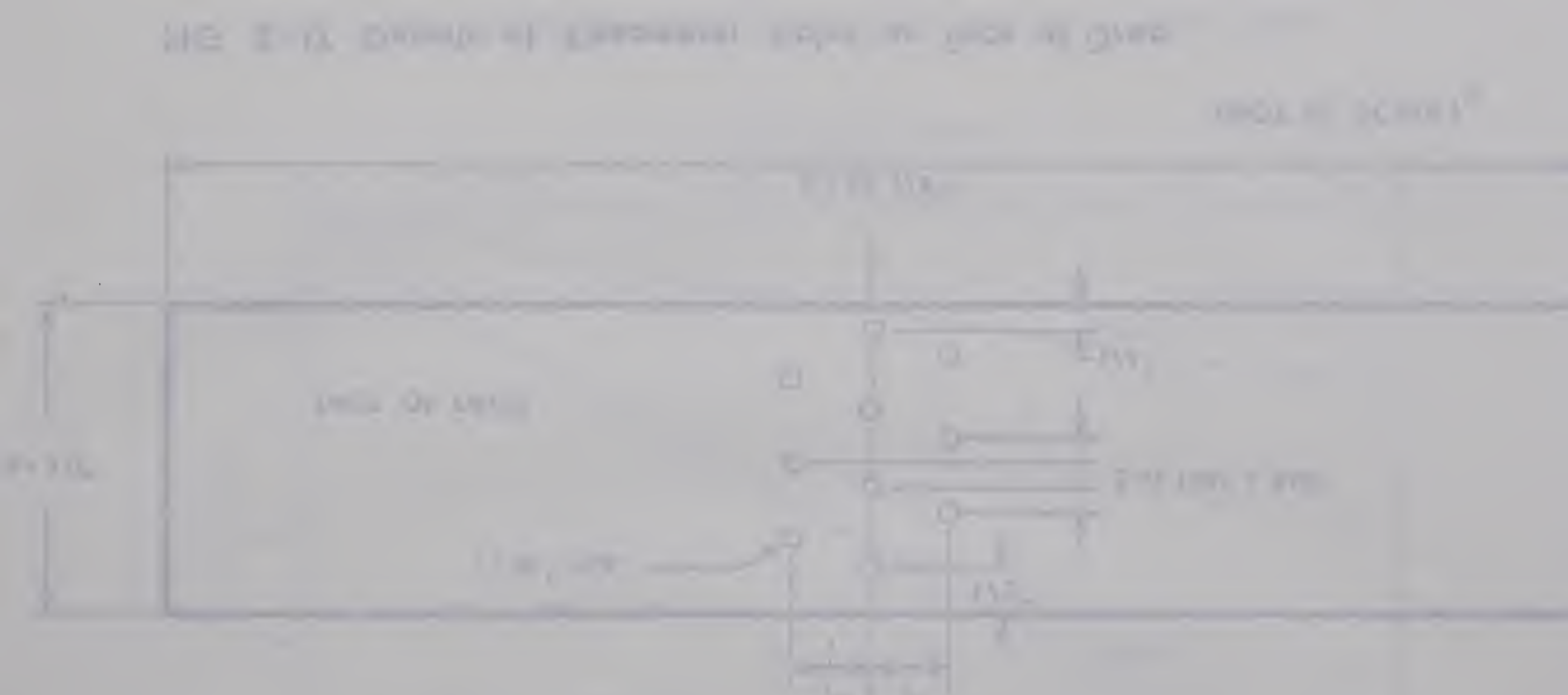

TABLE II-1

Experimental Data

Run No.	y_1 (in)	h (in)	$\frac{h}{y_1}$	L_e (in)	F_1	L_{rj} (in)	L_j (in)	y_t (in)
1-A	1.1	3	2.73	13.5	4.80	28	39	7.60
1-B	1.08	3	2.78	16.5	3.62	28	35	6.00
1-C	0.947	3	3.16	8.0	7.24	32	43	9.44
1-D	0.984	3	3.06	10.5	6.25	24	32	8.28
2-A	0.6	3	5.0	10.0	9.69	21.5	39	8.10
2-B	0.528	3	5.68	10.5	10.55	26.0	38	7.43
2-C	0.624	3	4.80	10.5	7.24	25.0	34	6.00
2-D	0.78	3	3.85	8.0	4.41	16.5	31	4.96
3-A	1.62	3	1.85	9.0	3.14	20.0	34	7.044
3-B	1.812	3	1.655	12.0	3.49	35.0	51.5	9.36
3-C	1.716	3	1.75	10.0	4.43	41.0	58	10.72
4-A	1.128	1.42	1.26	4.5	4.06	20.0	37	5.73
4-B	1.02	1.42	1.39	4.0	5.90	25.5	46	7.42
4-C	1.032	1.42	1.38	3.0	6.43	34.0	45	9.00

CHAPTER III

ANALYSIS OF RESULTS

Introduction

The experimental results were presented in a consolidated fashion in Figs. 2-2 to 2-15 in the previous chapter. These figures show that the supercritical stream enters the jump as a fully developed turbulent boundary layer. Then it undergoes diffusion as a curved jet, sandwiched between the standing eddy on the bottom and the surface roller on the top. After it hits the channel bed, it appears to behave like a plane turbulent wall jet with a return flow on top, up to the end of the surface roller. Beyond this, the wall jet degenerates into fully developed subcritical channel flow. In most of the cases studied, even at the end of the jump, that is, at the section at which the water surface becomes level and attains the tailwater depth, the velocity distribution has not attained the fully developed open channel velocity distribution. In the following sections, the different portions of the B-Jump are analysed separately with a view to explore the mechanics of this phenomenon.

Wall Jet

The wall jet could be defined as a jet of fluid impinging tangentially or at an angle on a boundary and covered by stationary or moving fluid. Fig. 3-1 shows the case of a plane turbulent wall jet, blowing tangentially on a smooth plate with a uniform velocity of U_o and depth

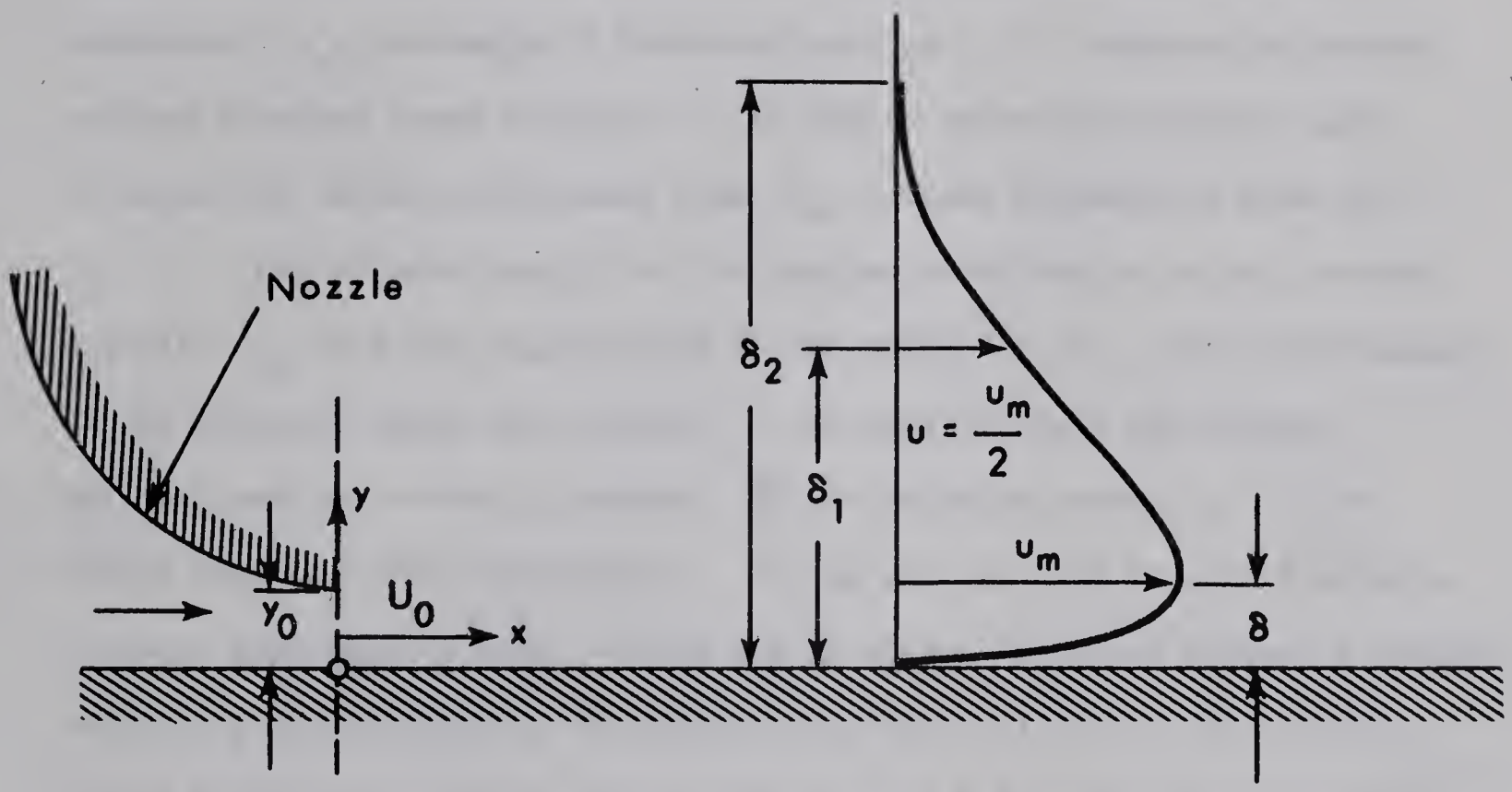

FIG. 3-1 The Plane Turbulent Wall Jet.

of y_o, the flat plate being covered by an infinite expanse of the ambient fluid and this is sometimes known as the classical wall jet. It has been found that in the fully developed portion of the wall jet, i.e. for $x/y_o \gtrsim 10$ to 15, where x is the longitudinal distance from the efflux section, the velocity distribution is "similar", in the sense that it is described by one single non-dimensional curve[14,15,16]. (Ref. 16 gives an extensive bibliography on wall jets). With reference to Fig. 3-1, the region close to the bed, in which the velocity increases from zero to a maximum of u_m, resembles a boundary layer and δ denotes the corresponding boundary layer thickness. The region above the boundary layer in which the velocity decreases from u_m to zero resembles a free jet.

The velocity scale for the similar distribution is the maximum velocity u_m and the length scale is the distance δ_1 from the boundary to the plane at which the velocity u is equal to half the maximum velocity and the velocity gradient $\frac{du}{dy}$ is negative, where y is the normal distance from the boundary. In the case of wall jets with adverse pressure gradients or with a rough bed or with an external stream, a single velocity profile could not be obtained and the wall jet has to be split into a boundary layer and a free mixing region and analysed separately[17]. This scheme is adopted in the present work.

Free Mixing Region

The velocity distribution profiles in the free mixing regions could be observed in Figs. 2-2 to 2-15. It was first attempted to see whether the velocity distribution in the free mixing region is similar.

It is done in Fig. 3-2, in which u/u_m is plotted against $\eta' = y - \delta / \delta_1 - \delta$. It is found that the velocity distribution is indeed similar and agrees very well with the curve for the plane turbulent wall jet under zero pressure gradient, which has been reproduced from Ref. 17. The scatter in the outer region, has been observed earlier by other investigators also[17]. This shows that even in the case of a reattached wall jet growing under an adverse pressure gradient and bounded by return flow on top, the velocity distribution in the free mixing region is similar and is essentially the same as that of the classical wall jet. In this connection, it should be mentioned that in a recent study of a plane turbulent jet impinging on a flat plate at different angles, Schauer and Eustis[18] obtained comparable results.

Next a study was made of the variation of the velocity and length scales. For the classical wall jet, the two scales are generally given[14,17] by the equations

$$\frac{u_m}{U_o} = 3.45 \left(\frac{x}{y_o}\right)^{-0.50} \qquad (3\text{-}01)$$

and

$$\frac{\delta_1}{y_o} = 0.50 + 0.065 \frac{x}{y_o} \qquad (3\text{-}02)$$

$$\frac{\delta_1 - \delta}{y_o} = 0.42 + 0.055 \frac{x}{y_o} \qquad (3\text{-}03)$$

The present results for the velocity scale are shown plotted in Fig. 3-3 with u_m/U_1 against x_2/y_1, where x_2 is the distance measured from the end of the eddy, which is the same as the reattachment line for the wall jet. A single curve could be drawn through the experimental points. In Fig. 3-3 it should be remembered that U_1 and y_1 are respectively the mean velocity and depth of the supercritical stream before the jump. Hence, it is not possible to compare this curve with Eq. 3-01, which is also shown plotted in Fig. 3-3.

The results for the length scale are shown plotted in Fig. 3-4 with $\delta_1 - \delta/y_1$ versus x_2/y_1. There is considerable scatter and the mean line drawn in Fig. 3-4 should be treated only as an approximation. Again, because of the considerations cited in the previous paragraph, the above results could not easily be compared with Eq. 3-03, which is also shown plotted in Fig. 3-4.

Boundary Layer Portion

The velocity distribution in the boundary layer portion is shown plotted in Fig. 3-5 on a double-log sheet. It was found that it is described by the power law type of equation written as

$$\frac{u}{u_m} = \left(\frac{y}{\delta}\right)^{1/n} \qquad (3\text{-}04)$$

with n = 8.5. The variation of δ/y_1 with x_2/y_1 is shown in Fig. 3-6. Their is considerable deviation from the mean curve drawn and this curve is considerably higher than the corresponding curve for the classical

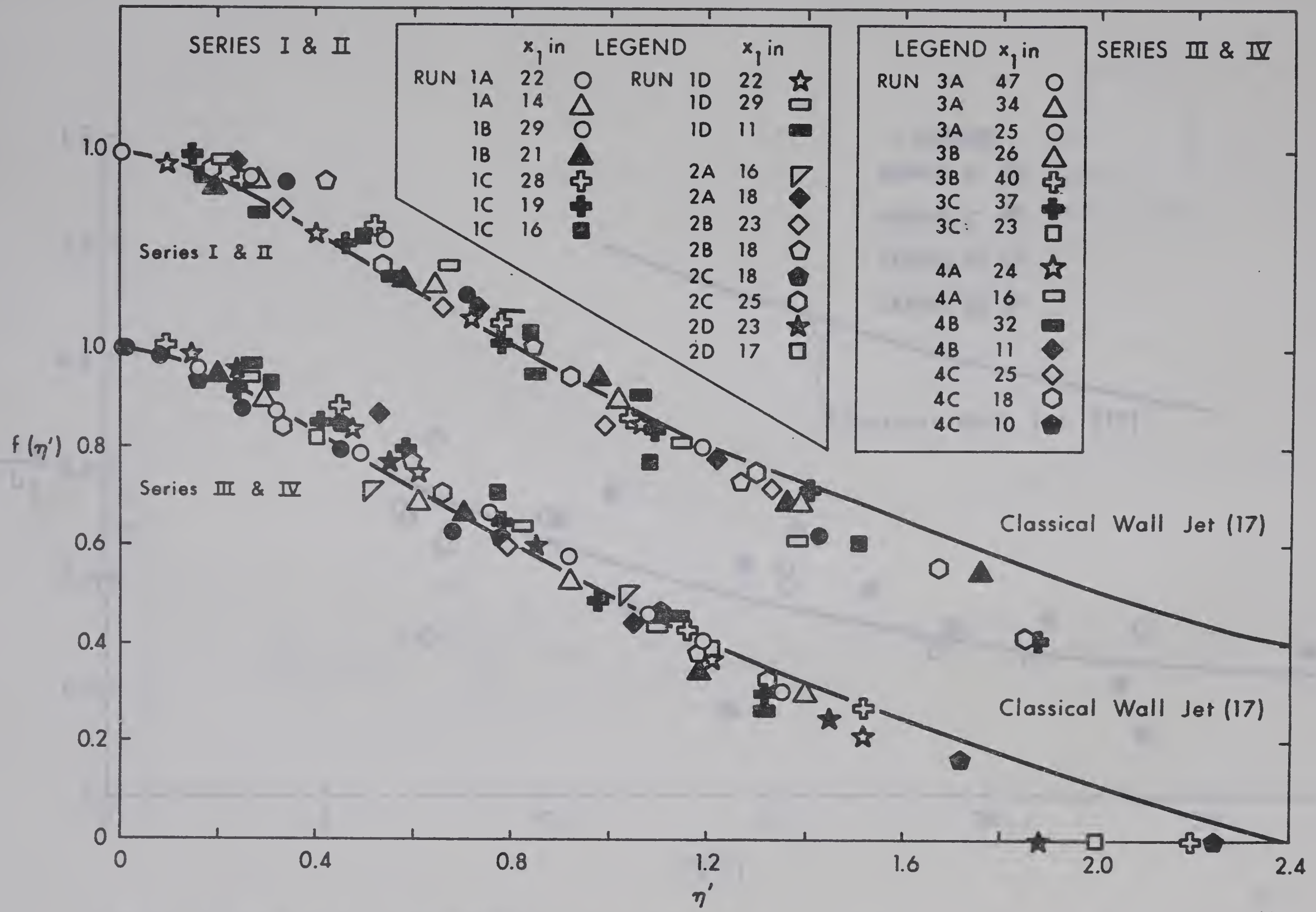

FIG. 3-2 Velocity Distribution — Free Mixing Region

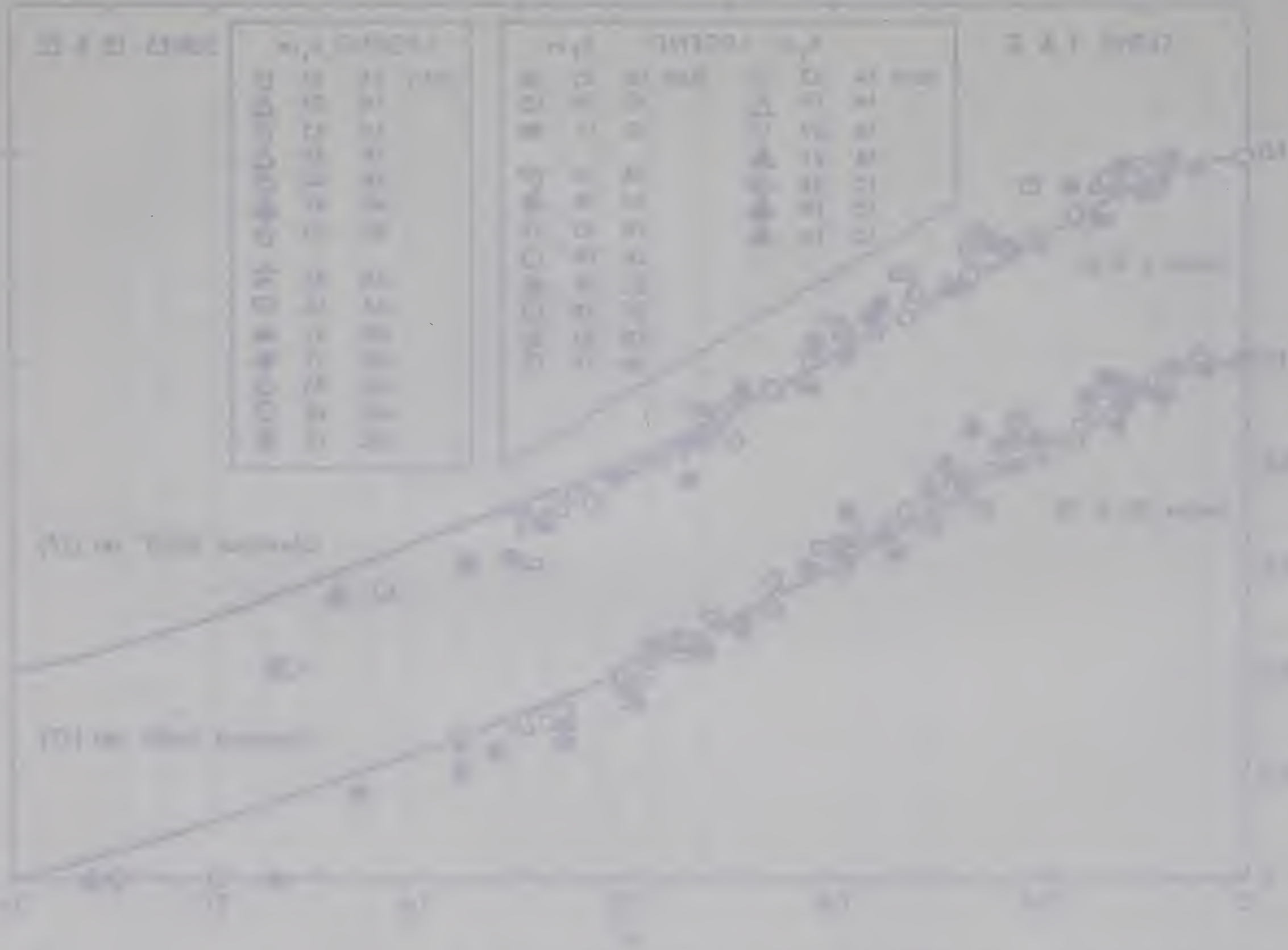

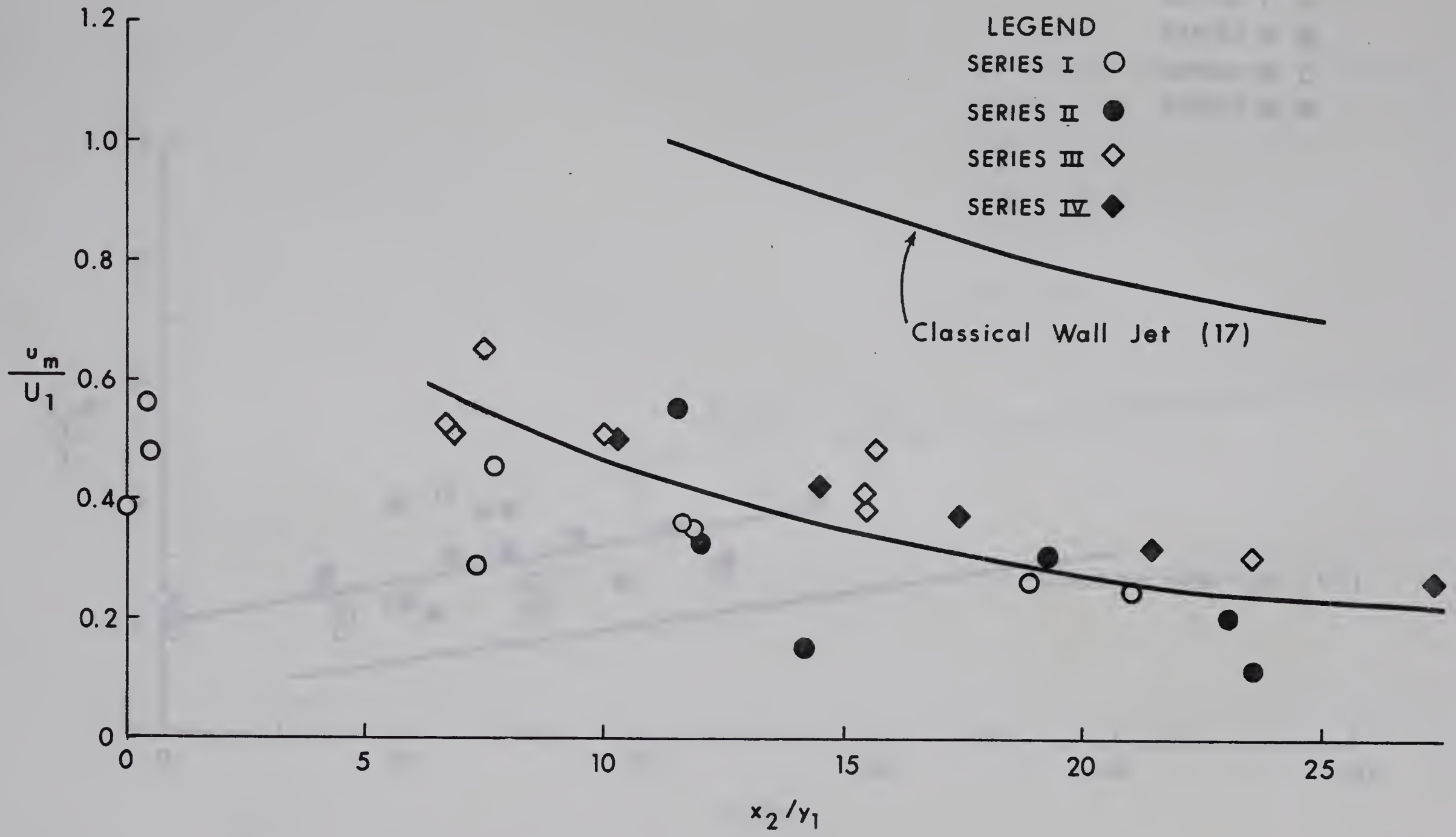

FIG. 3-3 Study of the Velocity Scale.

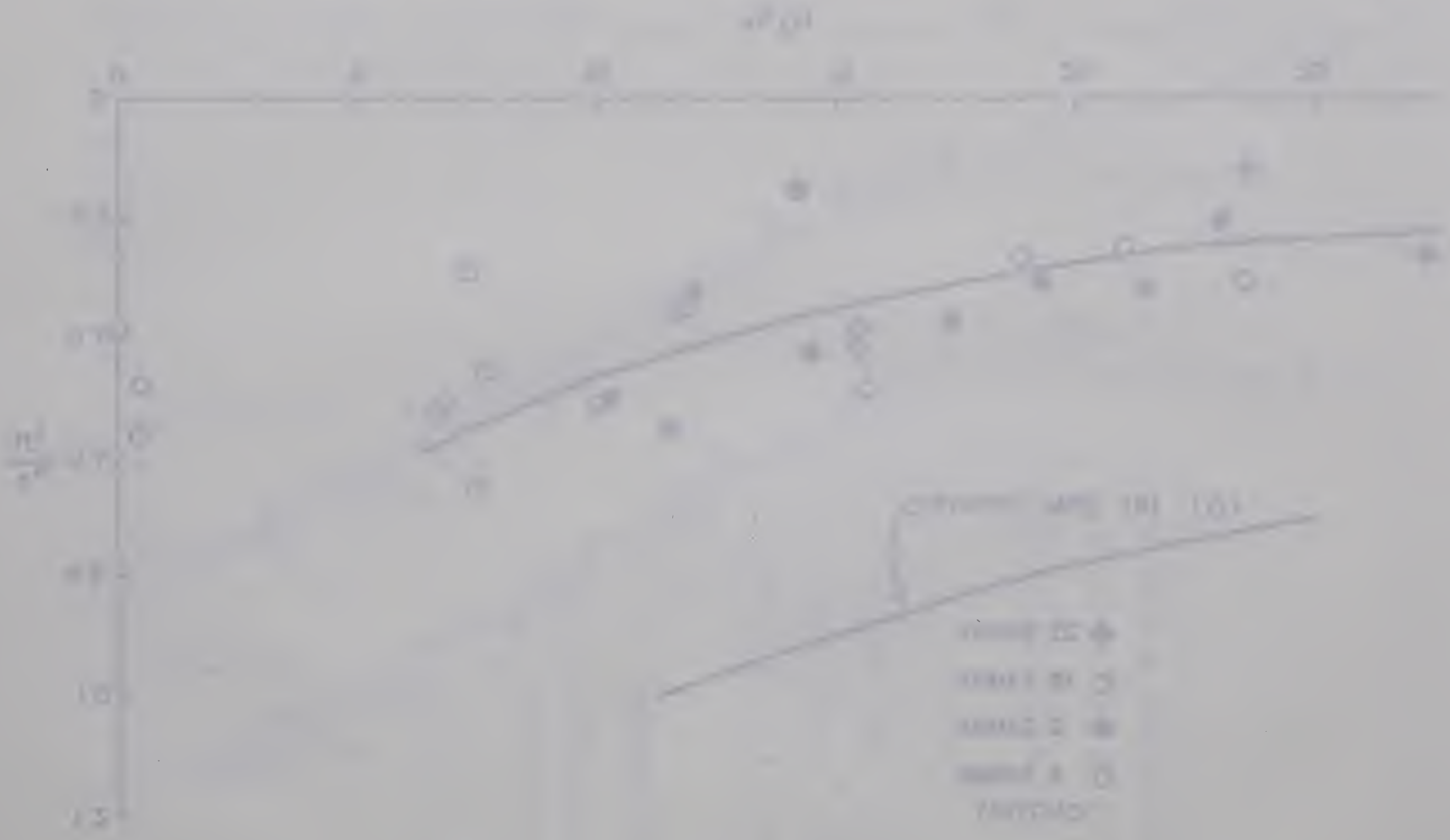

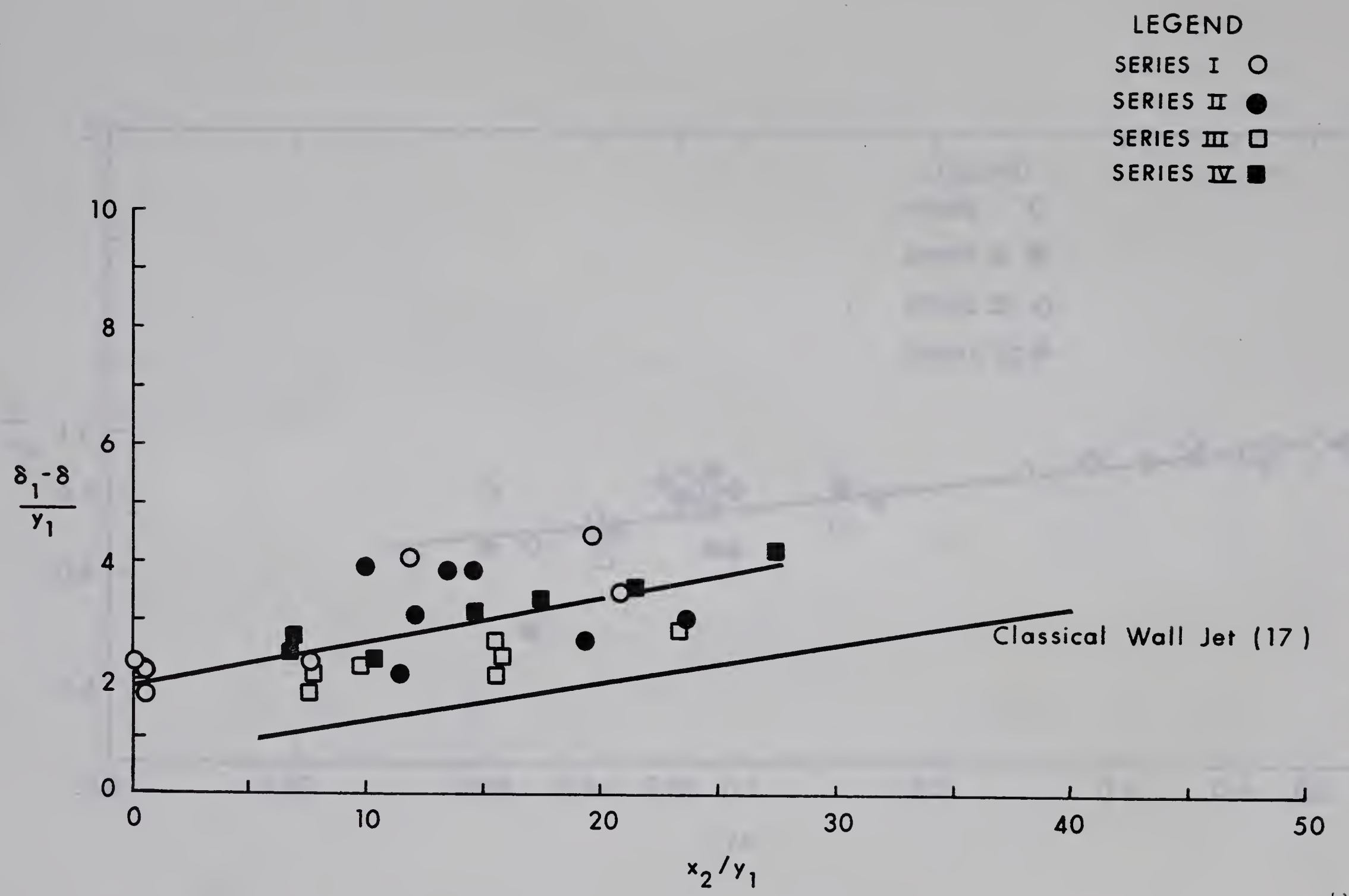

FIG. 3-4 Study of the Length Scale.

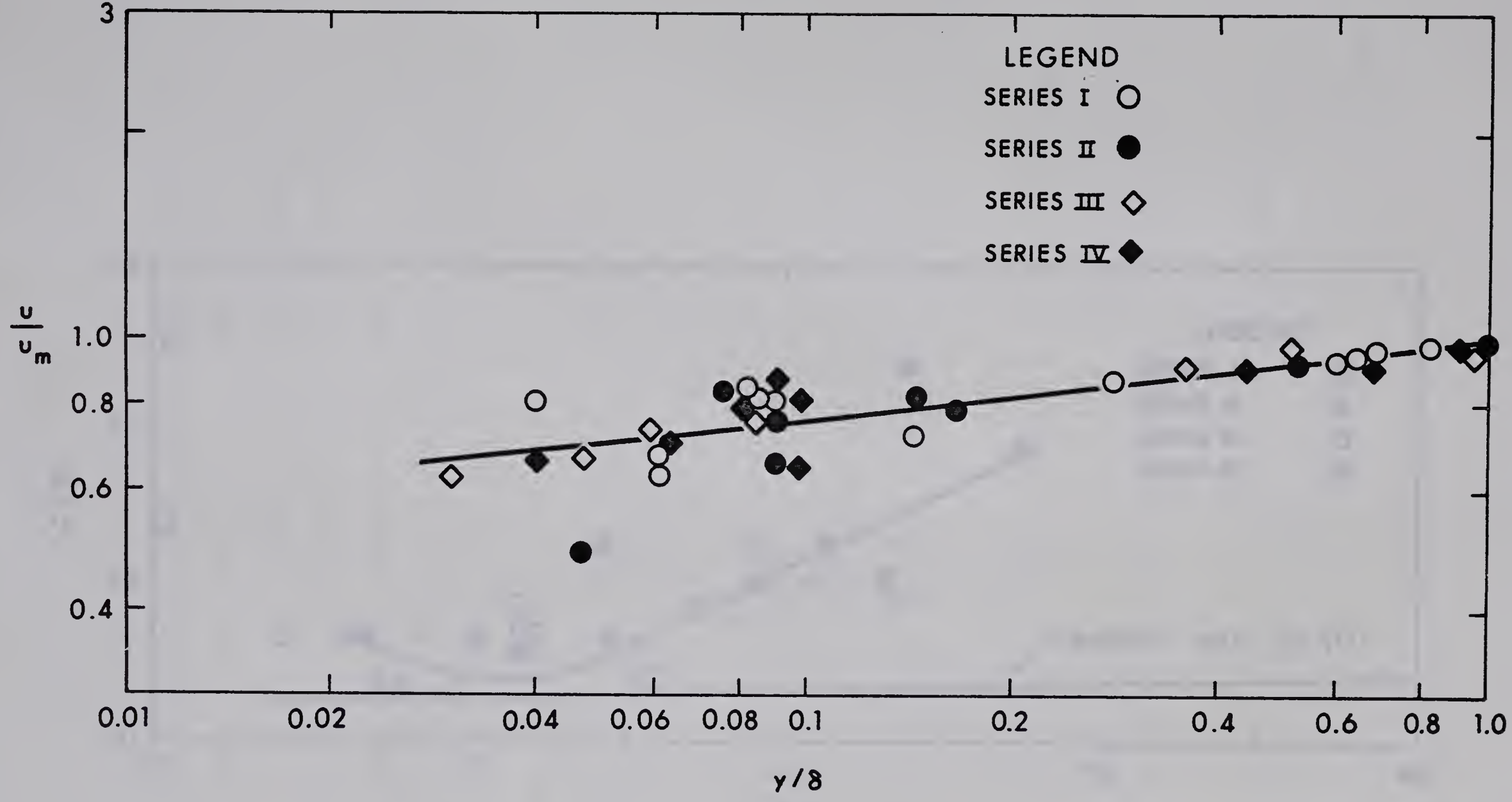

FIG. 3-5 Velocity Distribution – Boundary Layer Portion

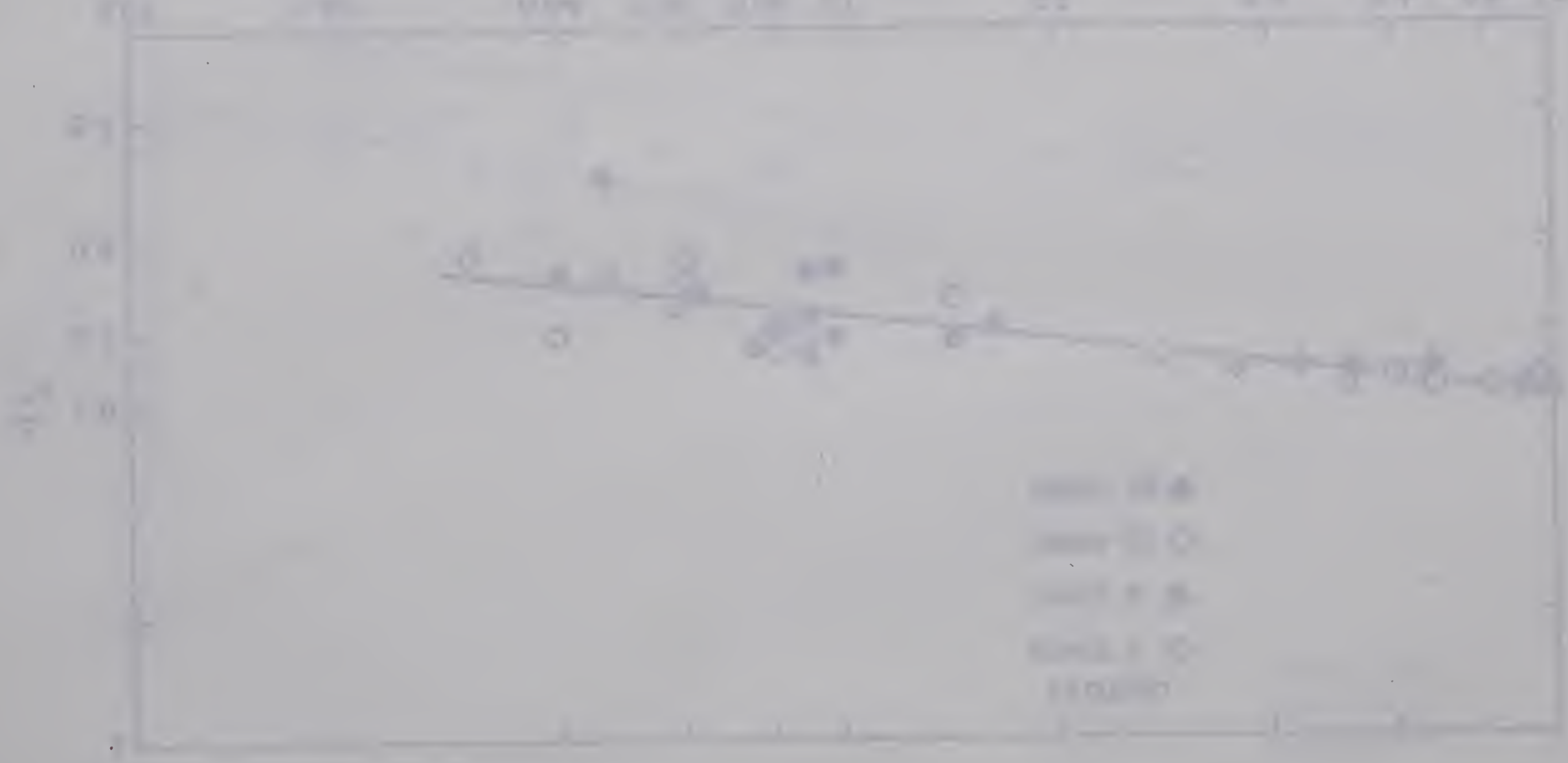

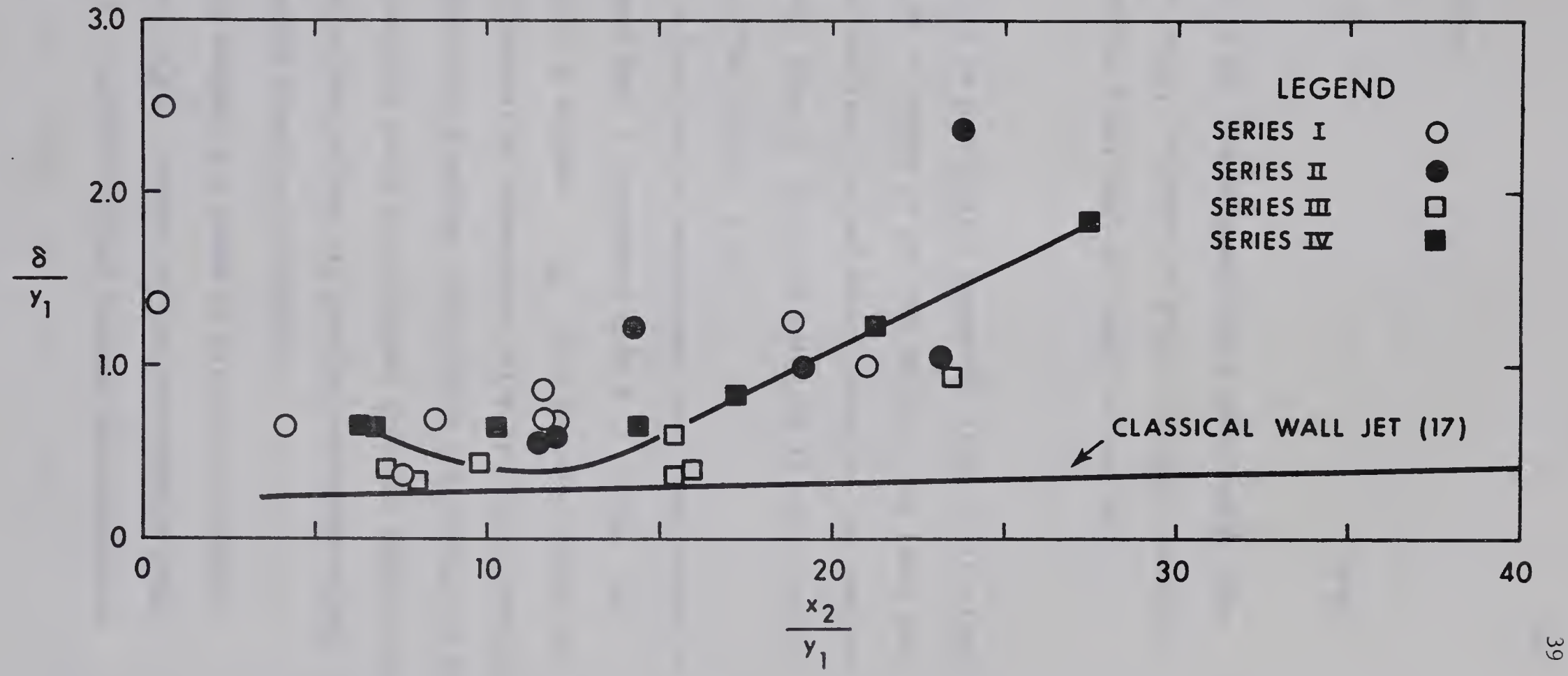

FIG. 3-6 Growth of the Boundary Layer

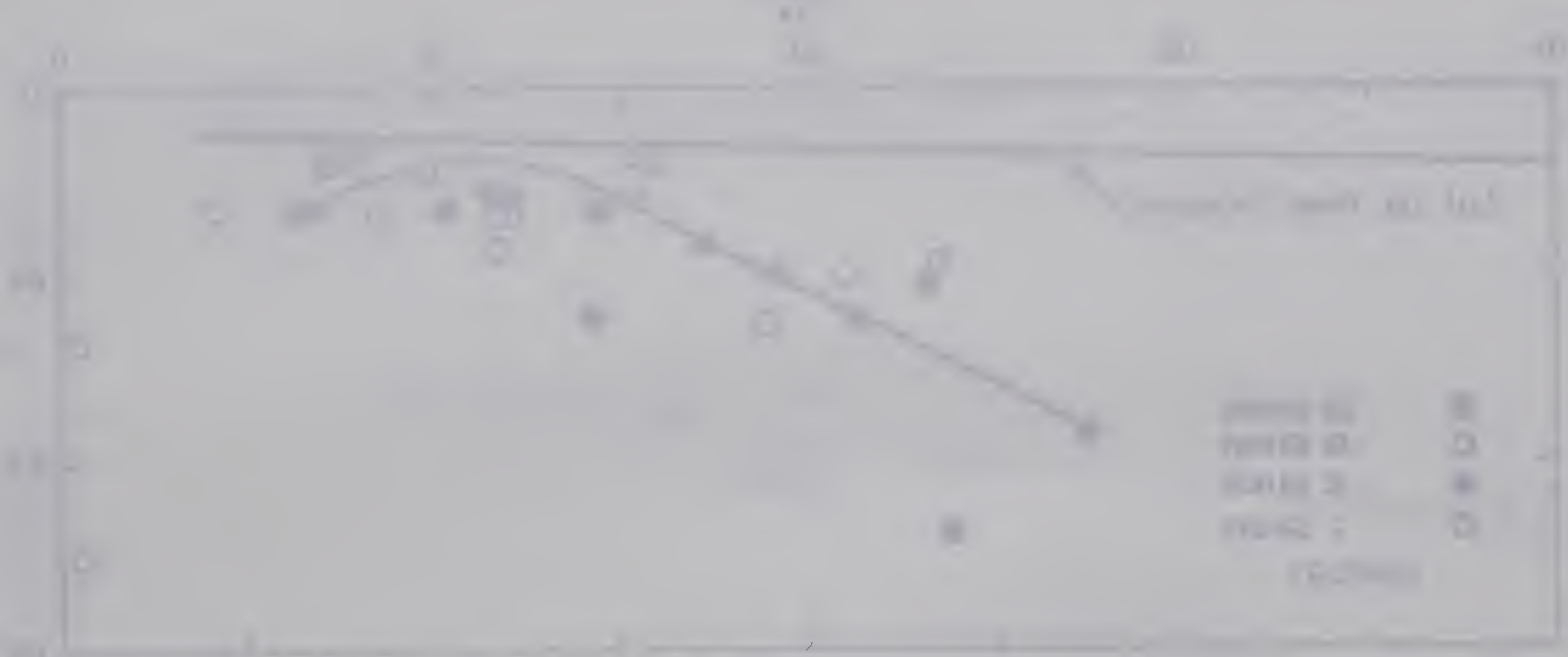

wall jet given by the equation

$$\delta \simeq 0.16 \quad \delta_1 \tag{3-05}$$

where δ_1 is given by Eq. 3-02. To be practically more useful, the variation of δ/y_1 with x_1/y_1 is shown in Fig. 3-7, which could be used, even without any knowledge regarding the length of the eddy.

Bed Shear Stress

The bed shear stress is practically important since it is closely connected with the initiation of motion of the bed material and hence with bed scour. As was mentioned earlier, the bed shear stress in the jump was measured by means of a Preston tube in 13 of the total of 14 runs, and the results are shown plotted in Fig. 3-8(a) to (d).

It is known that at the line of reattachment the shear stress is zero. In Fig. 3-8, it is seen that τ_o increases from a value of zero at the end of the eddy to a maximum τ_{om} at a certain section and then falls off, to eventually attain an asymptotic value at large distances.

An attempt was made to find whether the falling off portion of the shear stress curve for all the runs could be collapsed into one single curve. That is, is it possible that in the falling off portion, the shear stress distribution in the longitudinal direction is similar?

The results of this attempt are shown in Fig. 3-9, in which τ_o / τ_{om} is plotted against x_3 / λ where x_3 is the distance from the section of τ_{om} and λ is the distance between the sections at

which τ_o is respectively equal to τ_{om} and $\tau_{om}/2$. It is seen that the shear stress distribution is indeed described very well by one single curve at least for values of τ_o/τ_{om} from 1.0 to 0.3, below which there is considerable scatter.

For the shear stress distribution discussed above, the non-dimensionalising stress is τ_{om} and the length scale is λ. After a number of unsuccessful plots, it was found that $C'_{fm} = \tau_{om}/\rho U_1^2/2$ varies mainly with F_1 as shown in Fig. 3-10 and appears to be independent of h/y_1 at least in the range studied. As shown in Fig. 3-11, the dimensionless length scale λ/y_1 was found to vary mainly with F_1. If x_o is the distance to the section of maximum shear stress from the face of the drop, x_o/h was found to decrease linearly with F_1 as shown in Fig. 3-12. Now using the results presented in this section, the bed shear stress distribution in the major portion of the reattached wall jet could be predicted and this prediction is believed to be satisfactory for practical purposes.

Free Jet

It was mentioned earlier that the supercritical stream enters the jump as a fully grown turbulent boundary layer and in the region before it hits the downstream bed, it behaves like a free jet confined between the standing eddy on the bottom and the surface roller on the top. Only for the early portion of this region does it behave like a straight jet and in the remaining portion it becomes considerably curved. The velocity measurements made were not sufficient for analysing the diffusion of this curved jet, and the analysis is limited to only the portion of the essentially straight jet where the velocity distribution is symmetrical about

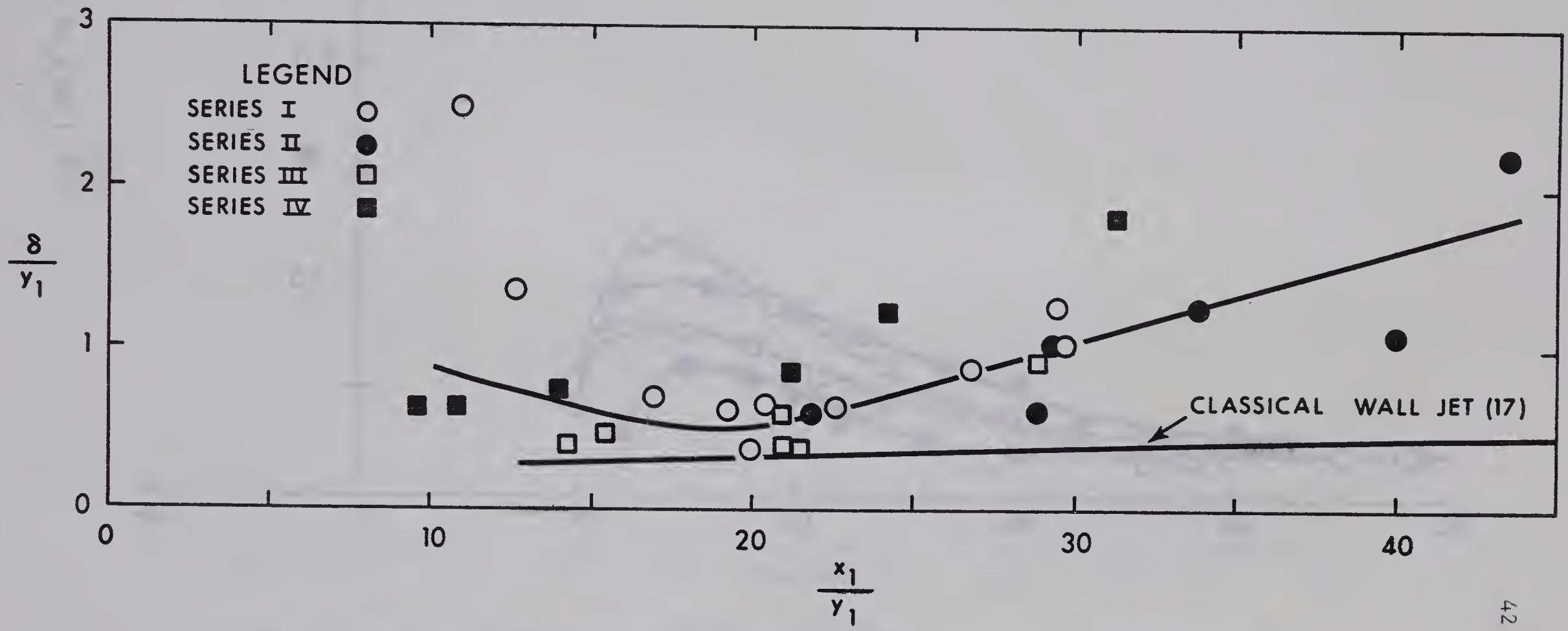

FIG. 3-7 Growth of Boundary Layer — Alternate Plot

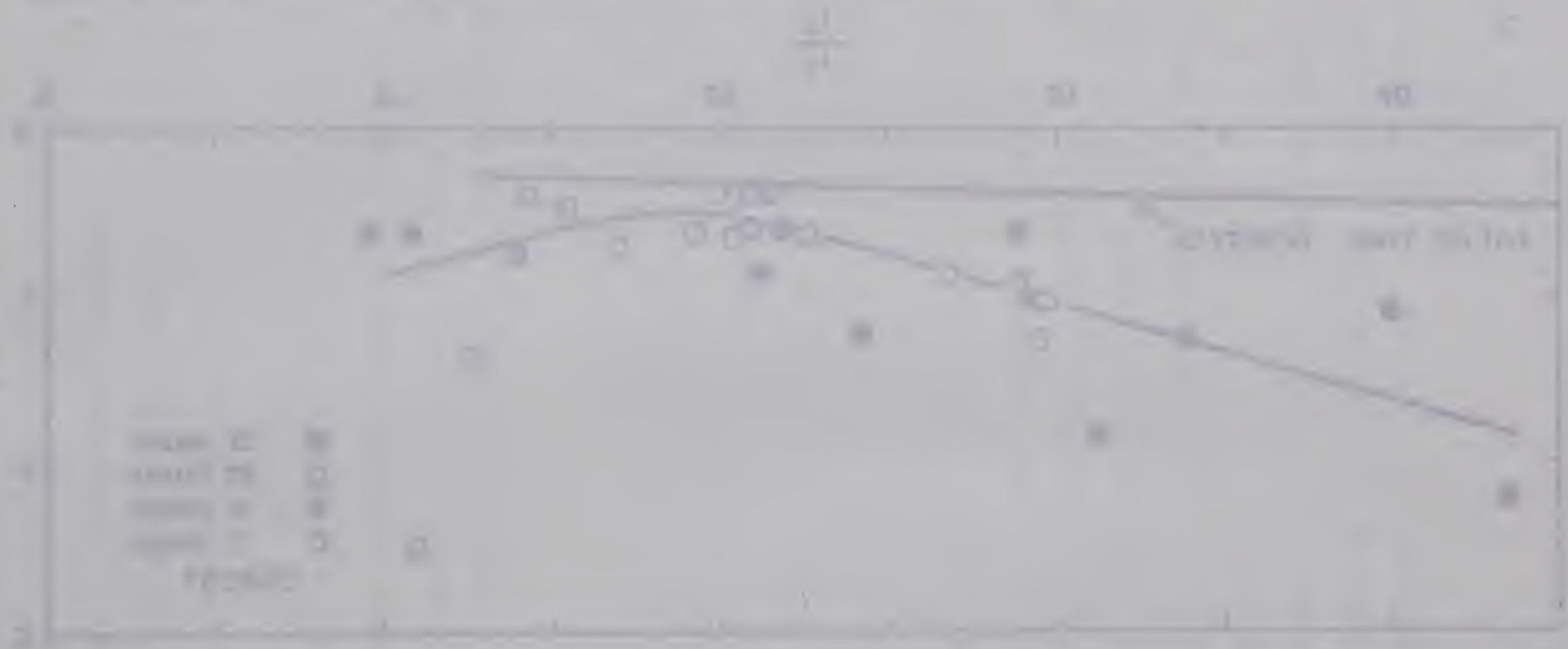

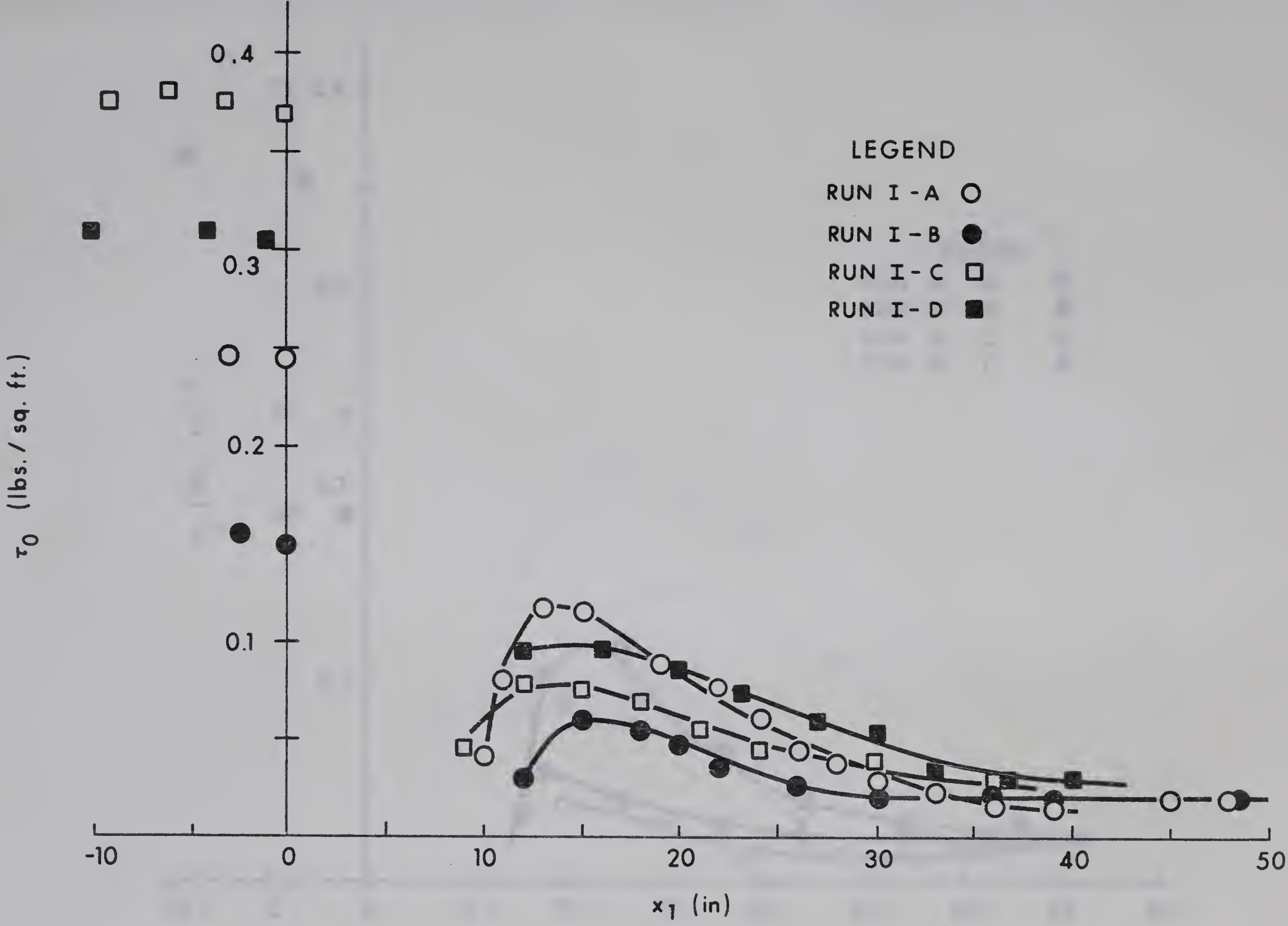

FIG. 3-8 (a) Bed Shear Stress Measurements (Series I)

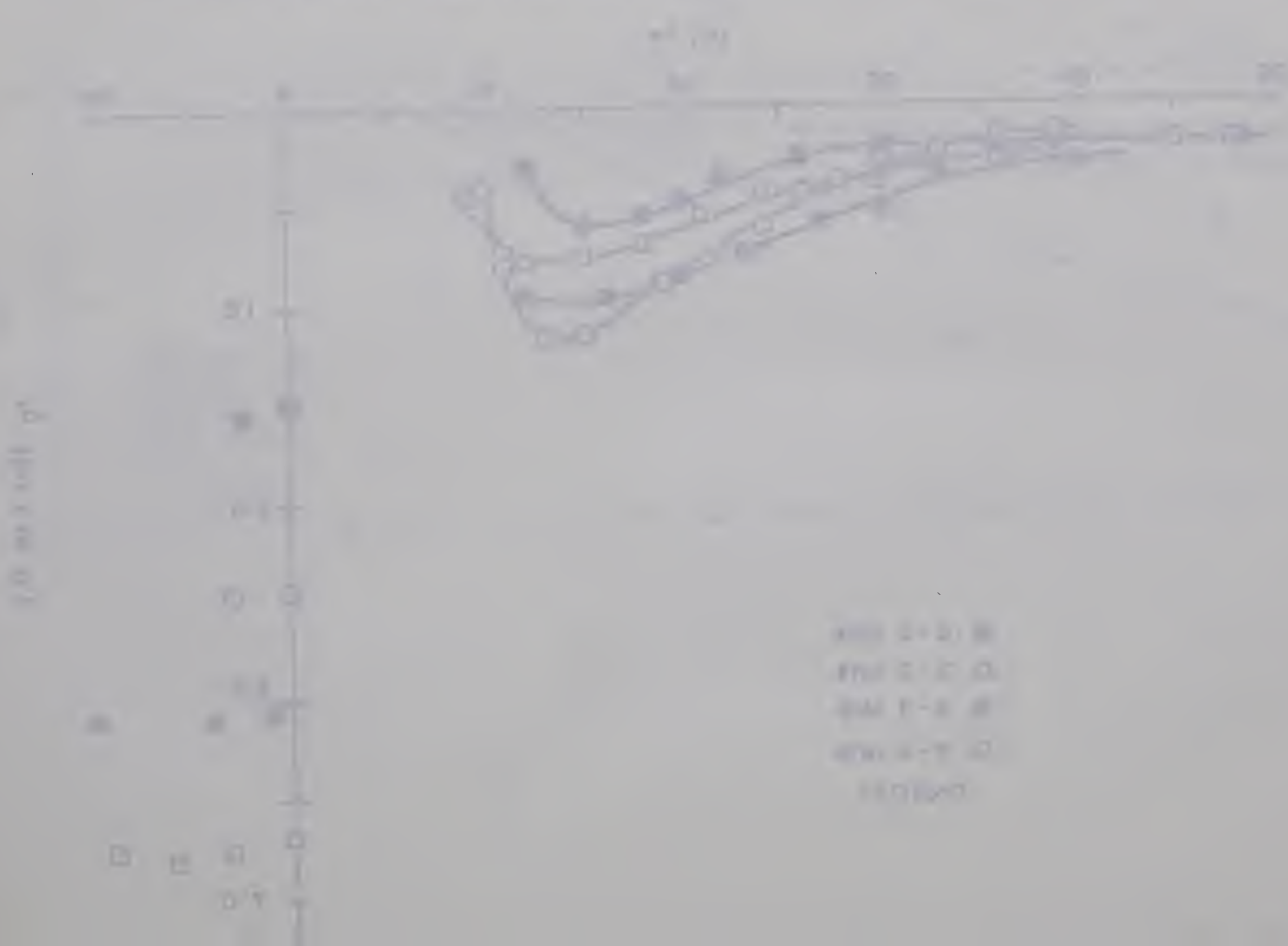

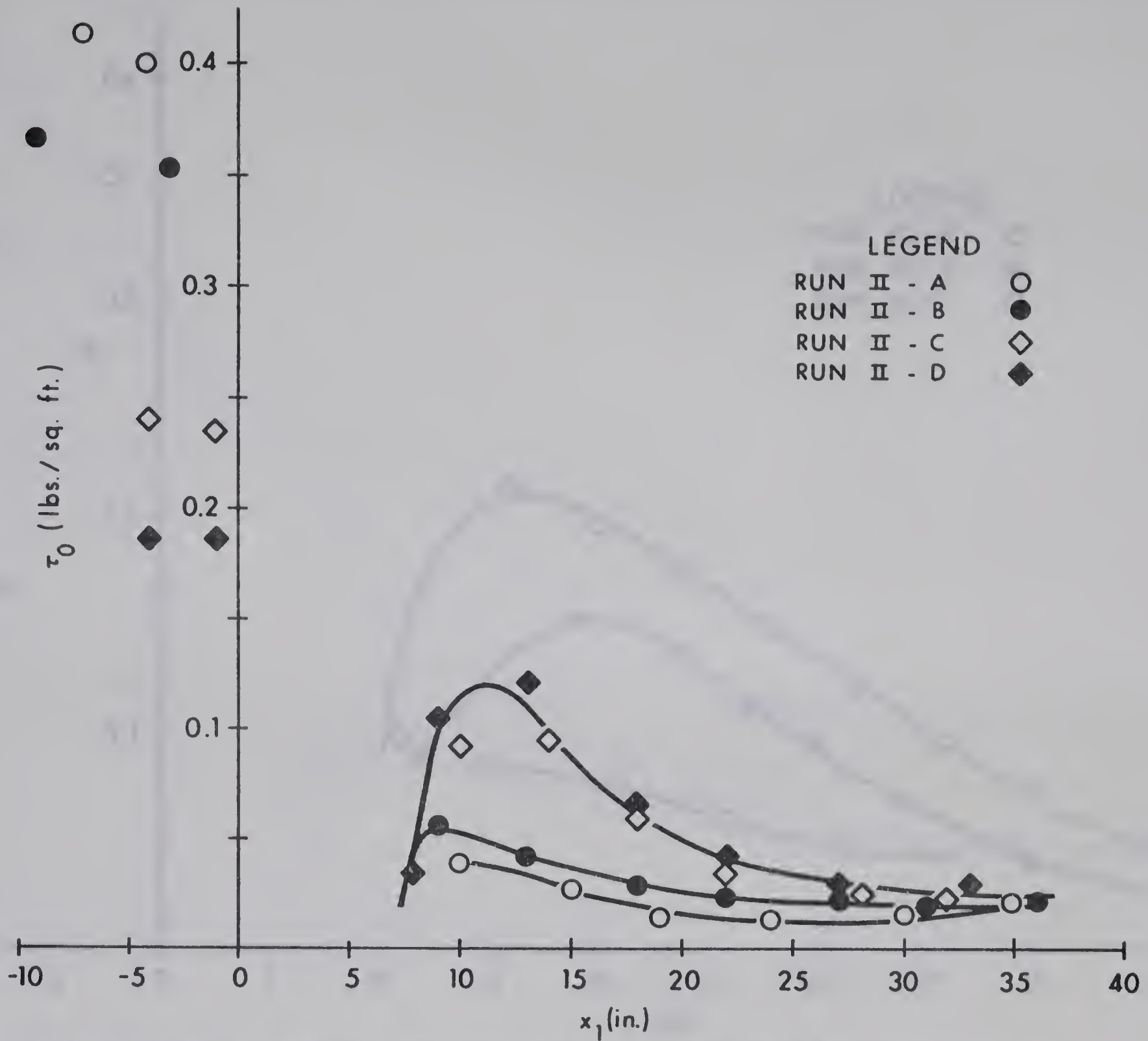

FIG. 3-8 (b) Bed Shear Stress Measurement (Series II)

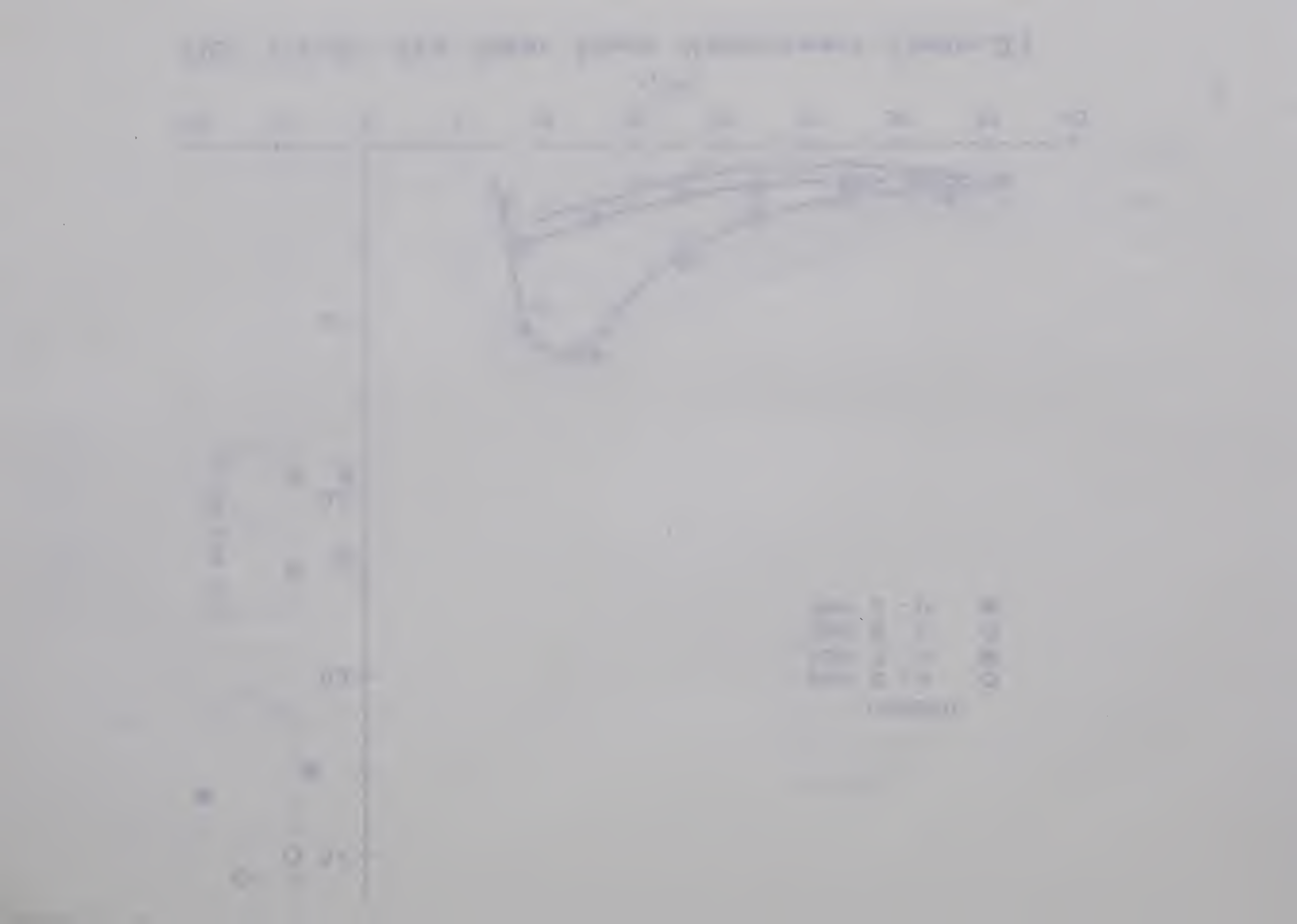

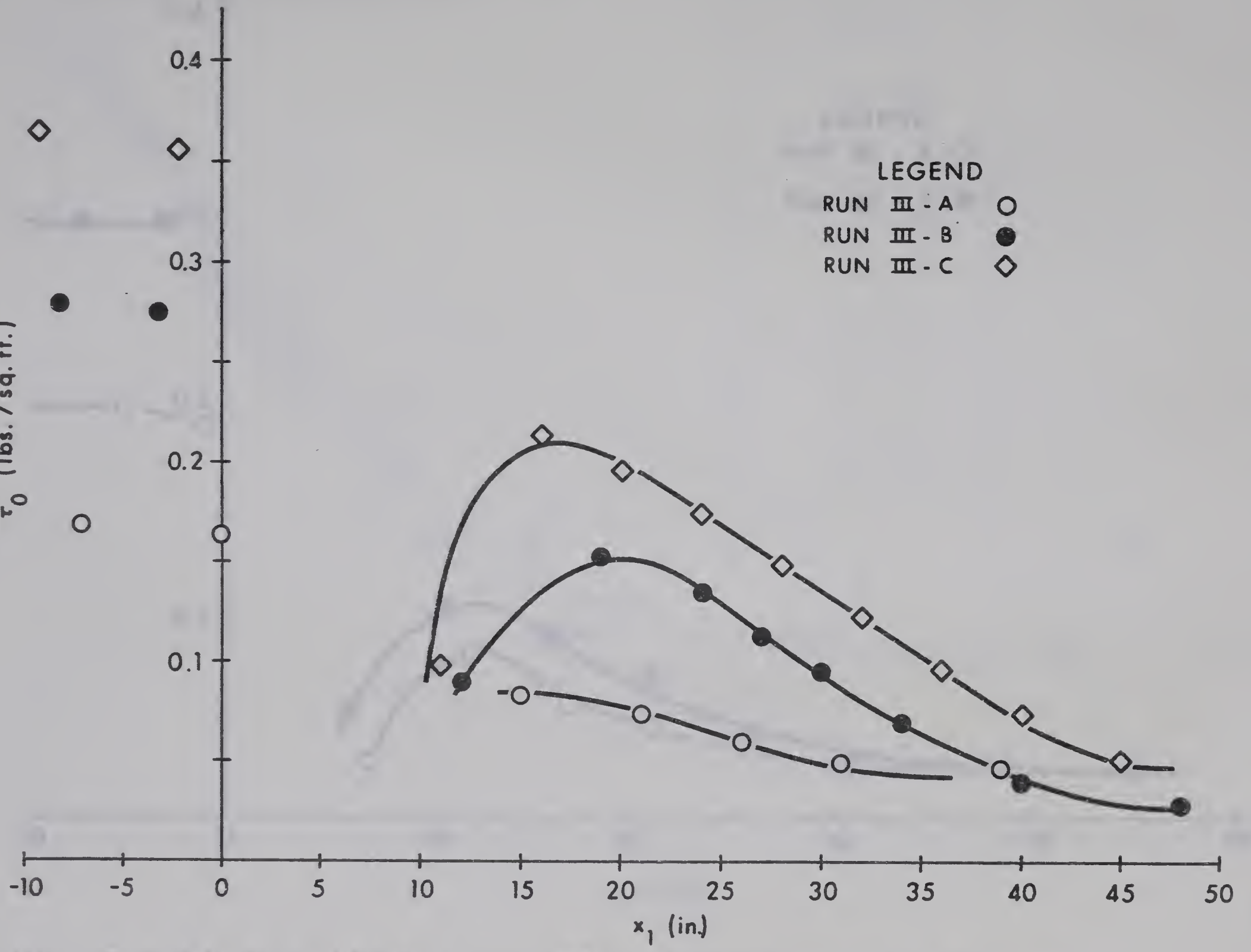

FIG. 3-8 (c) Bed Shear Stress Measurements (Series III)

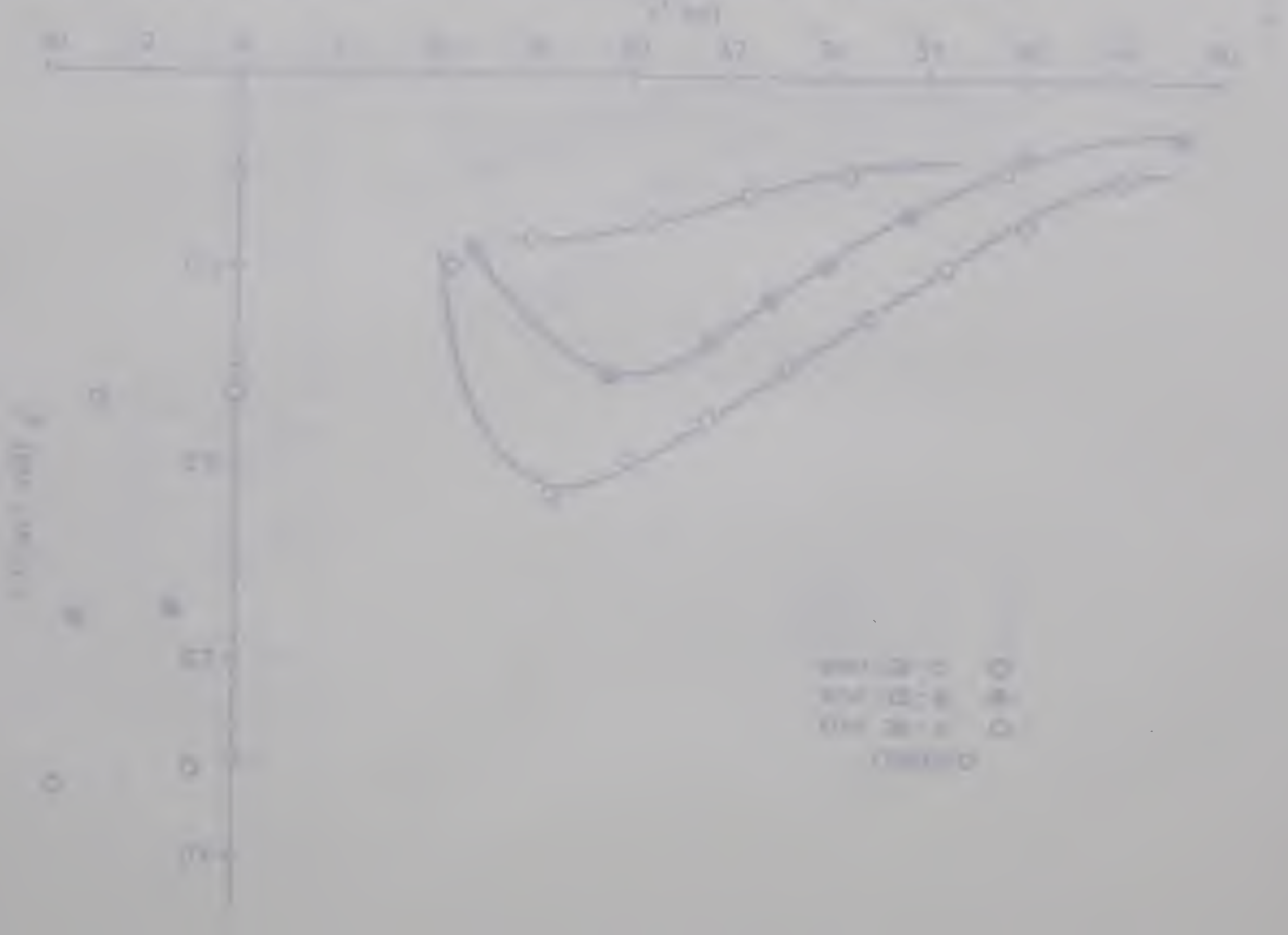

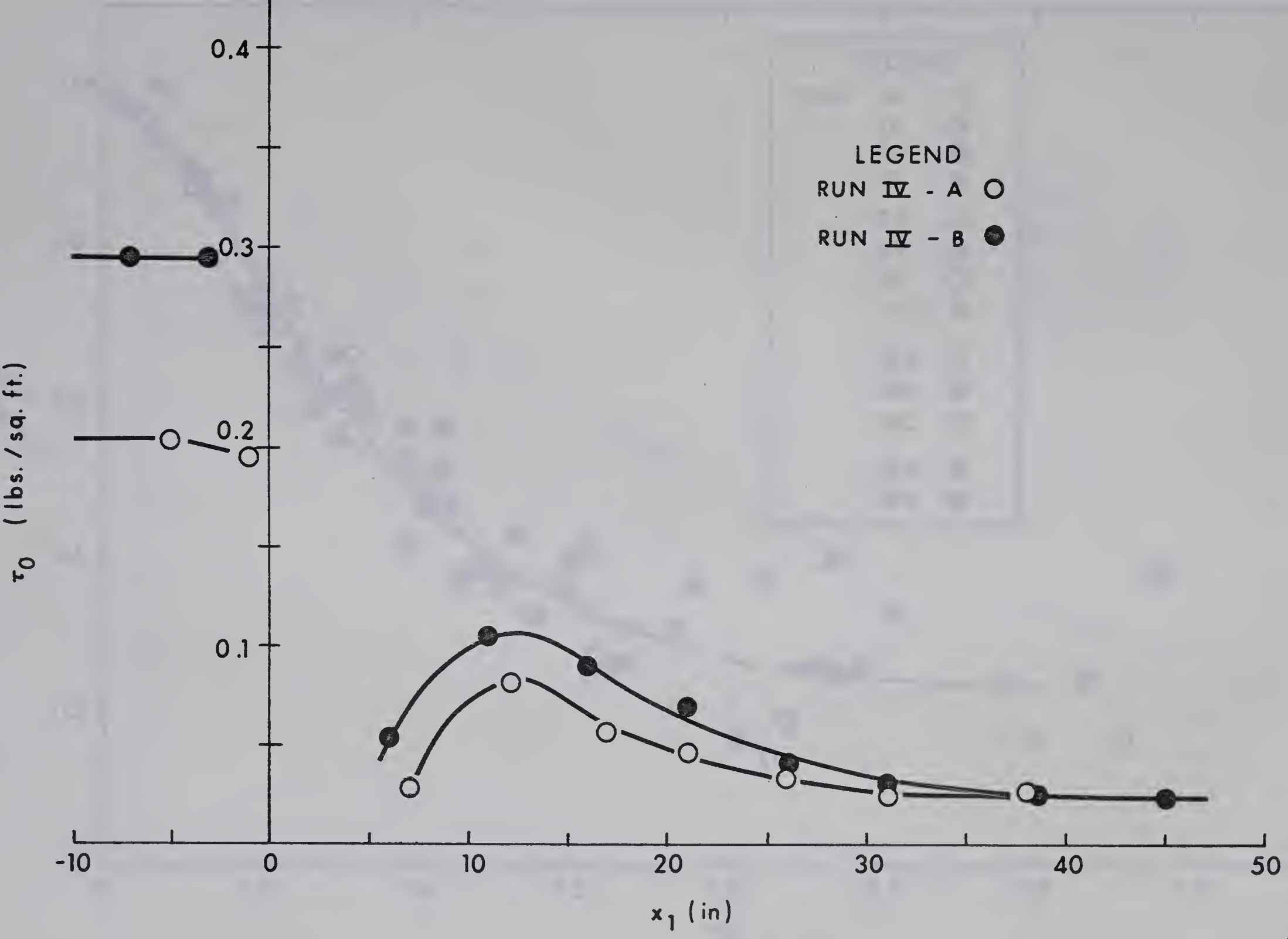

FIG. 3-8 (d) Bed Shear Stress Measurements (Series IV)

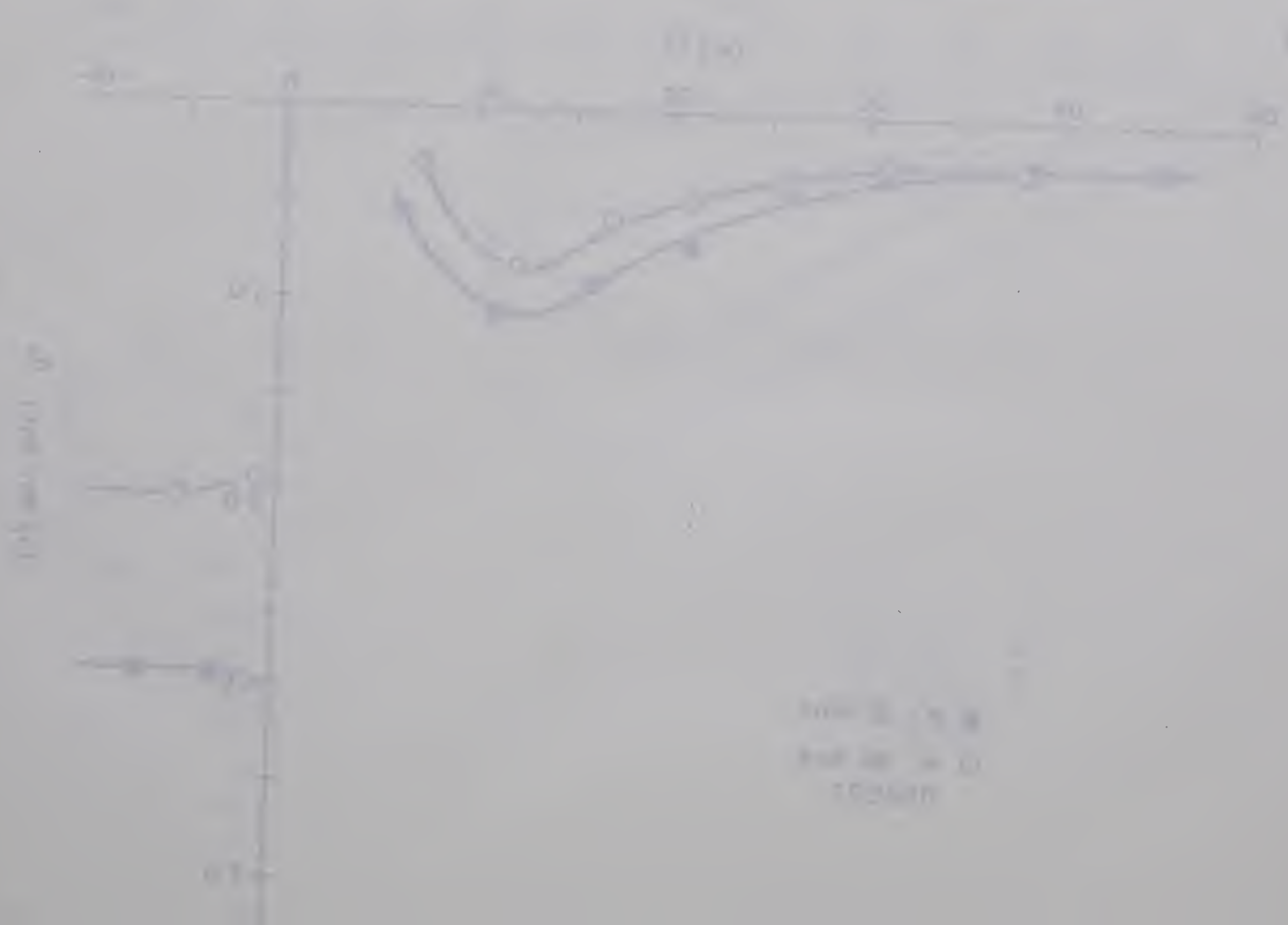

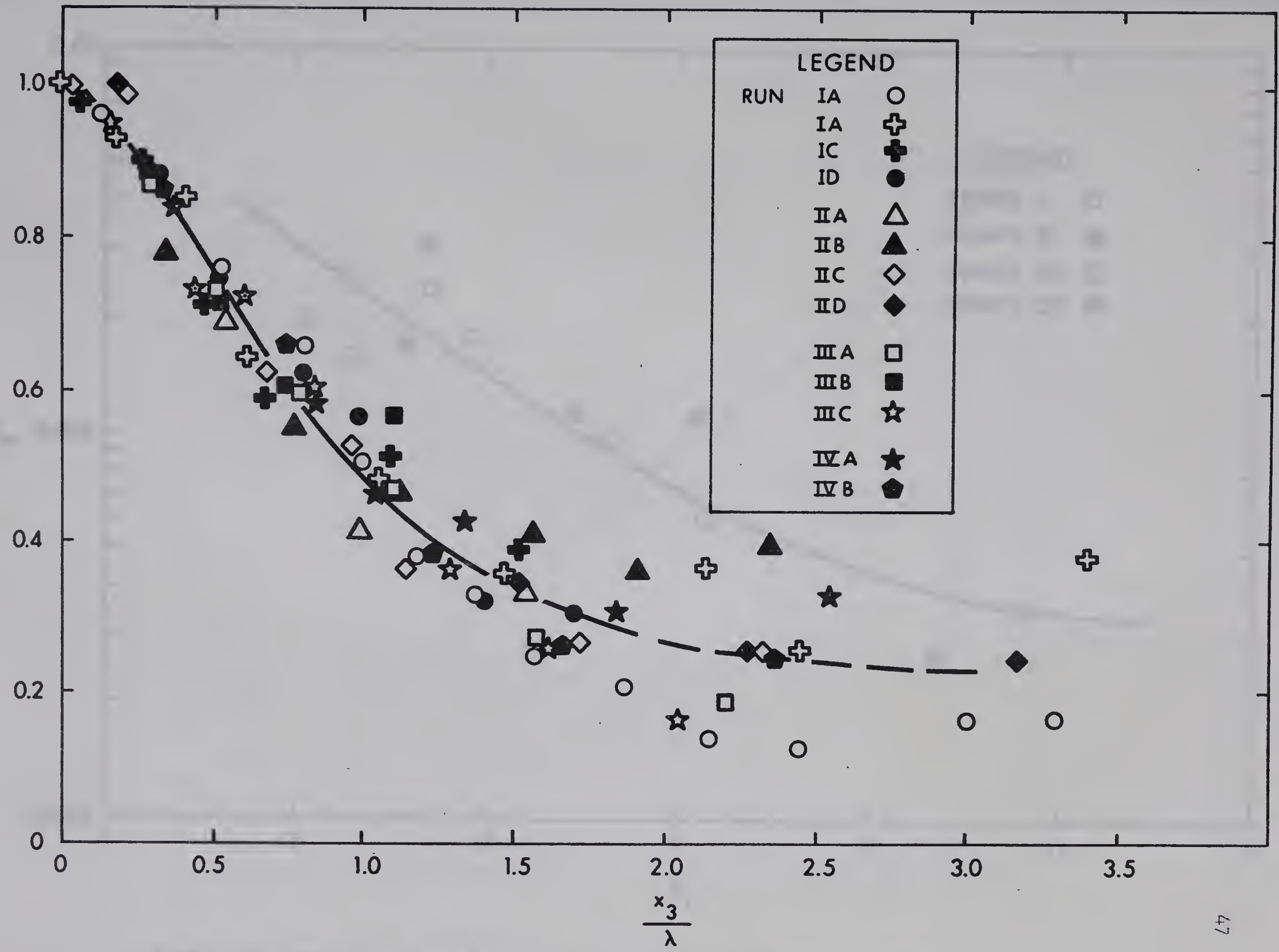

FIG. 3-9 Generalized Distribution of Bed Shear Stress

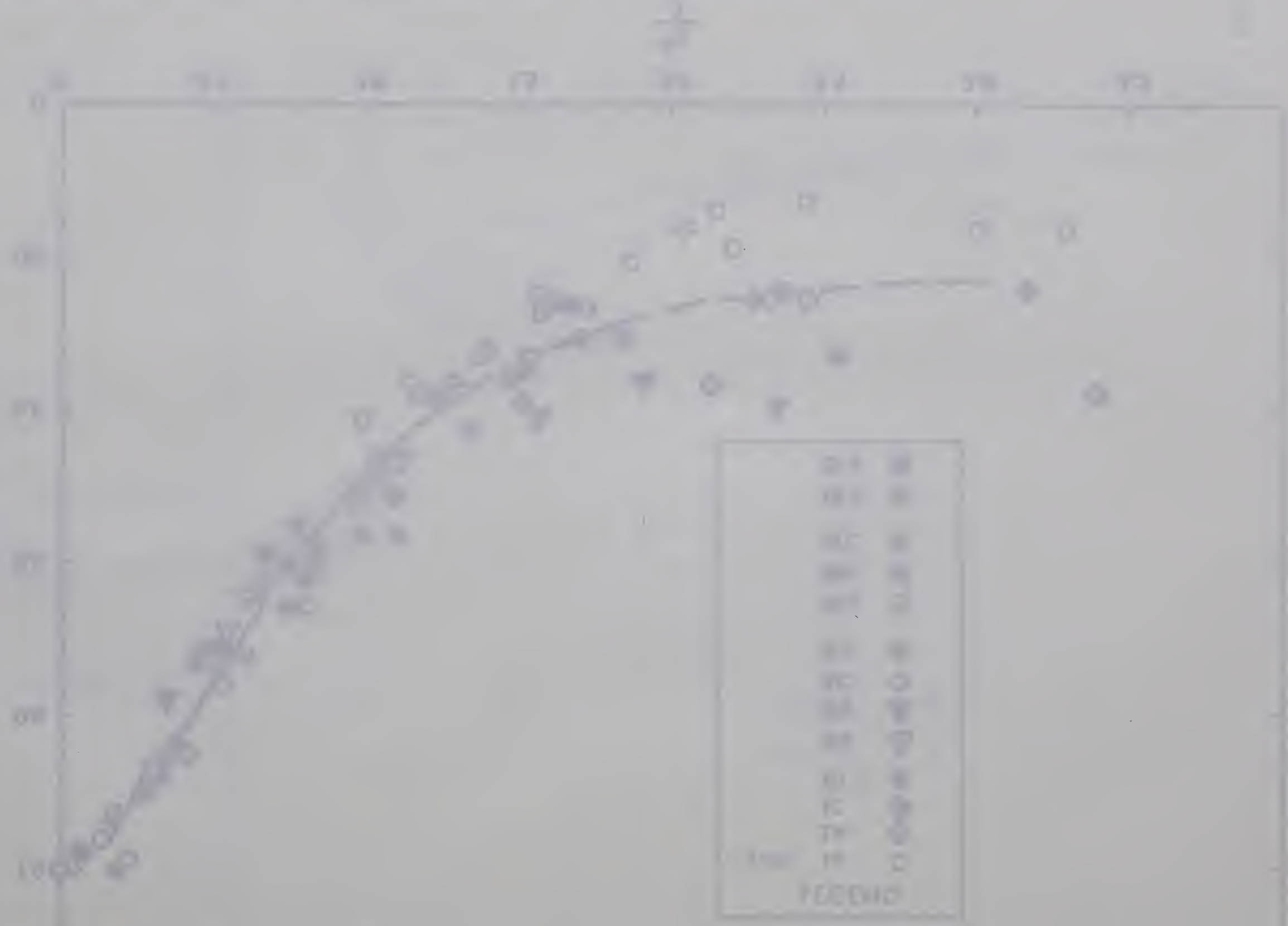

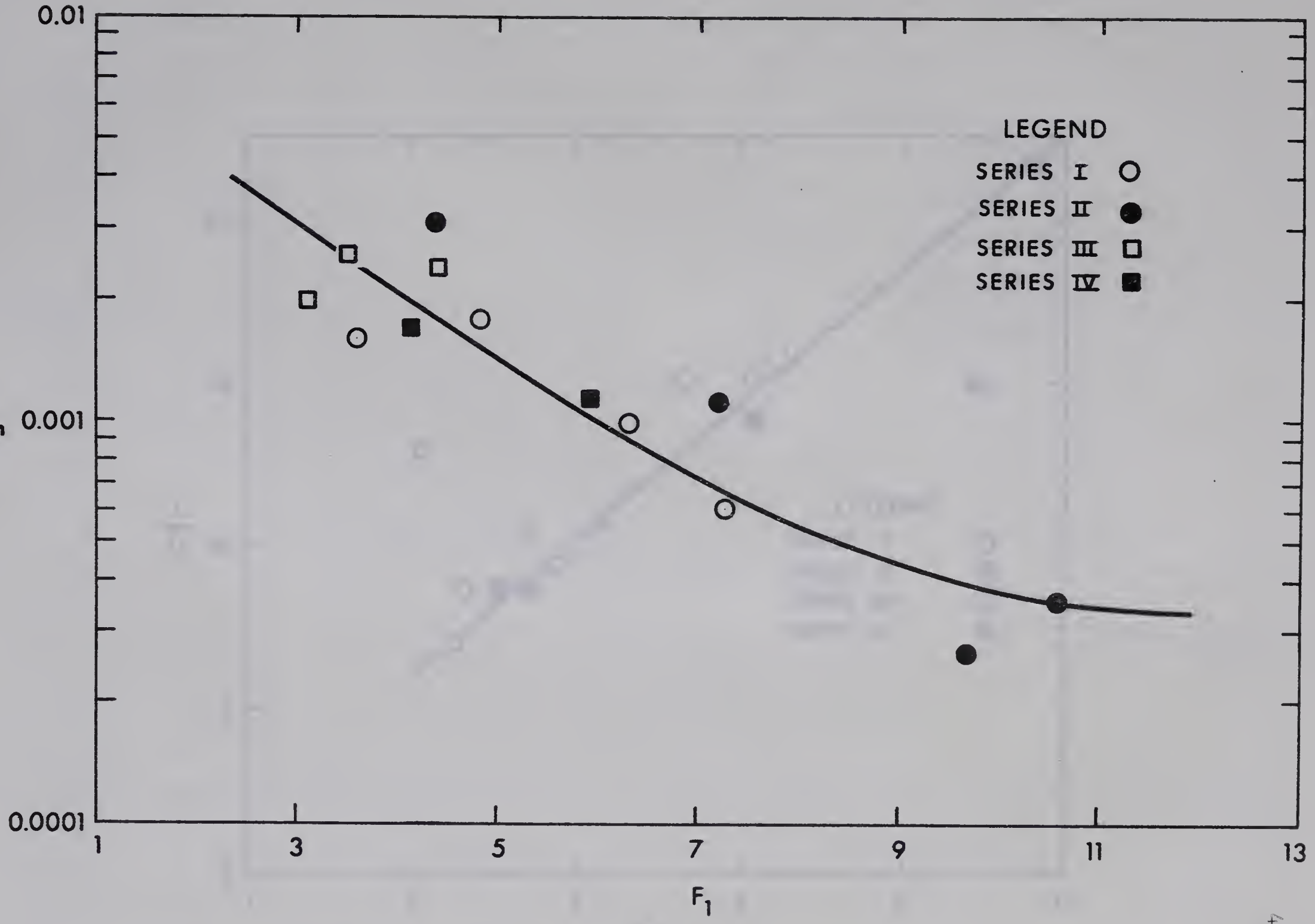

FIG. 3-10 Study of τ_{0m}

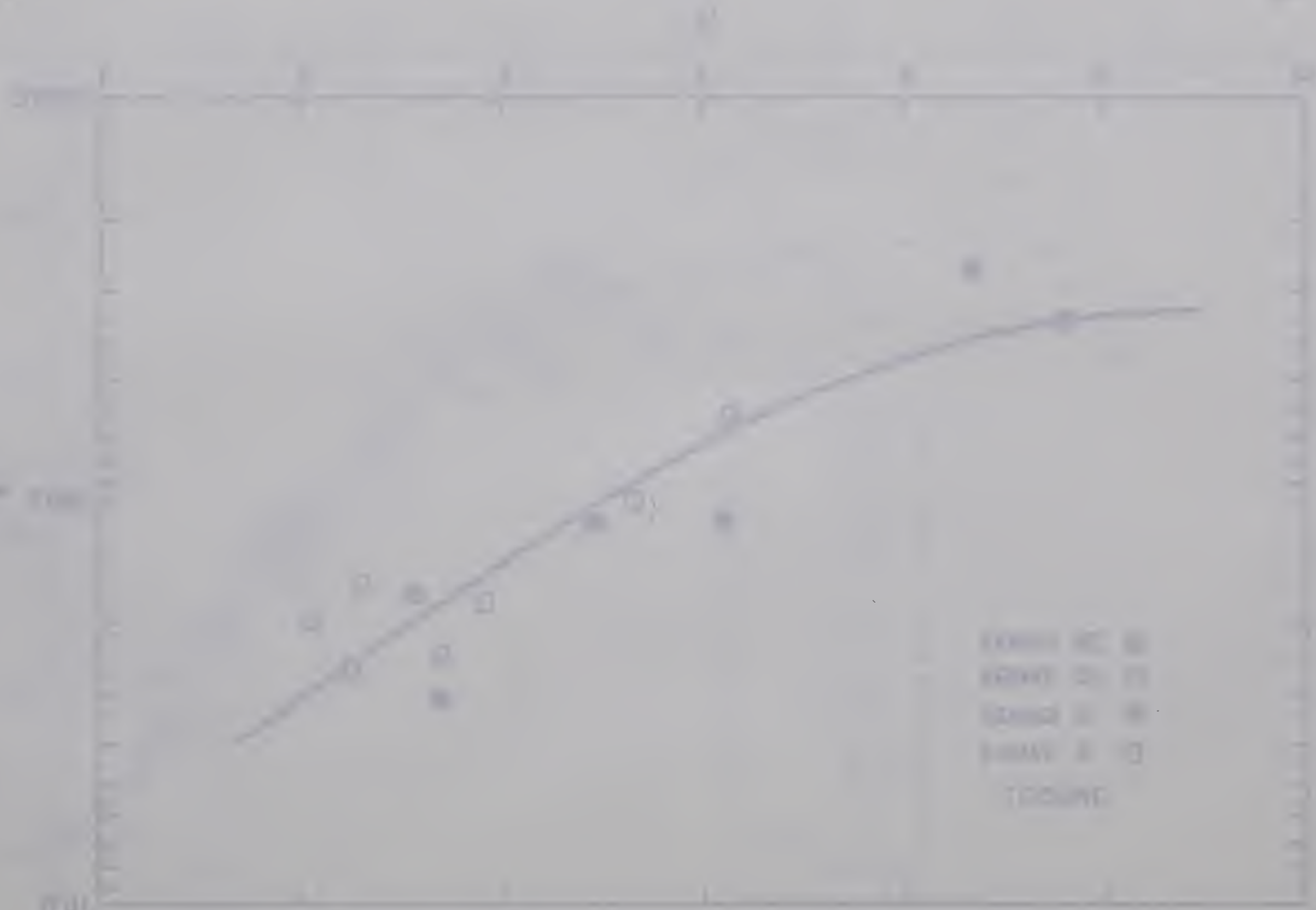

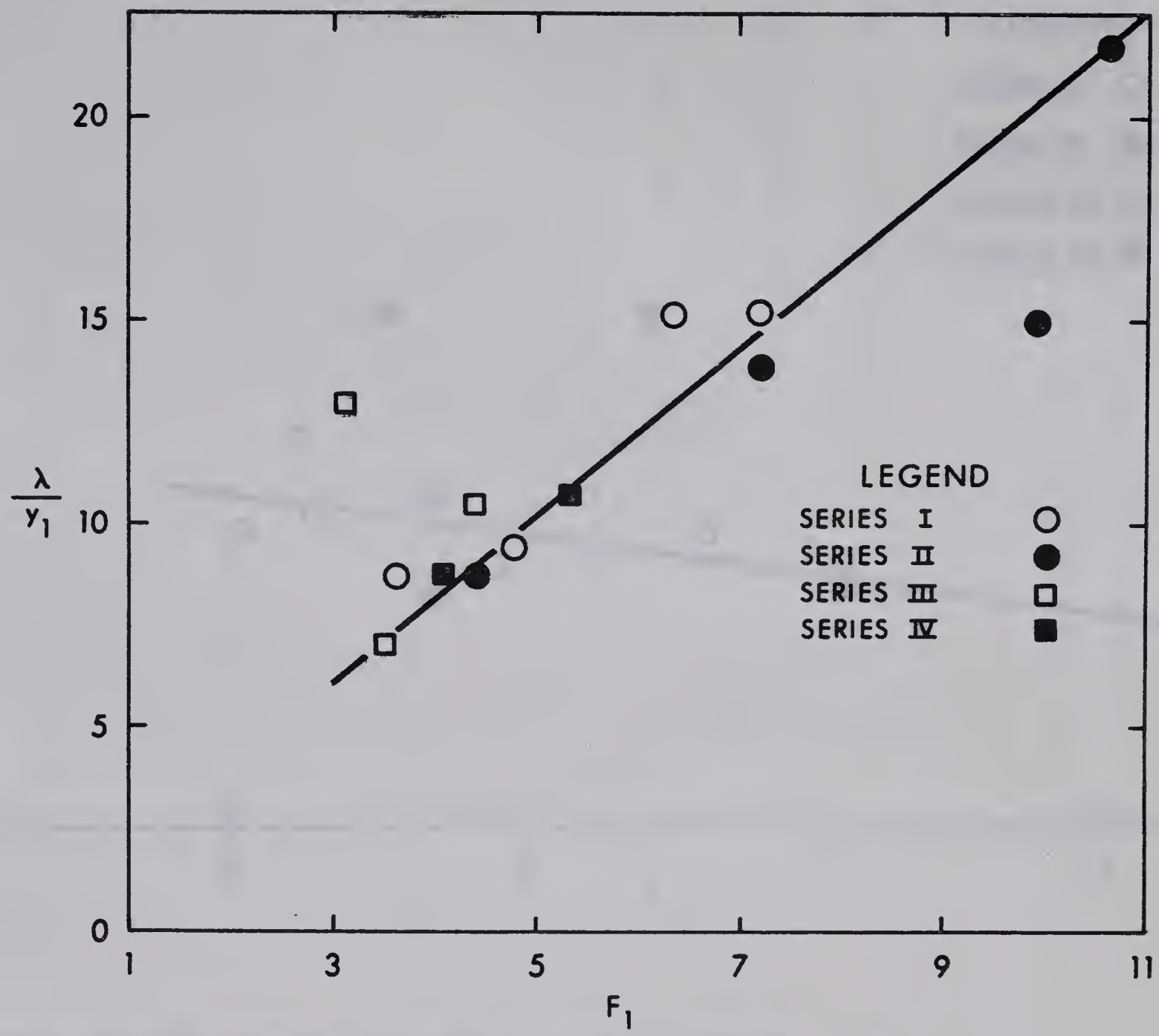

FIG. 3-11 Study of the Length Scale λ

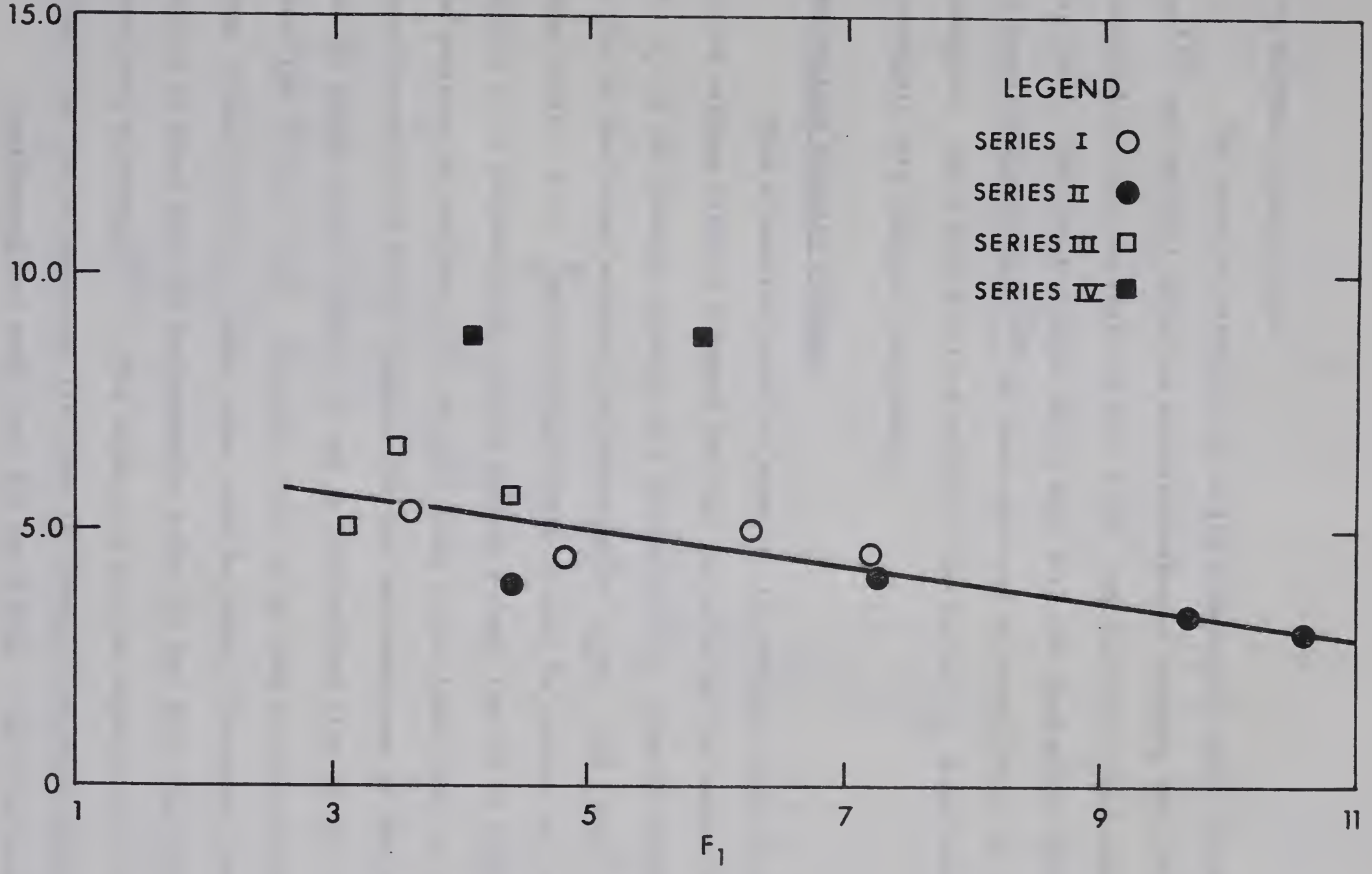

FIG. 3-12 Variation of x_0/h with F_1

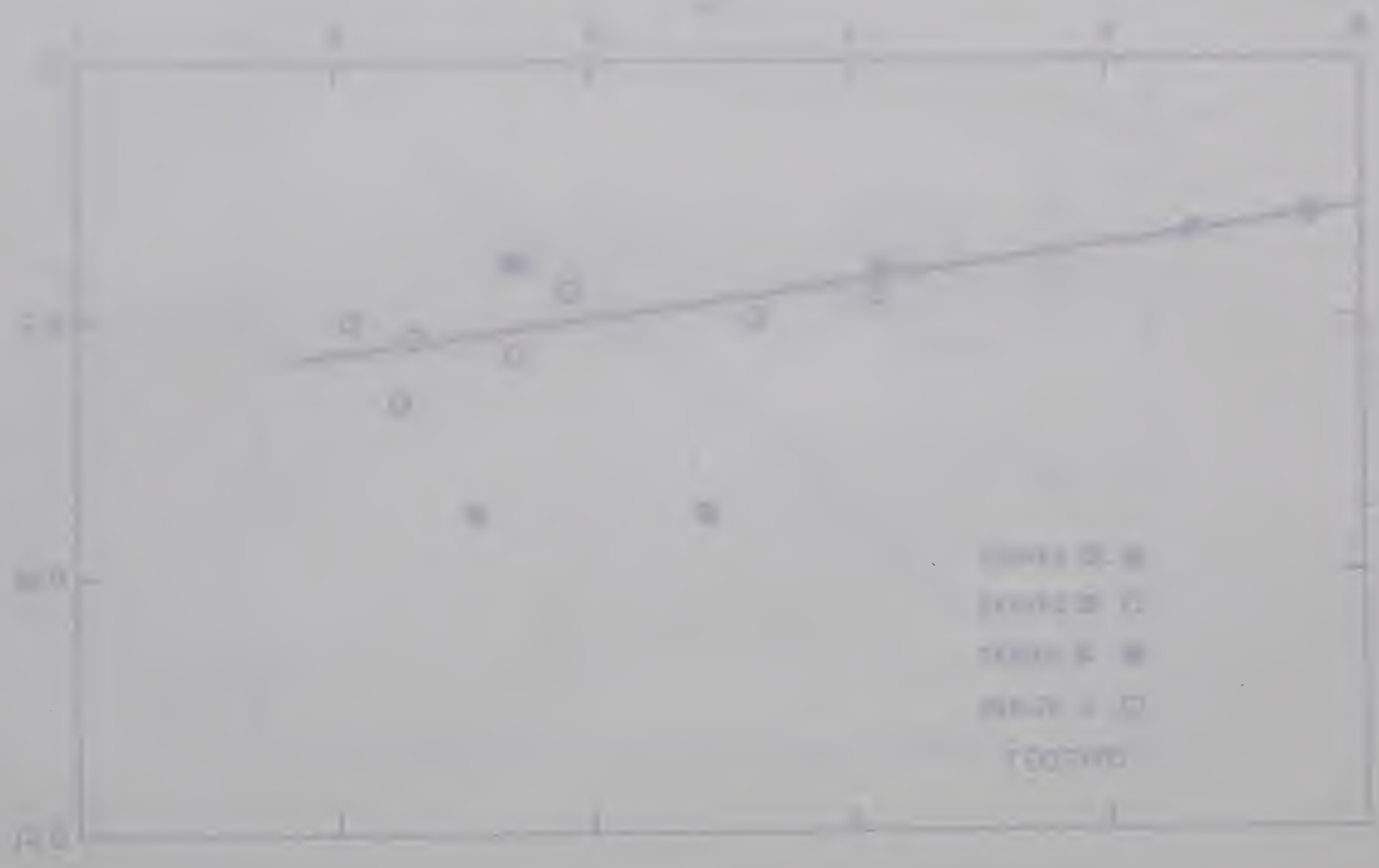

the maximum velocity point.

The velocity distribution in the symmetrical region of the free jet[19] was analysed using the standard method of studying free jet velocity distribution (see the inset in Fig. 3-13), and the results are shown in Fig. 3-13. The results agree fairly well with the theoretical curve due to Goertler and Tollmien[20] in some cases and in others there is considerable deviation. For a more detailed analysis, the curved jet should be probed thoroughly with suitable instruments.

The Maximum Velocity Filament

From a practical point of view, it is useful to know the location of the maximum velocity filament and also the value of the maximum velocity. If u_m is the maximum velocity at a distance of x_4 from the beginning or toe of the B-Jump studied, the variation of u_m/U_1 with x_4/y_1 is shown in Fig. 3-14. [Before going further it must be pointed out that in general it is believed that for the maximum B-Jump, the toe is always at the position of the drop. But in this study it was found that for the lower supercritical Froude numbers, the toe was downstream of the drop and for higher Froude numbers, it was on the upstream side of the drop. (See Figs. 2-2 to 2-15)]. From Fig. 3-14, it is seen that for the wide range of data involved, a mean curve could be drawn. This mean curve is seen to be lower than the corresponding curve for the free jump which is taken from Rajaratnam[16]. This shows in a way the superiority of the B-Jump over the corresponding free jump for energy dissipation purposes.

Considering the mean curve for the B-Jump, a detailed study

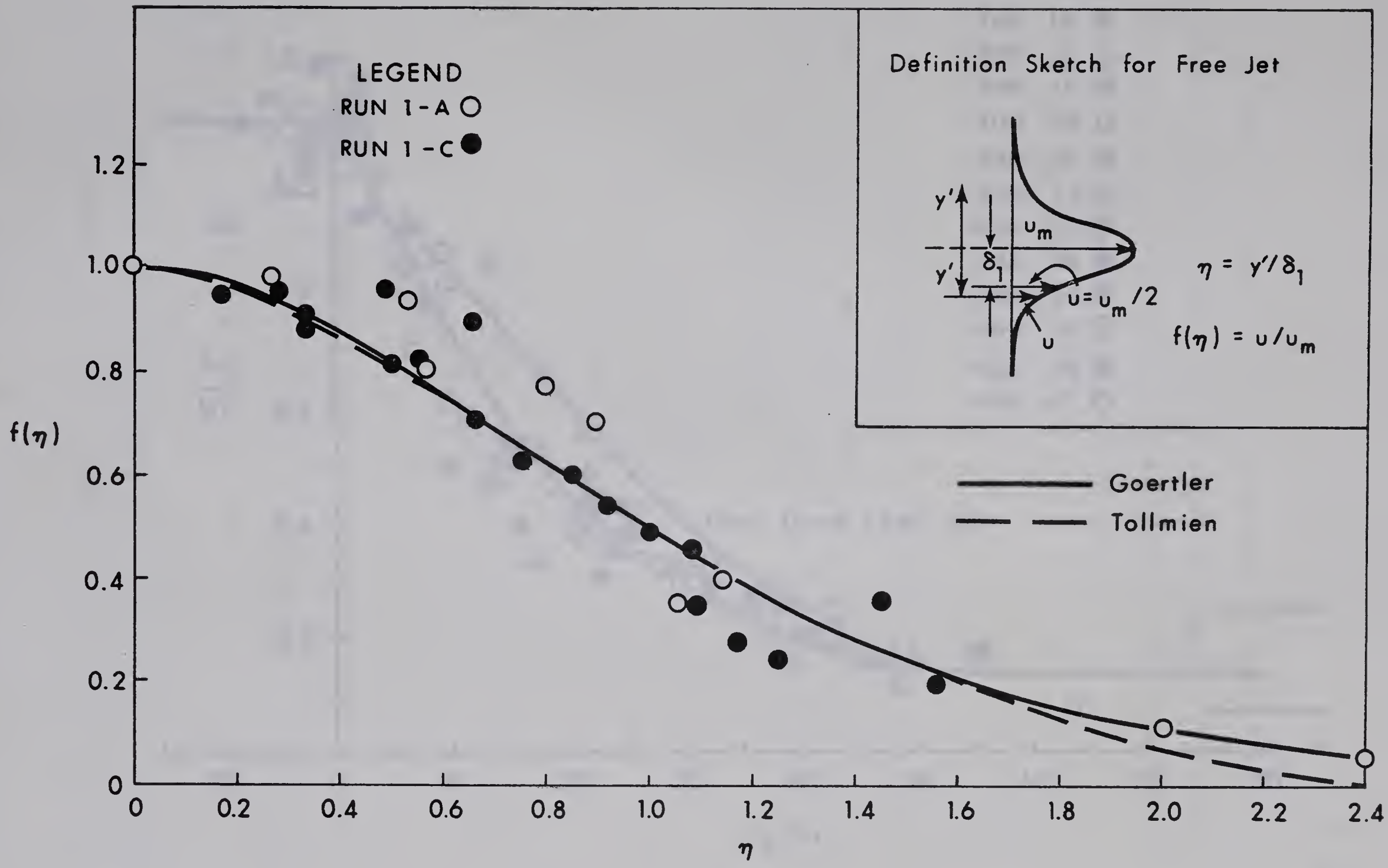

FIG. 3-13 Velocity Distribution – Plane Free Jet.

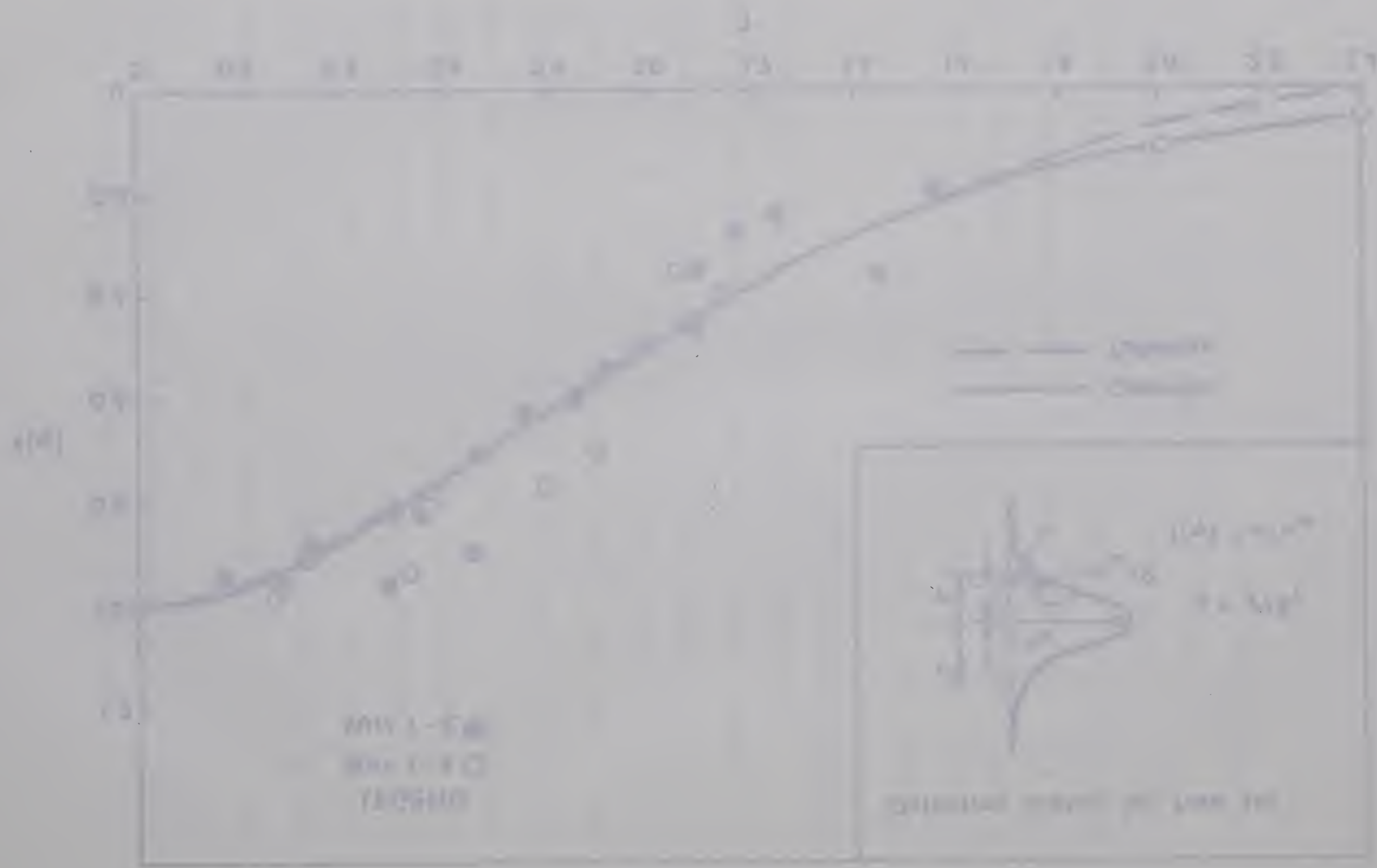

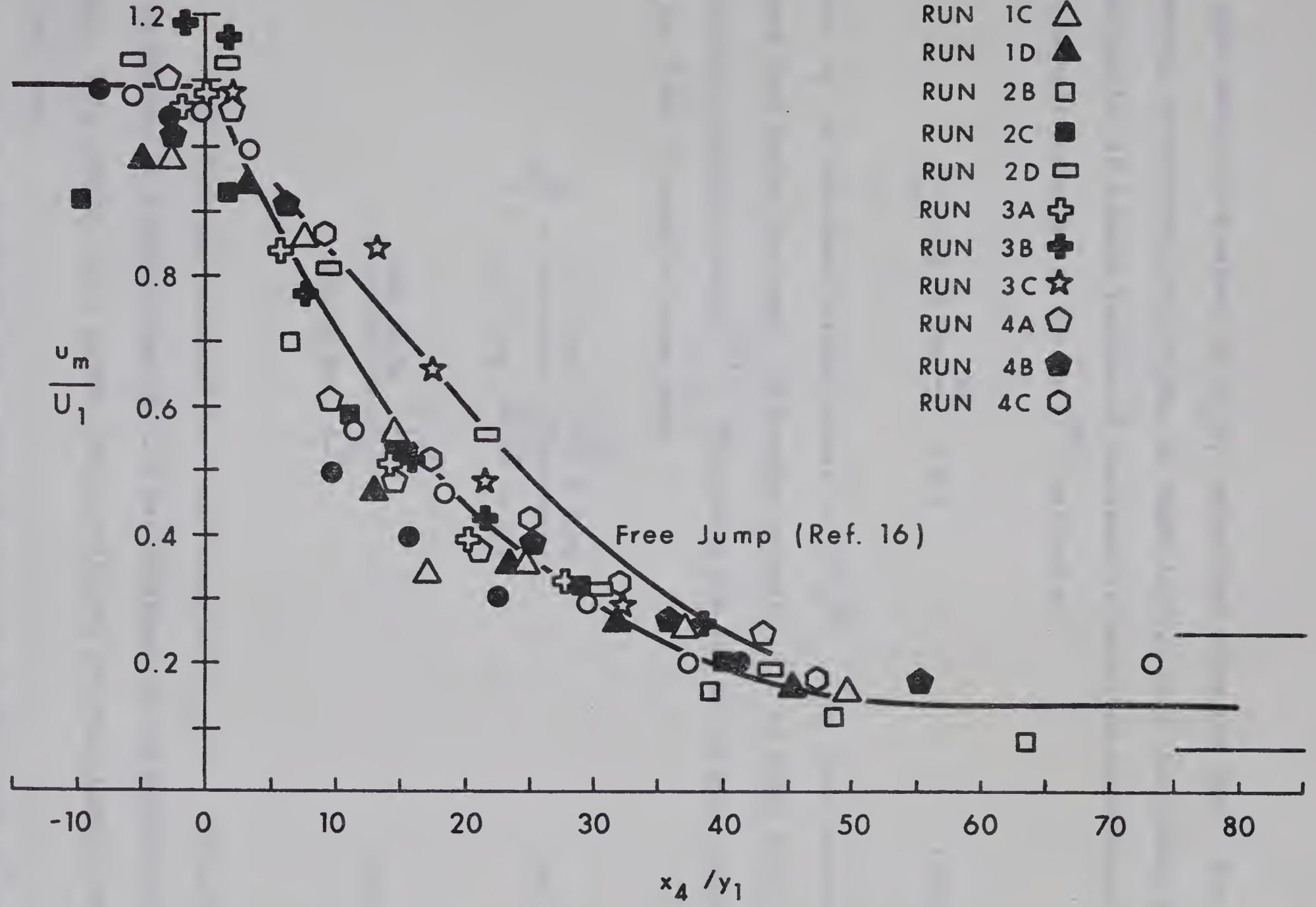

FIG. 3-14 Variation of u_m / U_1 with x_4 / y_1.

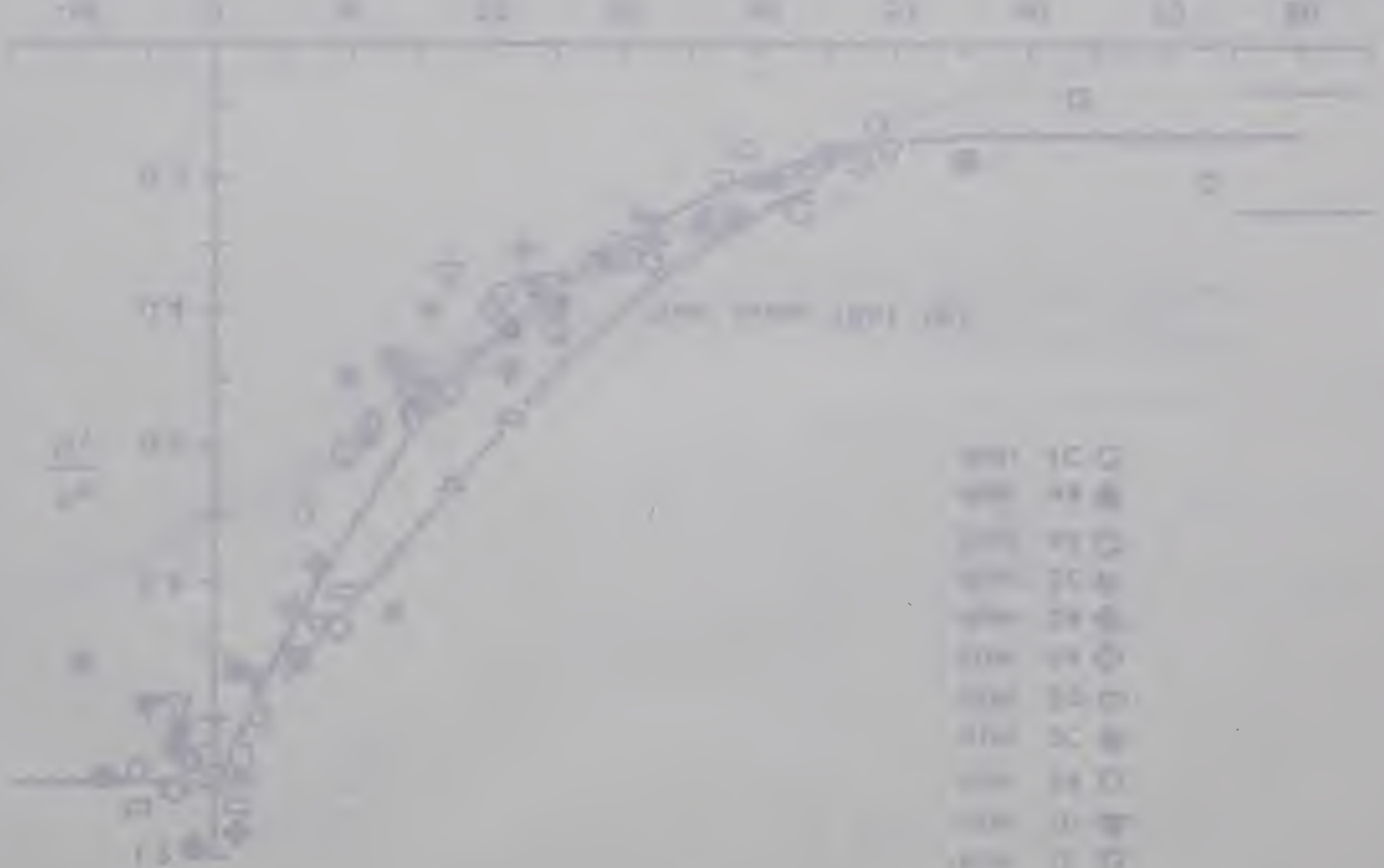

is next made of the values of u_m/U_1 before and after the jump. Considering the supercritical stream, as shown in Fig. 3-15, the velocity distribution in a major portion of the depth is described satisfactorily by the well known law of the wall[20] written as

$$\frac{u}{u_*} = 5.75 \log \frac{yu_*}{\nu} + 5.5 \qquad (3\text{-}06)$$

where u_* is the shear velocity equal to $\sqrt{\tau_o/\rho}$. For this supercritical stream just before the jump, the maximum velocity u_m is taken as the centerline surface velocity[21]. Then using the law of the wall, given by Eq. 3-06, it could be shown that

$$\frac{u_m}{U_1} = \frac{5.75 \log \frac{y_1 u_*}{\nu} + 5.50}{5.75 \log \frac{y_1 u_*}{\nu} + 3.0} \qquad (3\text{-}07)$$

$$= \frac{\log (9.04 \frac{y_1 u_*}{\nu})}{\log (3.33 \frac{y_1 u_*}{\nu})} \qquad (3\text{-}08)$$

Eq. 3-08 was evaluated in a wide range of $y_1 u_*/\nu$ from 200 to 10,000 and an average value of 1.10 was obtained for the entire practical range. This average value agrees fairly well with the experimental data in Fig. 3-14.

Coming to the other boundary of the curve in Fig. 3-14, the experimental data indicated that the velocity distribution at the end of the jump

is appreciably different from the fully developed distribution in sub-critical channel flow. Still for the sake of getting a control value, fully developed channel distribution was assumed to exist at the end of the jump.

At the end of the jump

$$\frac{u_m}{U_1} = \frac{u_m}{U_t} \cdot \frac{U_t}{U_1} \qquad (3\text{-}09)$$

where U_t is the mean velocity at this section. Eq. 3-09 was evaluated for the extreme values for the range of F_1 from 3.0 to 10.0 and h/y_1 from 1.0 to 6.0. Using the momentum equation (Eq. 1-04) of the B-Jump, a more extensive plot of which is given in Fig. 3-16, the boundary values were found to be 0.075 and 0.25. These limiting values shown in Fig. 3-14, appear to contain the entire width of the data at the lower level.

The dimensionless configuration of the maximum velocity filament is shown in Fig. 3-17, in which $\bar{y}$ is the depth of the filament below the surface of the supercritical stream and x_4 is the distance from the beginning of the jump. The mean curve given in Fig. 3-17 along with Fig. 3-14 could be used to predict the location of the maximum velocity filament and the magnitude of the maximum velocity at the desired section.

Junction Velocity

It is interesting to find the development of the velocity in the centerline of the junction plane, which is the extension of the upstream bed. Up to the end of the drop, the junction plane velocity u_j should

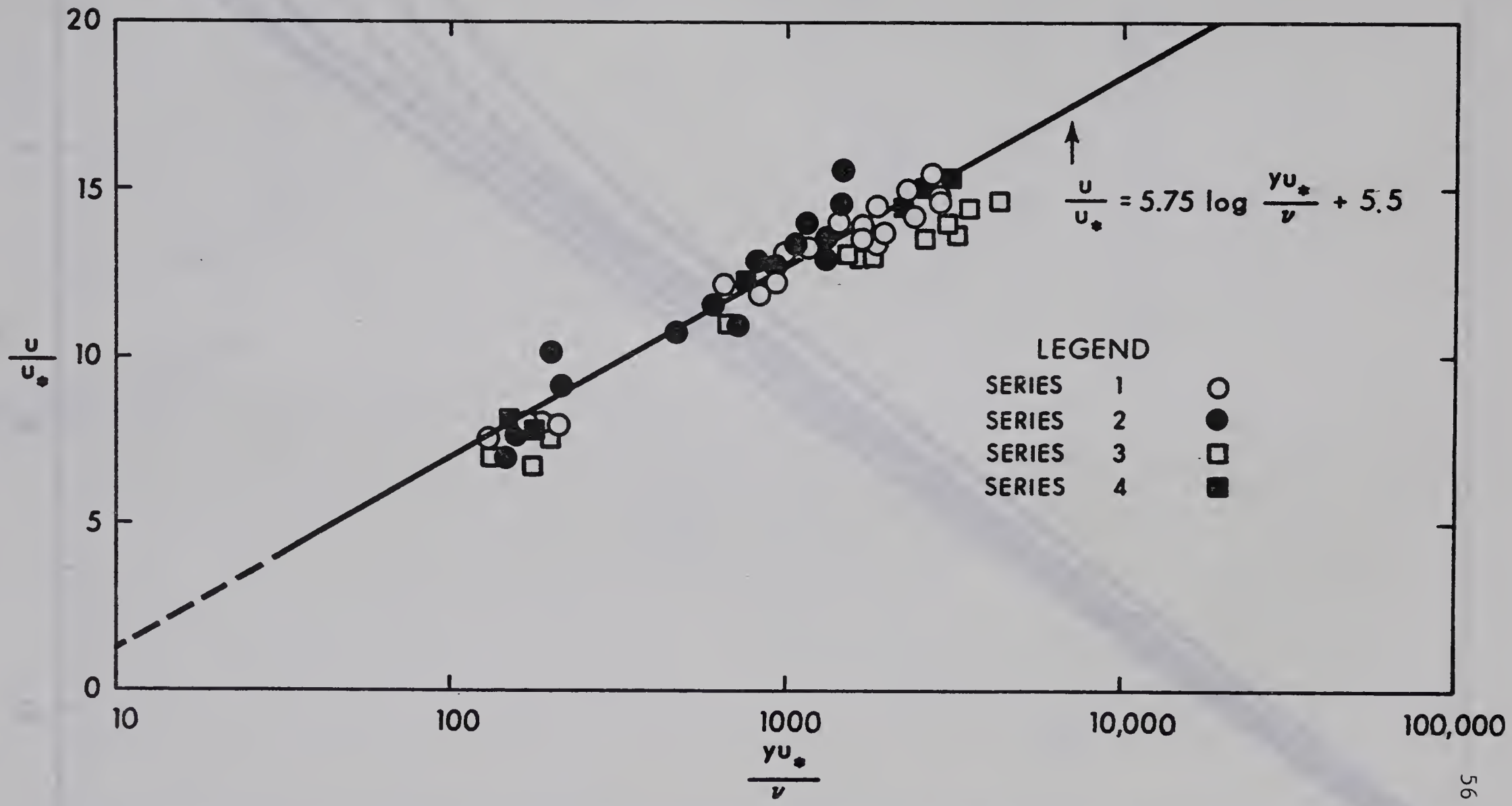

FIG. 3-15 Velocity Distribution in the Supercritical Stream

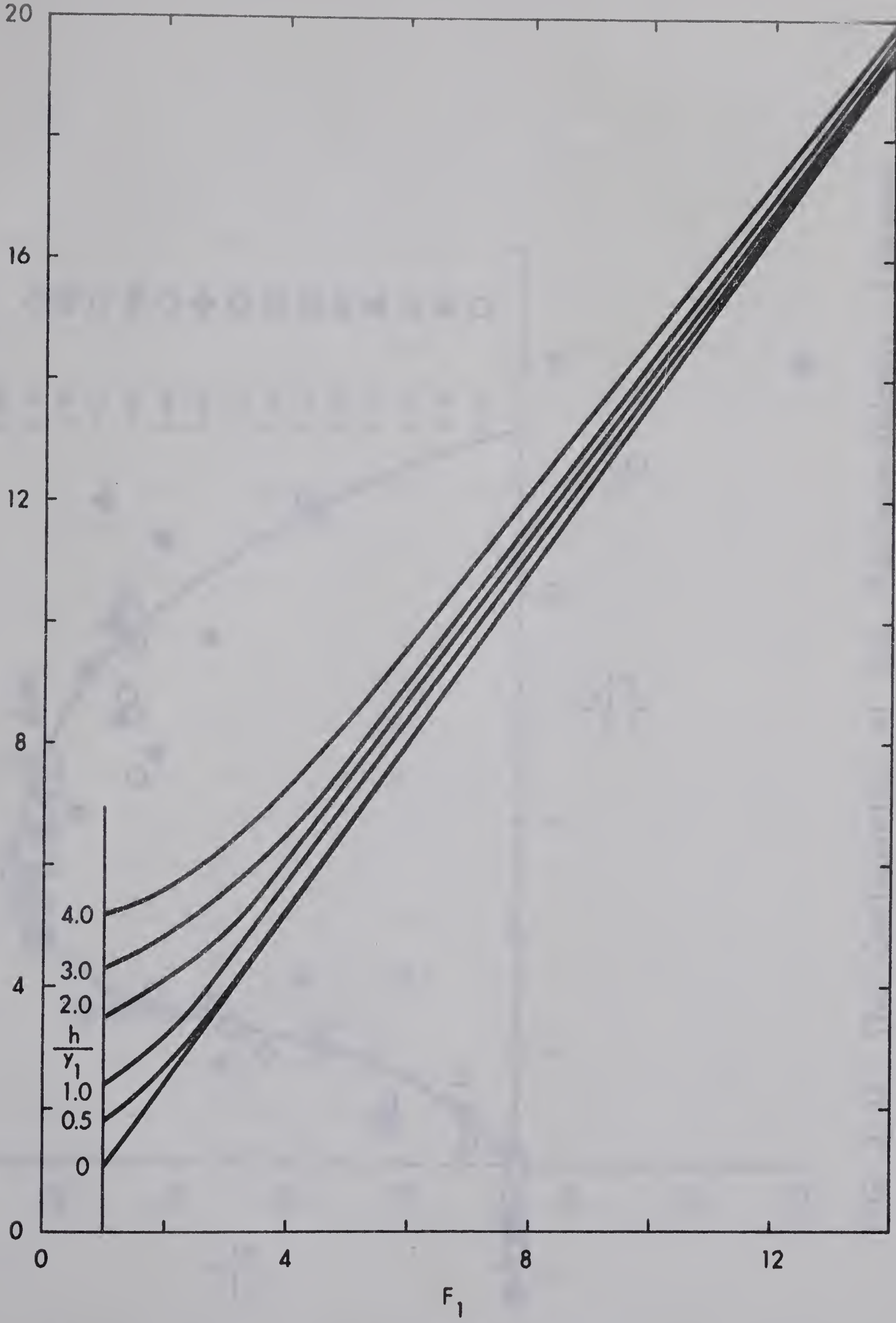

FIG. 3-16 Plot of the Momentum Equation for B-Jump

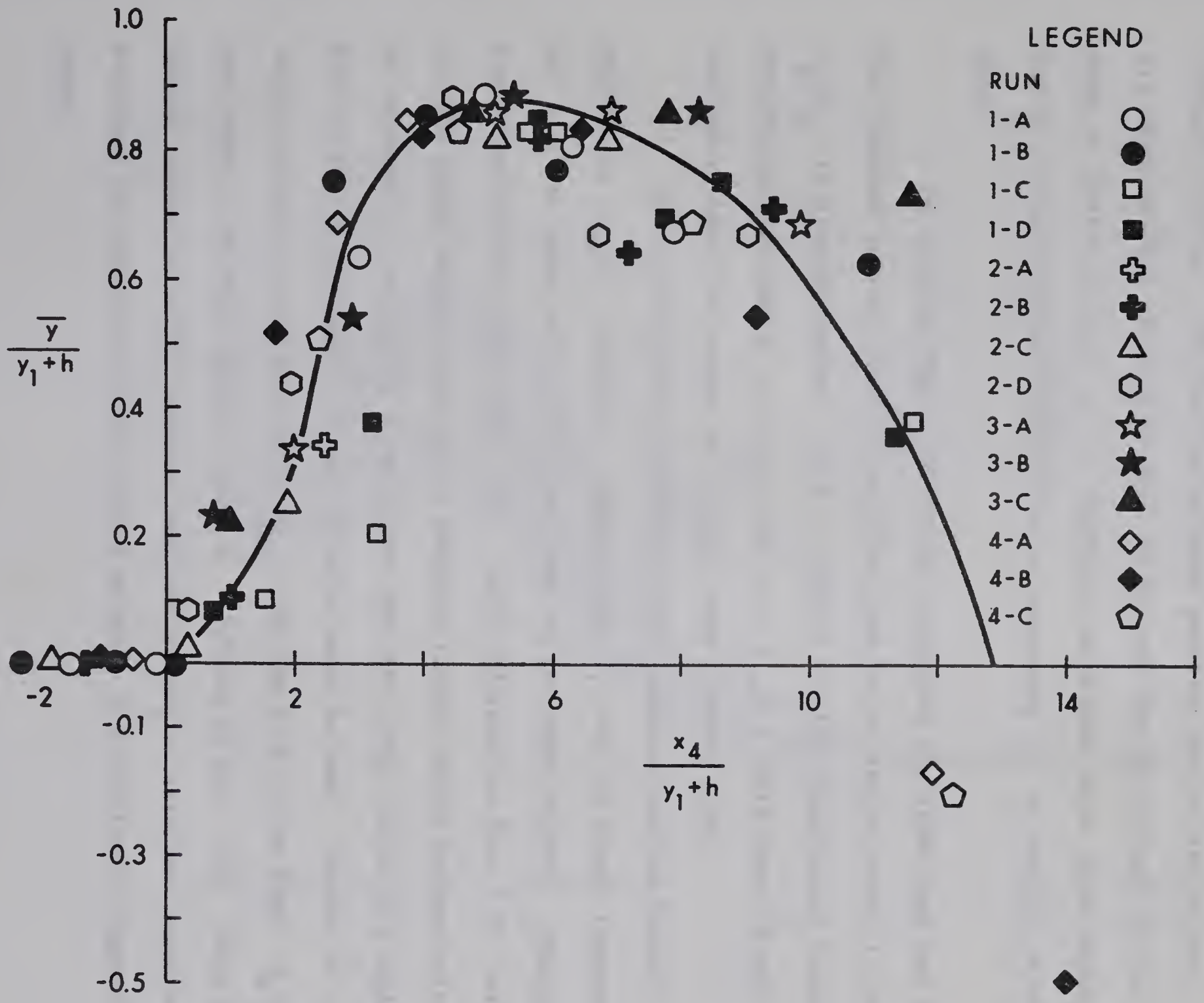

FIG. 3-17 The Configuration of the Maximum Velocity Filament

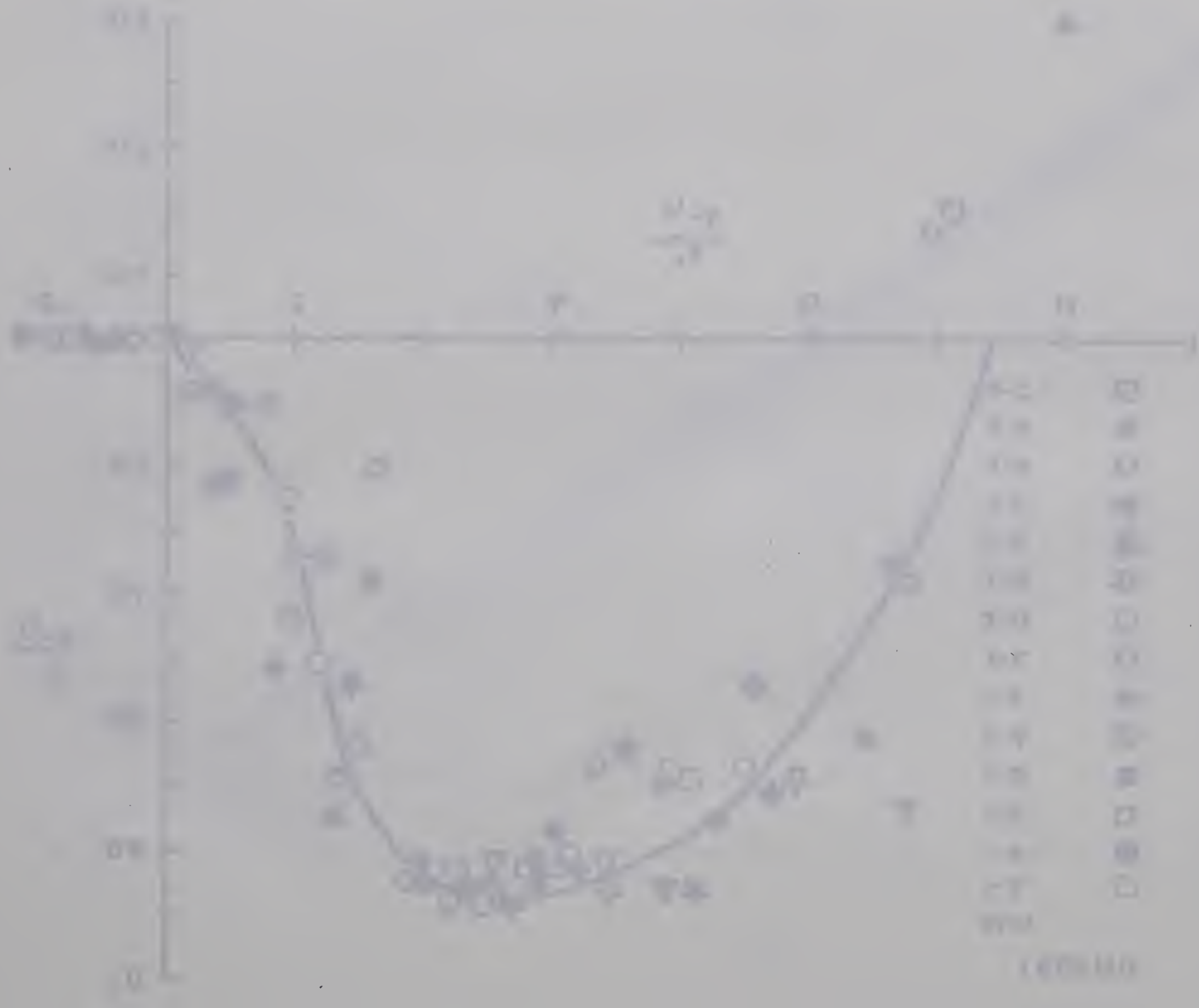

be zero because of the property of "no slip" of real fluids. Then with the distance x_1 from the junction plane, it increases to a maximum value of u_{jm} and decreases rapidly first and slowly later on to assume an asymptotic value. The junction velocity profiles for all the 14 runs are shown in Figs. 3-18(a) to (d). It is seen that at the end of the drop, a finite value of u_j is observed, which must be at least partly due to the experimental difficulties in measuring u_j at the tip of the drop.

As shown in Fig. 3-19, it was found that the right hand arm of the junction velocity profile could be given by one single curve, in which u_j/u_{jm} is plotted against x_5/θ, where θ is the longitudinal distance between sections where $u_j = u_{jm}$ and $u_j = u_{jm}/2$. This curve is well defined at least for values of u_j/u_{jm} down to about 0.30.

It was found that the dimensionless maximum junction velocity written as u_{jm}/U_1 varies mainly with F_1 and is almost independent of h/y_1 as shown in Fig. 3-20, at least in the range studied. Regarding the dimensionless length scale θ/y_1, with reference to Fig. 3-21, points for the fourth series could not be obtained (unless daring extrapolation is resorted to) and if the three points with the large scatter are neglected, for preliminary purposes a linear relation could be used. Further if x_m is the distance of the section of u_{jm} from the face of the drop, $x_m/y_1 + h$ was found to decrease linearly with F_1 as shown in Fig. 3-22. Using the results presented in this section some preliminary calculations could be performed for calculating the junction velocity distribution in comparable cases.

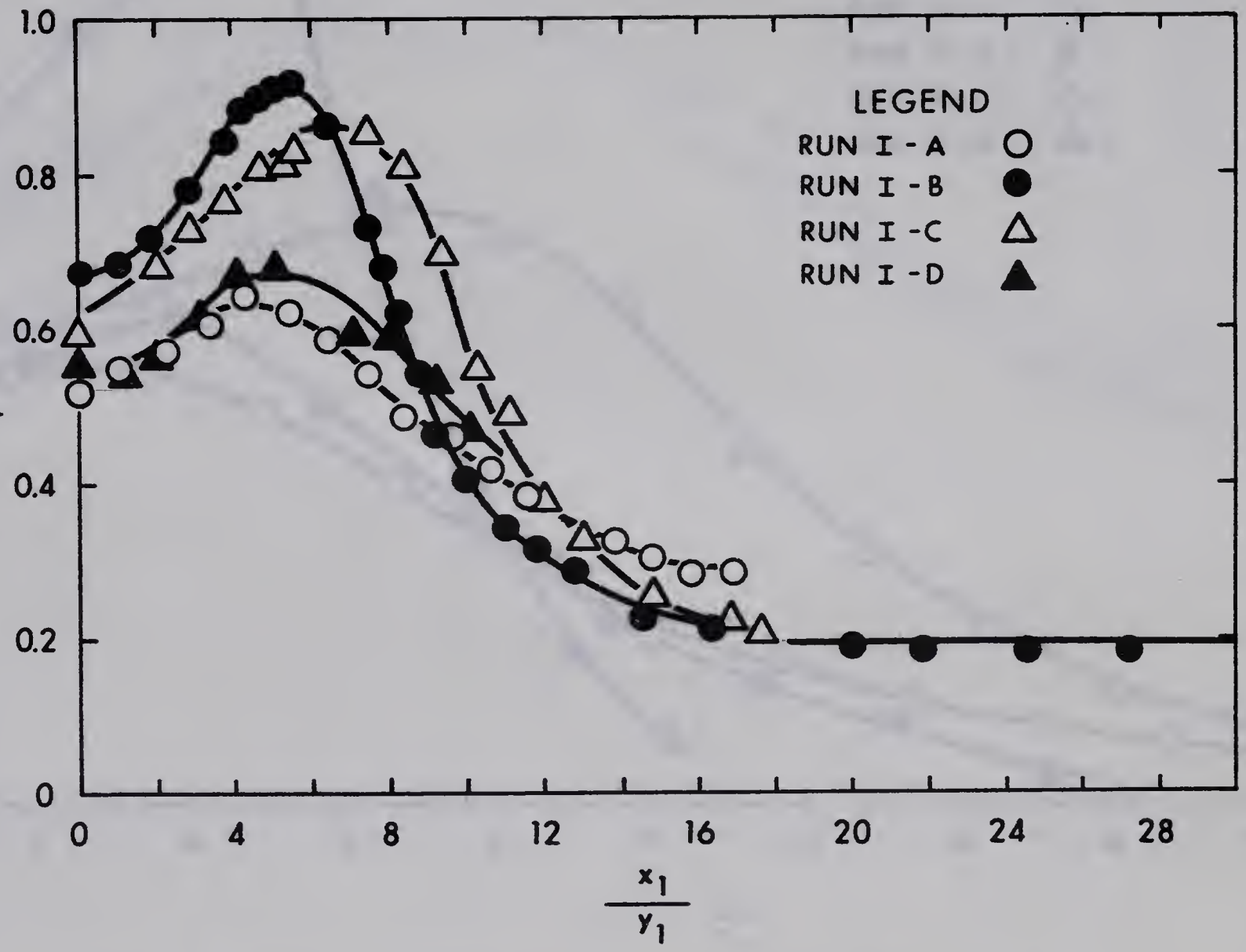

FIG. 3-18(a) Junction Velocity Profiles (Series I)

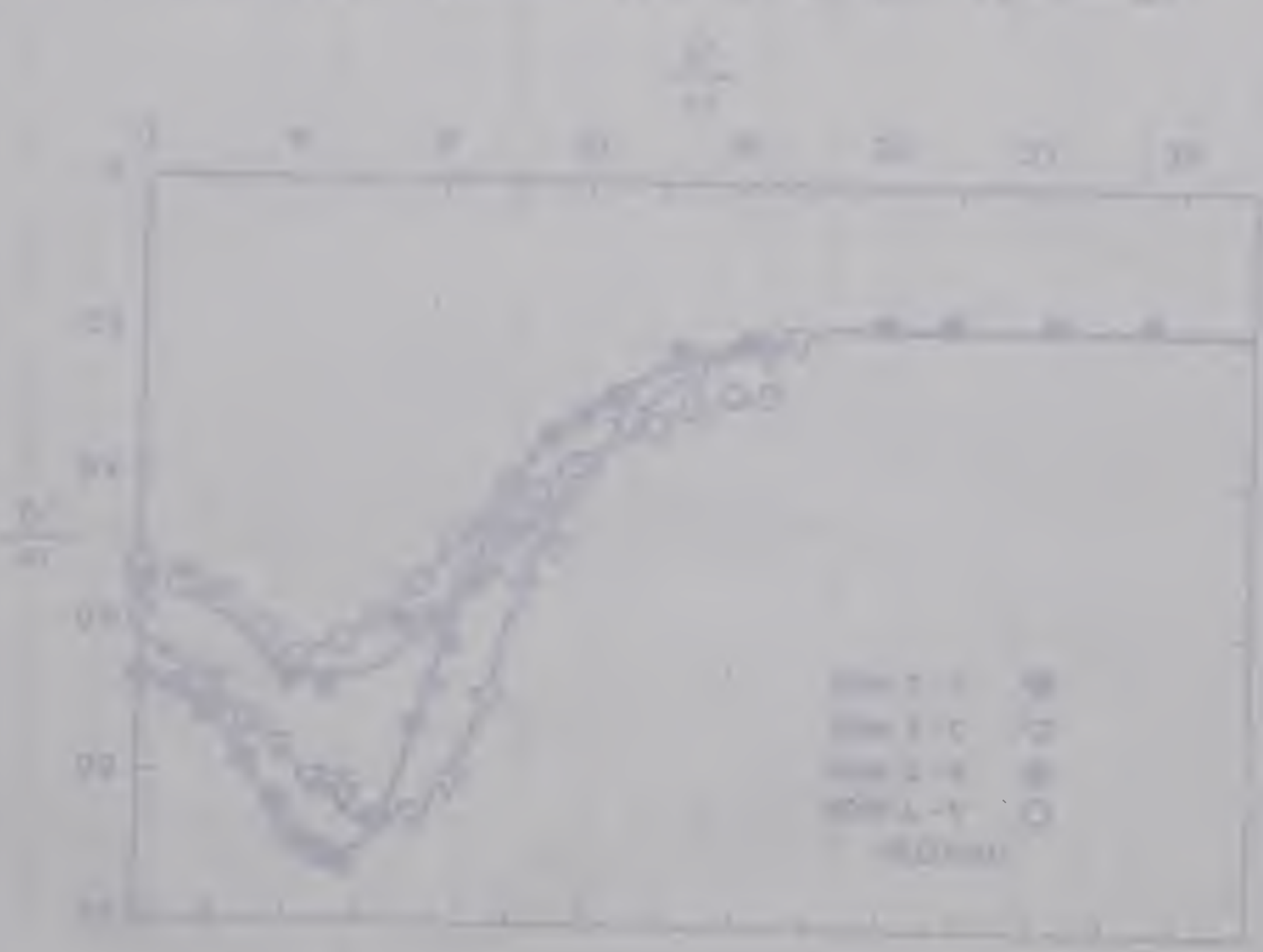

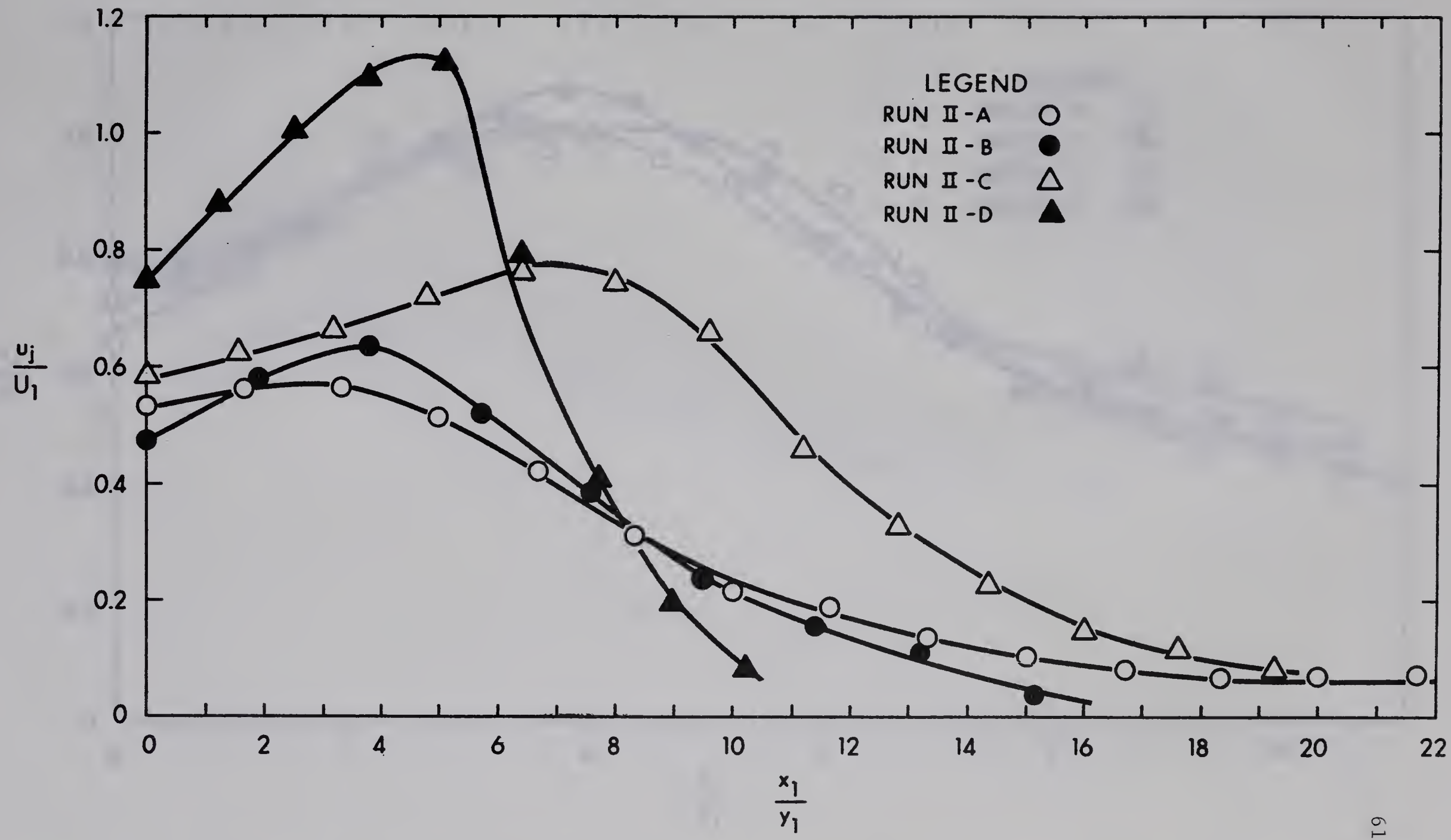

FIG. 3-18(b) Junction Velocity Profiles (Series II)

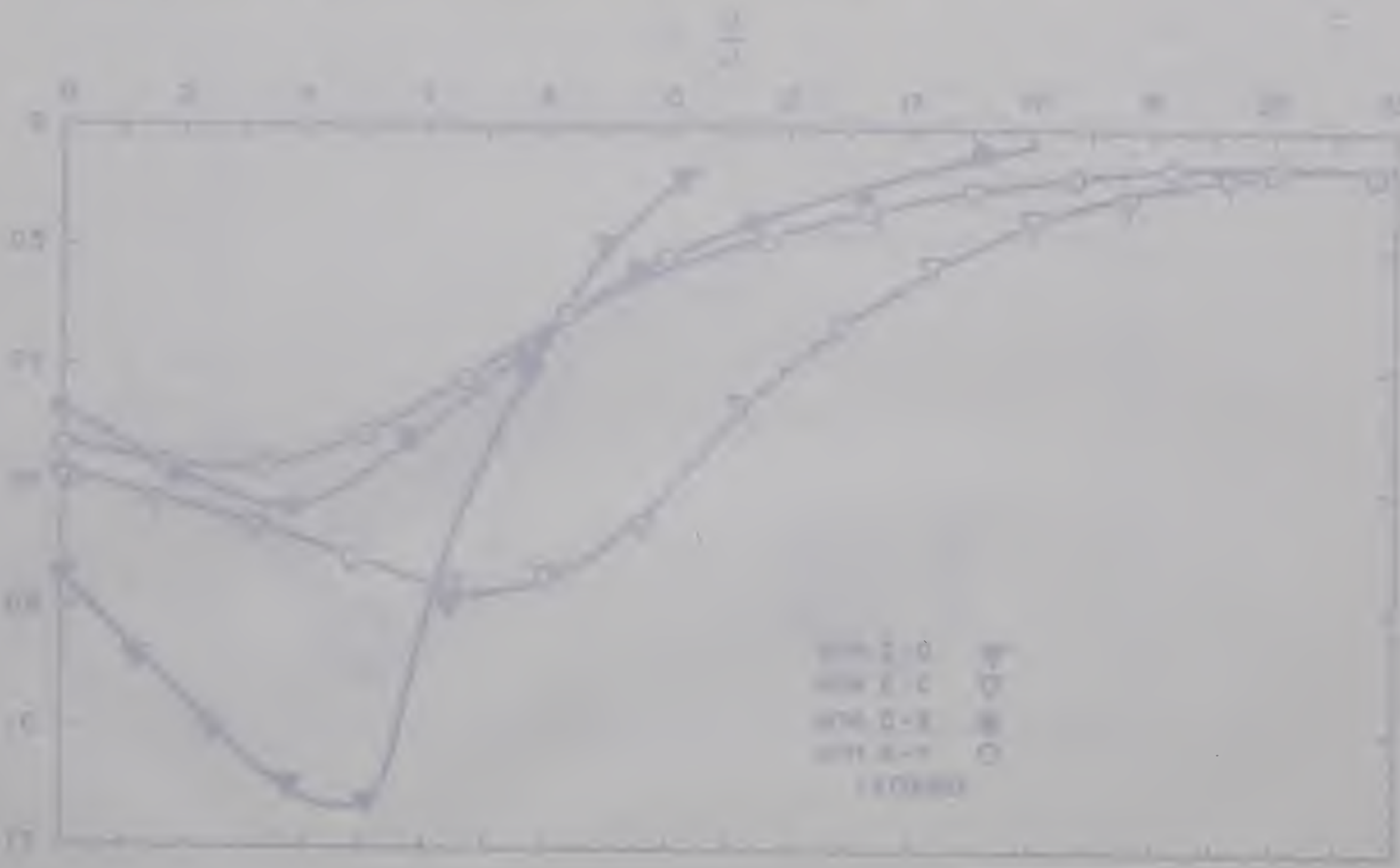

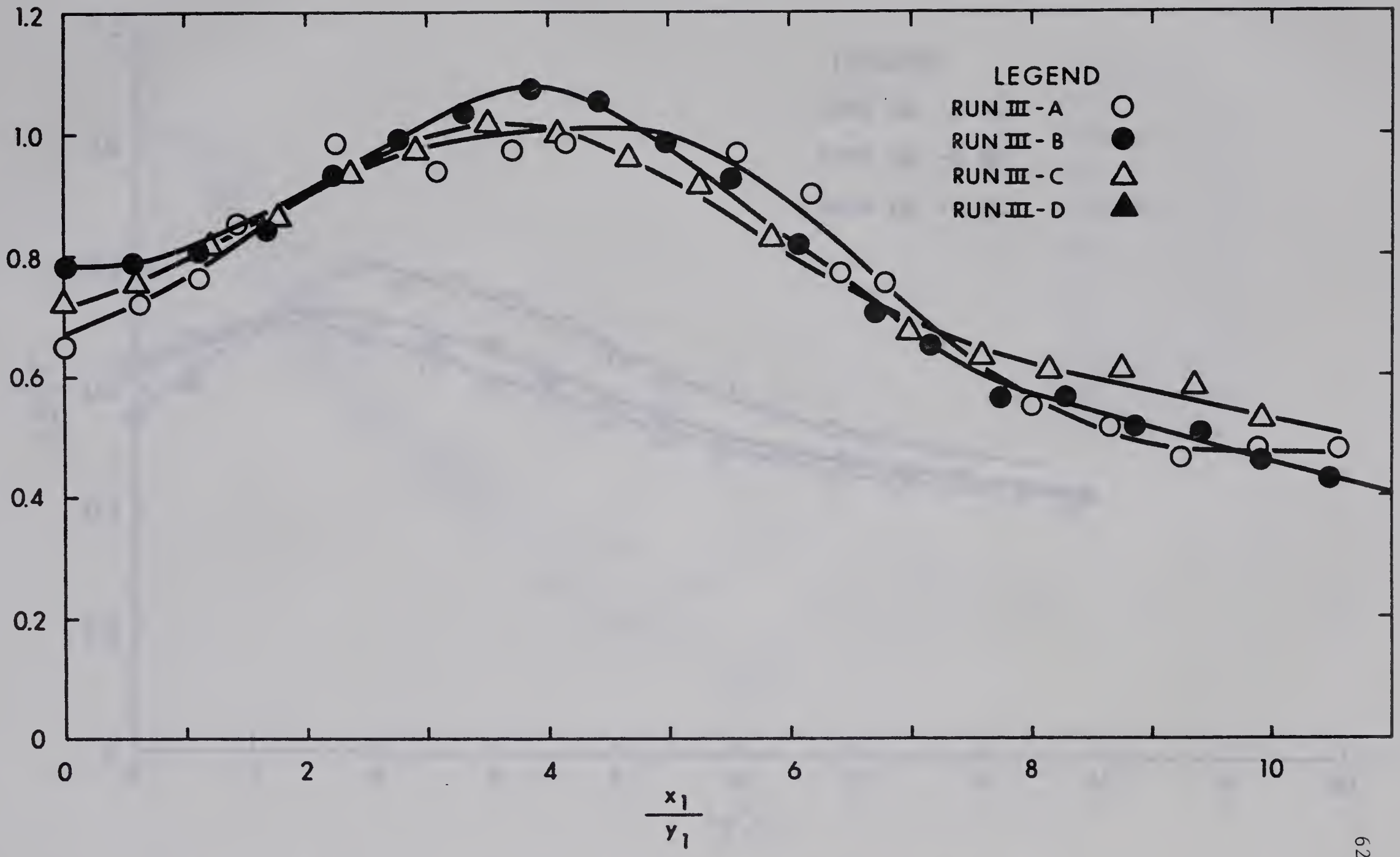

FIG. 3-18(c) Junction Velocity Profiles (Series III)

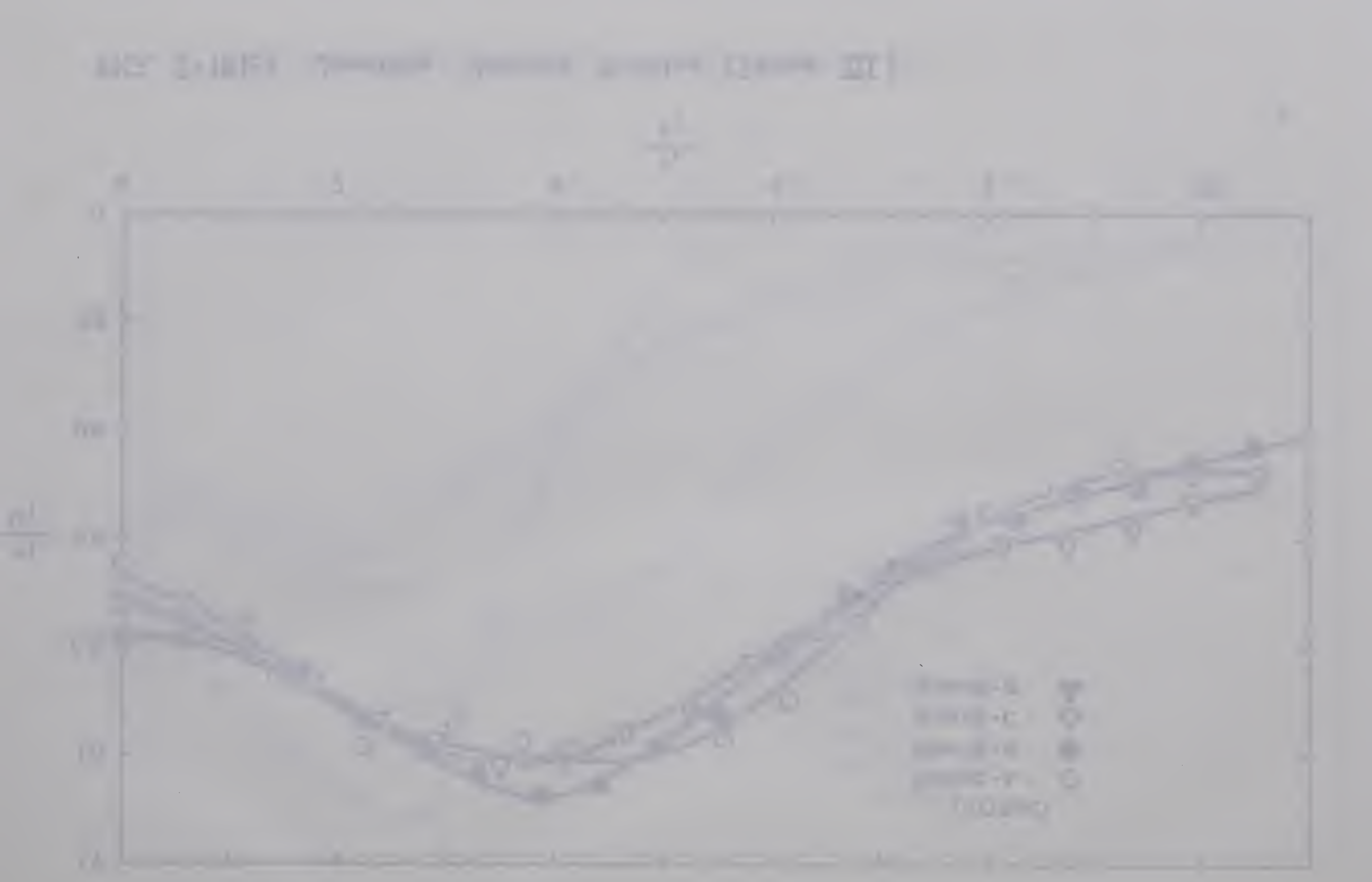

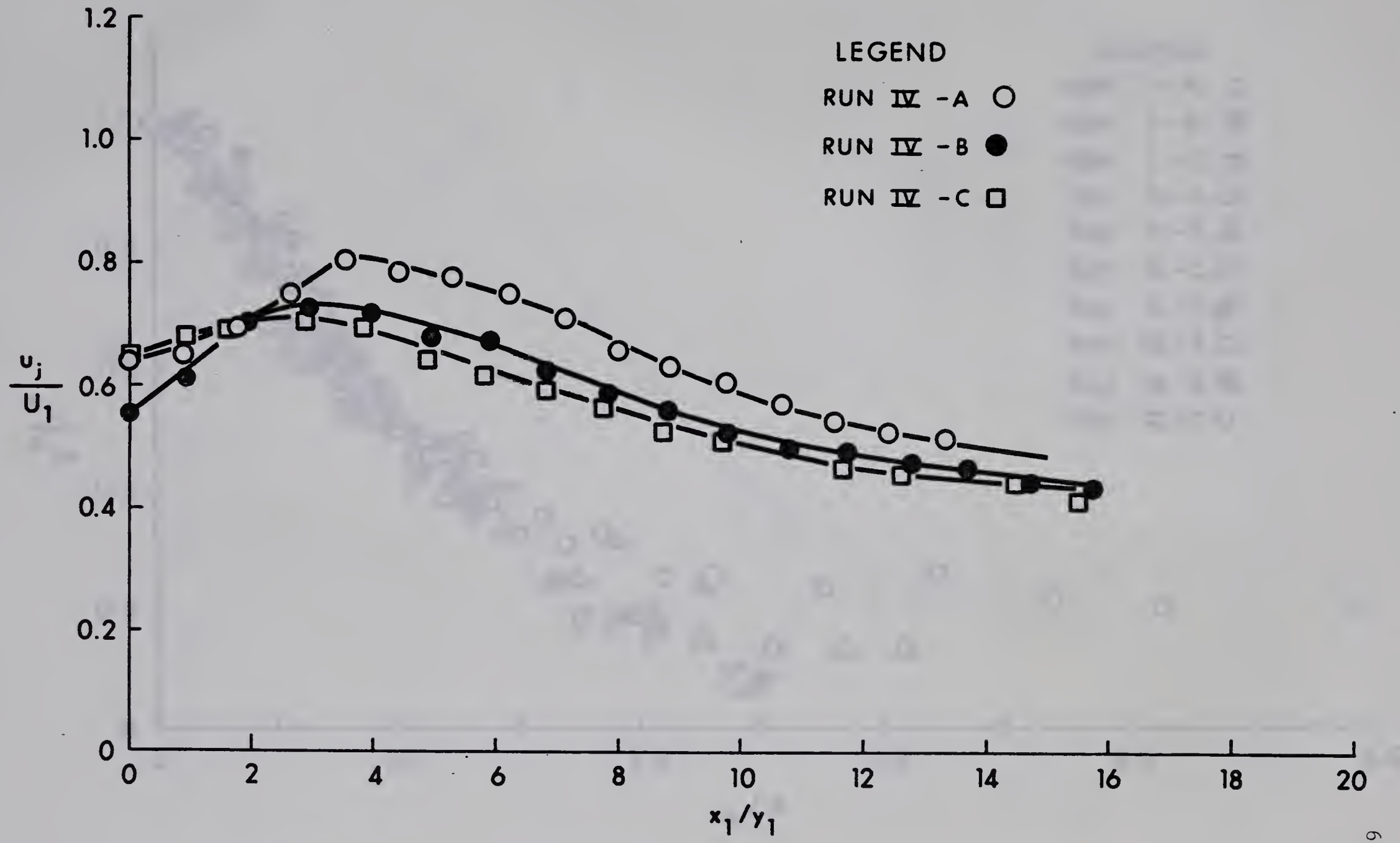

FIG. 3-18 (d) Junction Velocity Profiles (Series IV)

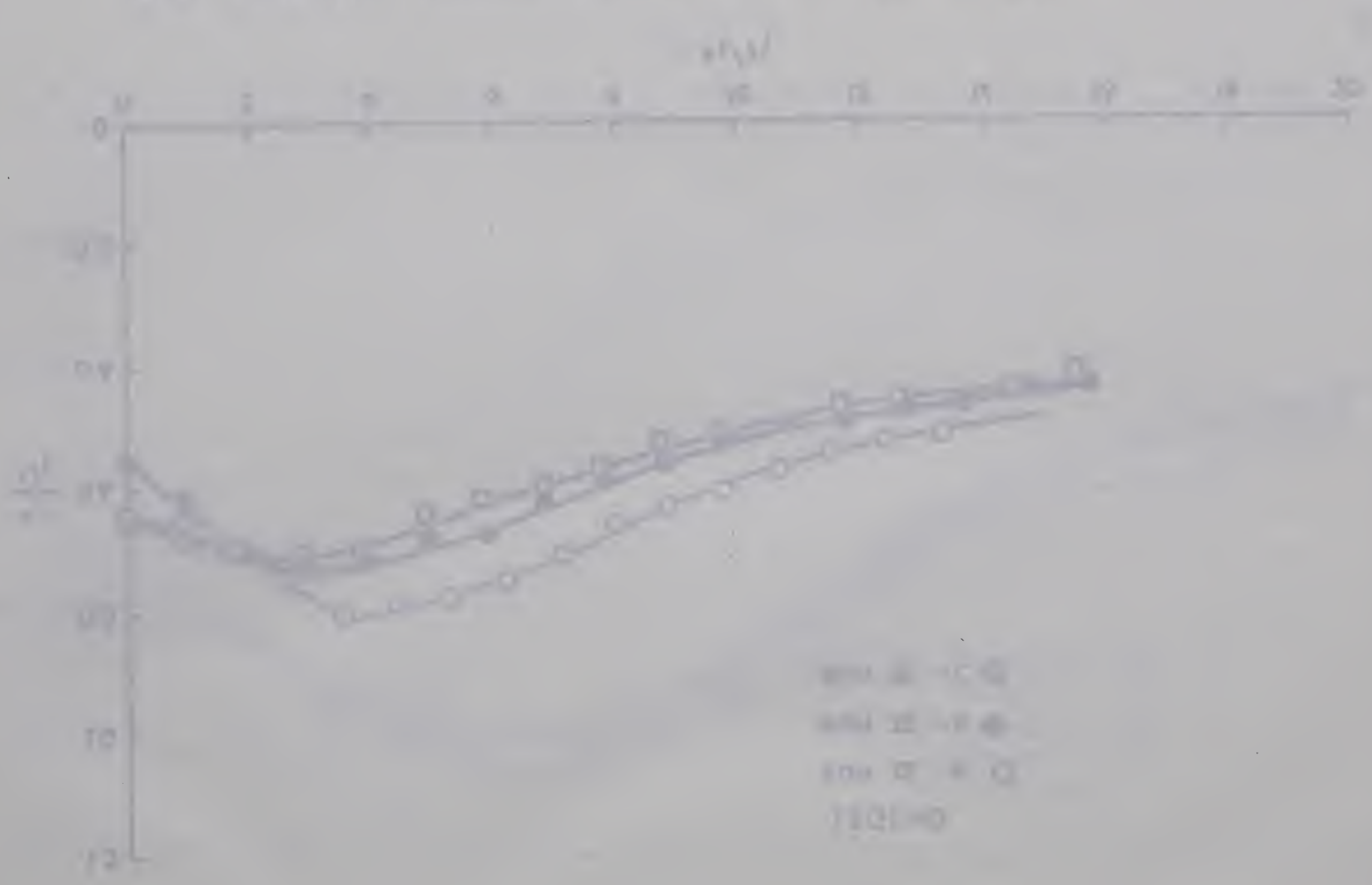

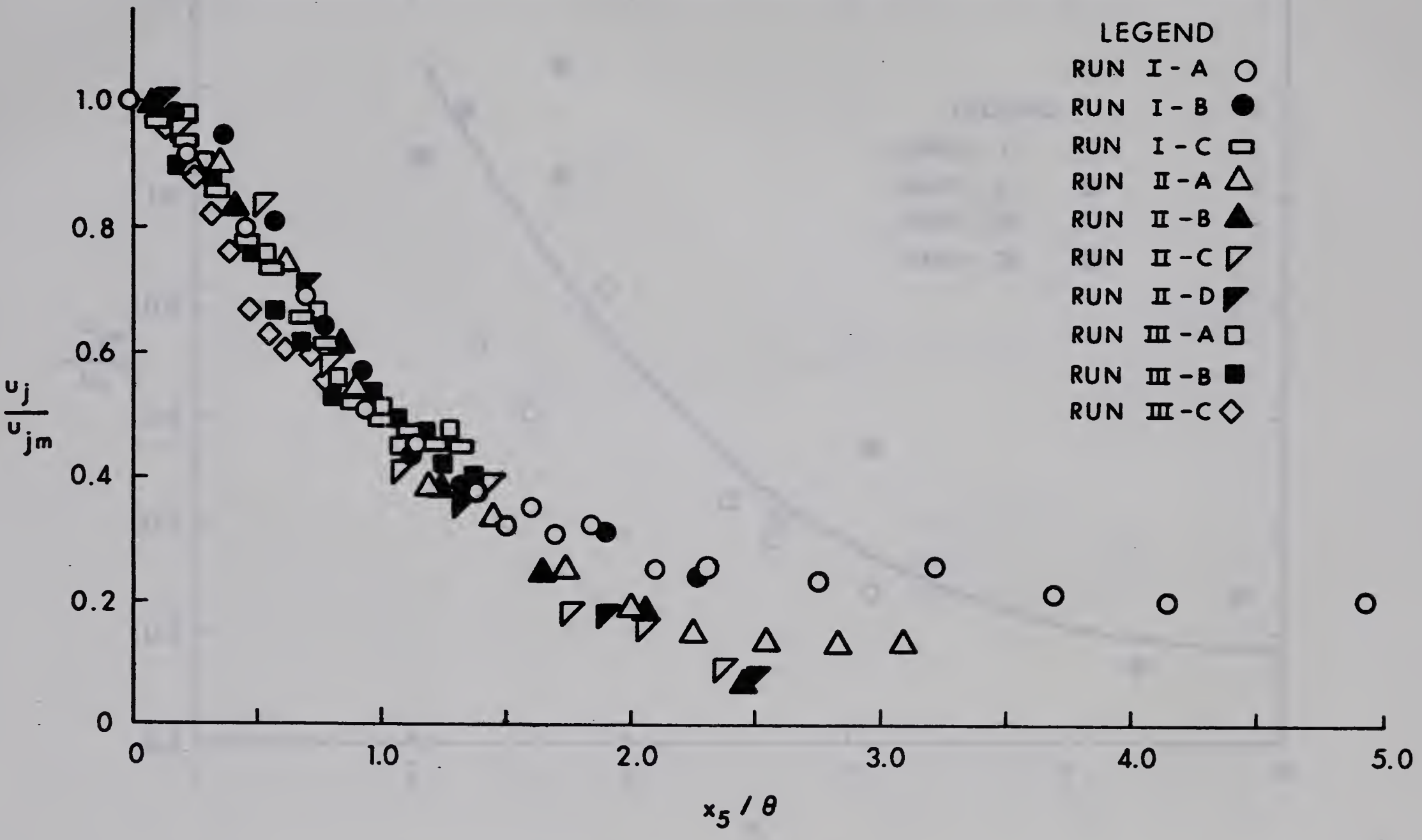

FIG. 3-19 Dimensionless Junction Velocity Distribution.

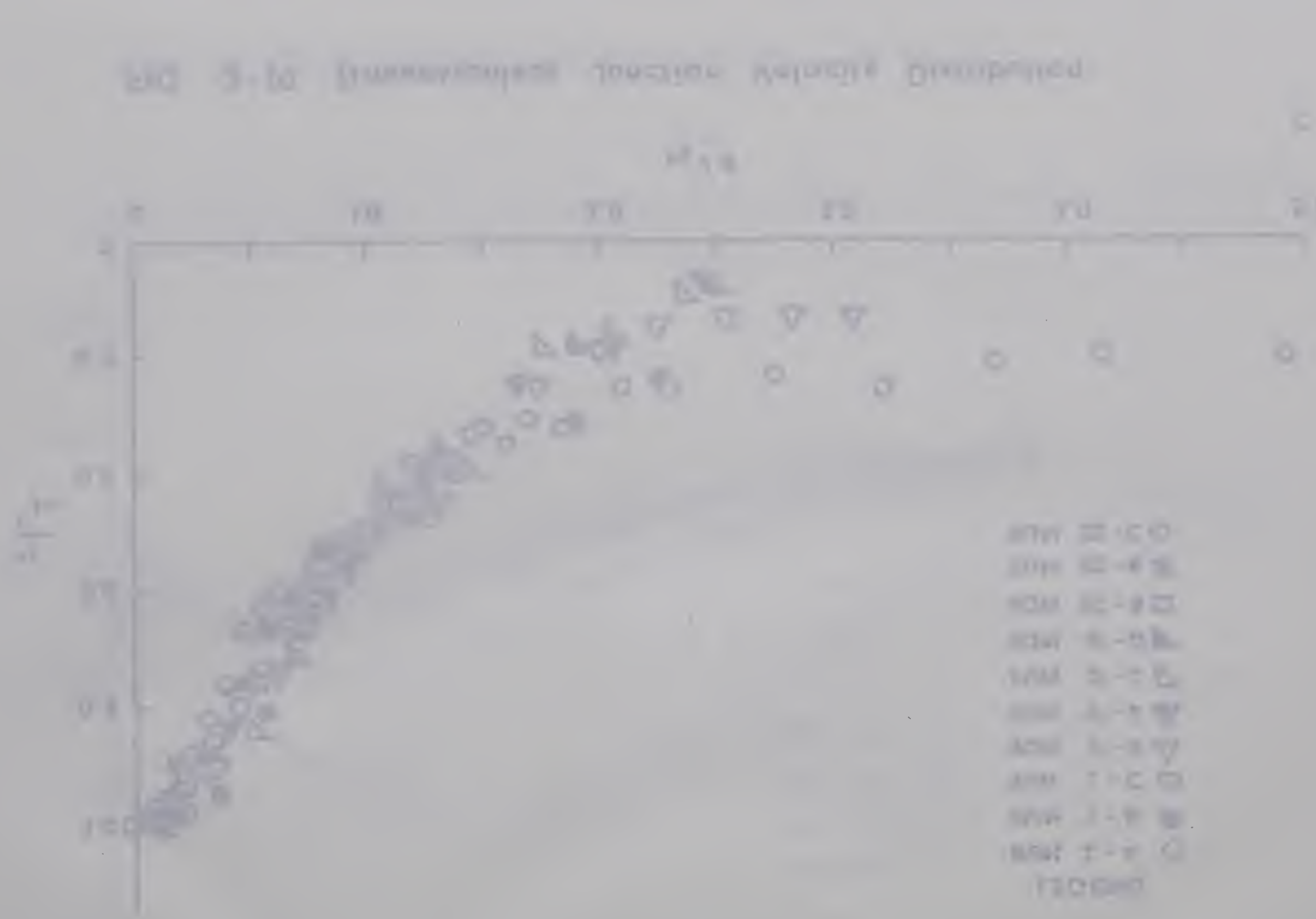

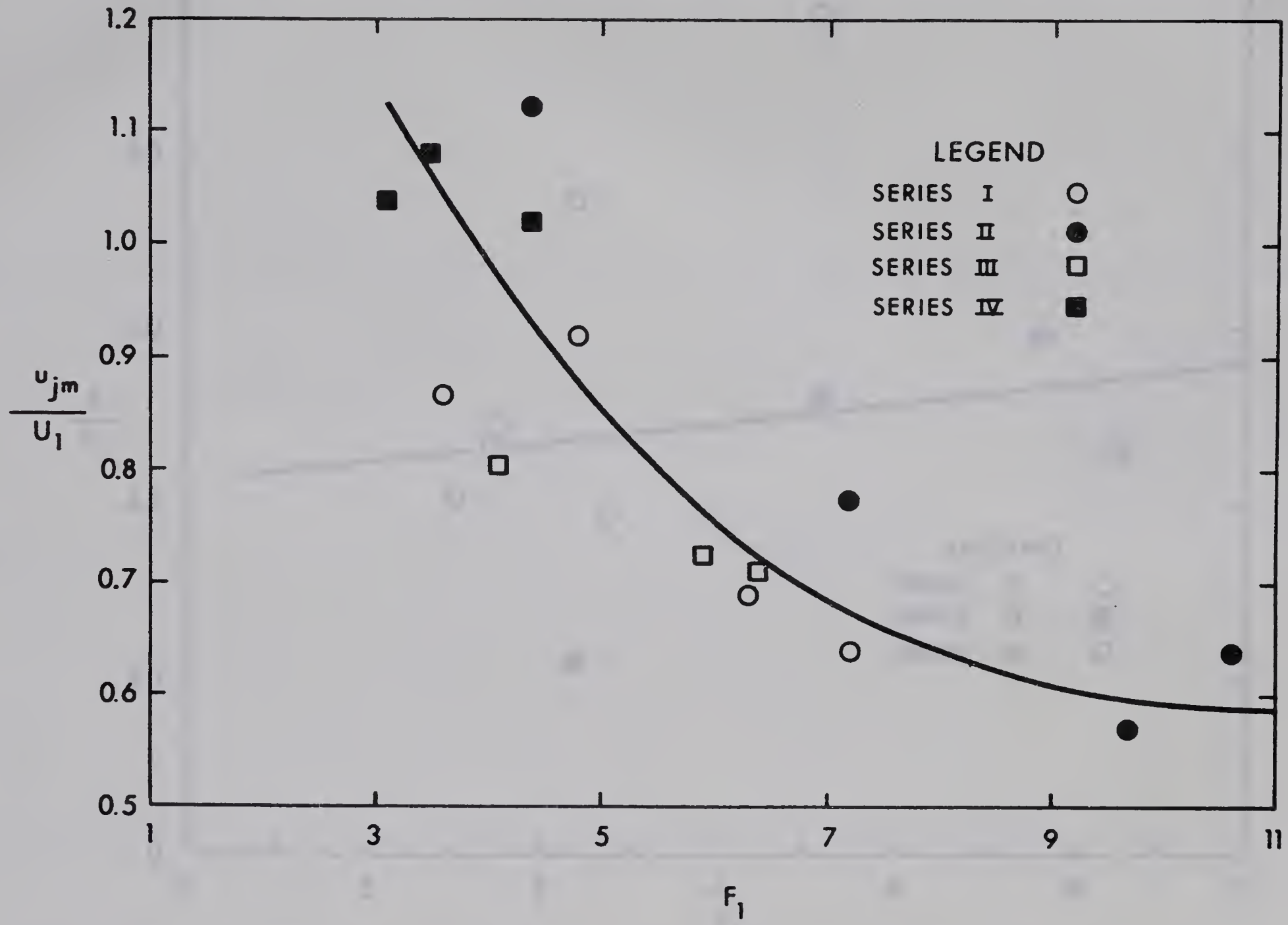

FIG. 3-20 Variation of $\frac{u_{jm}}{U_1}$ with F_1

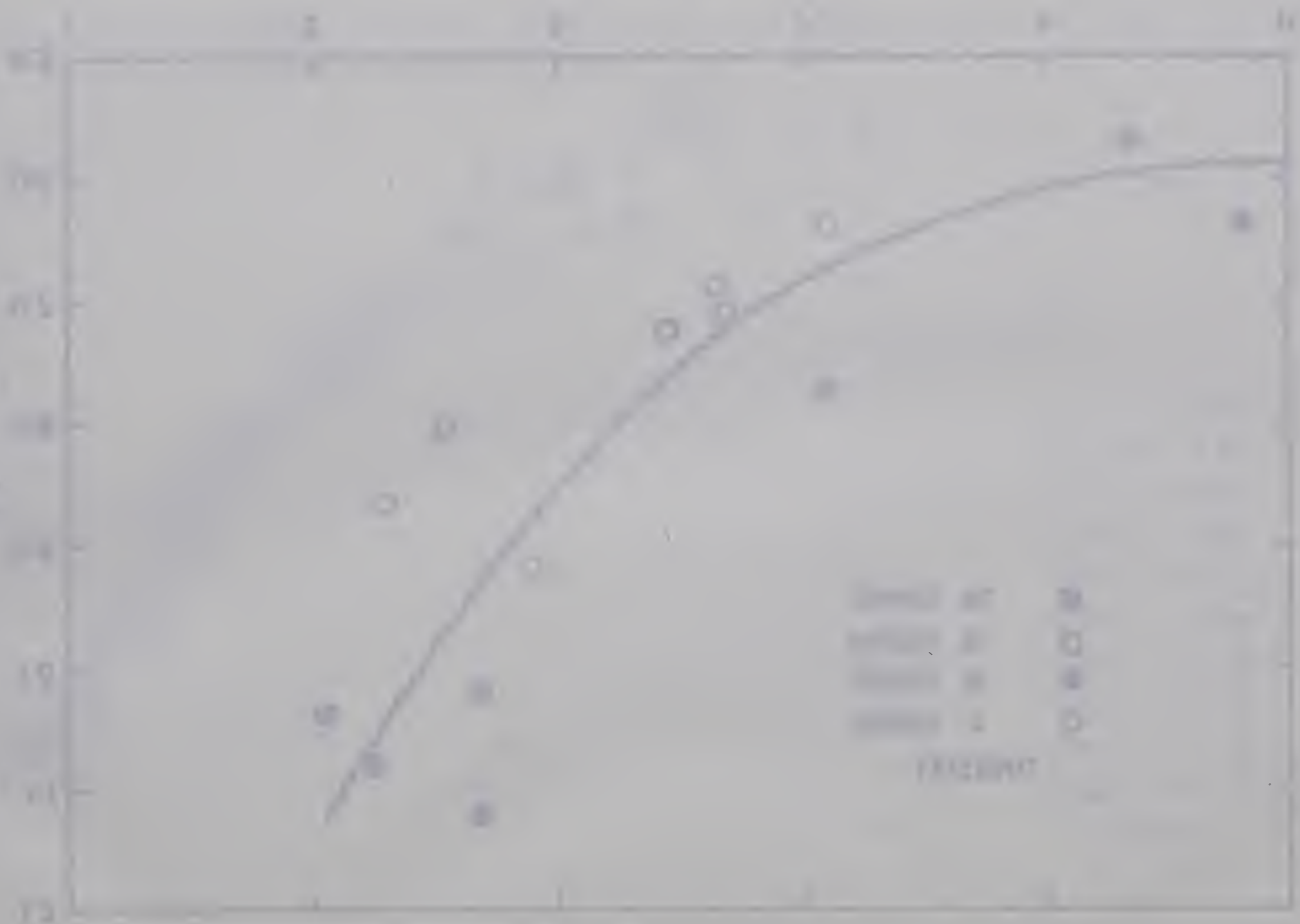

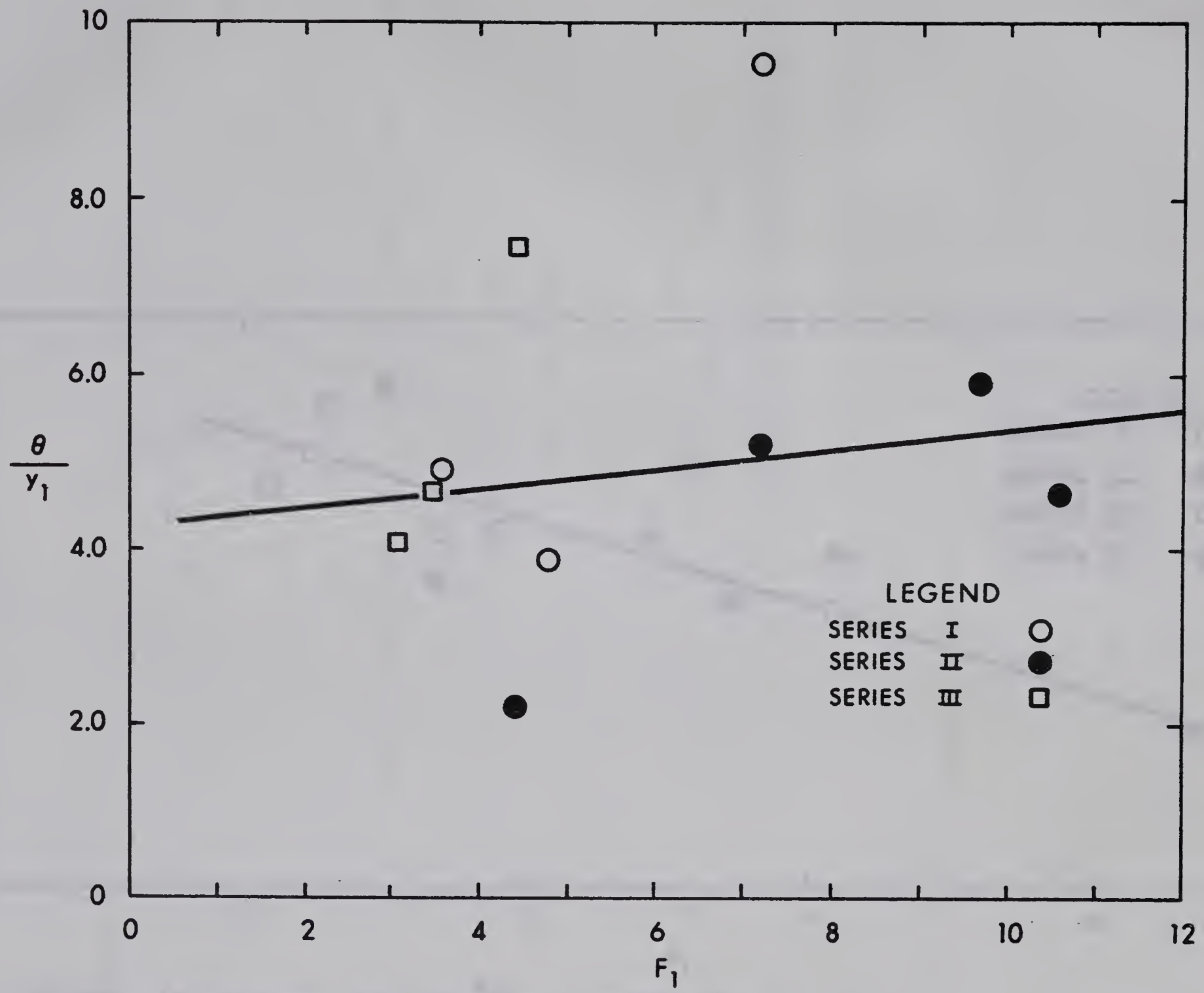

FIG. 3-21 Length Scale for Junction Velocity Distribution

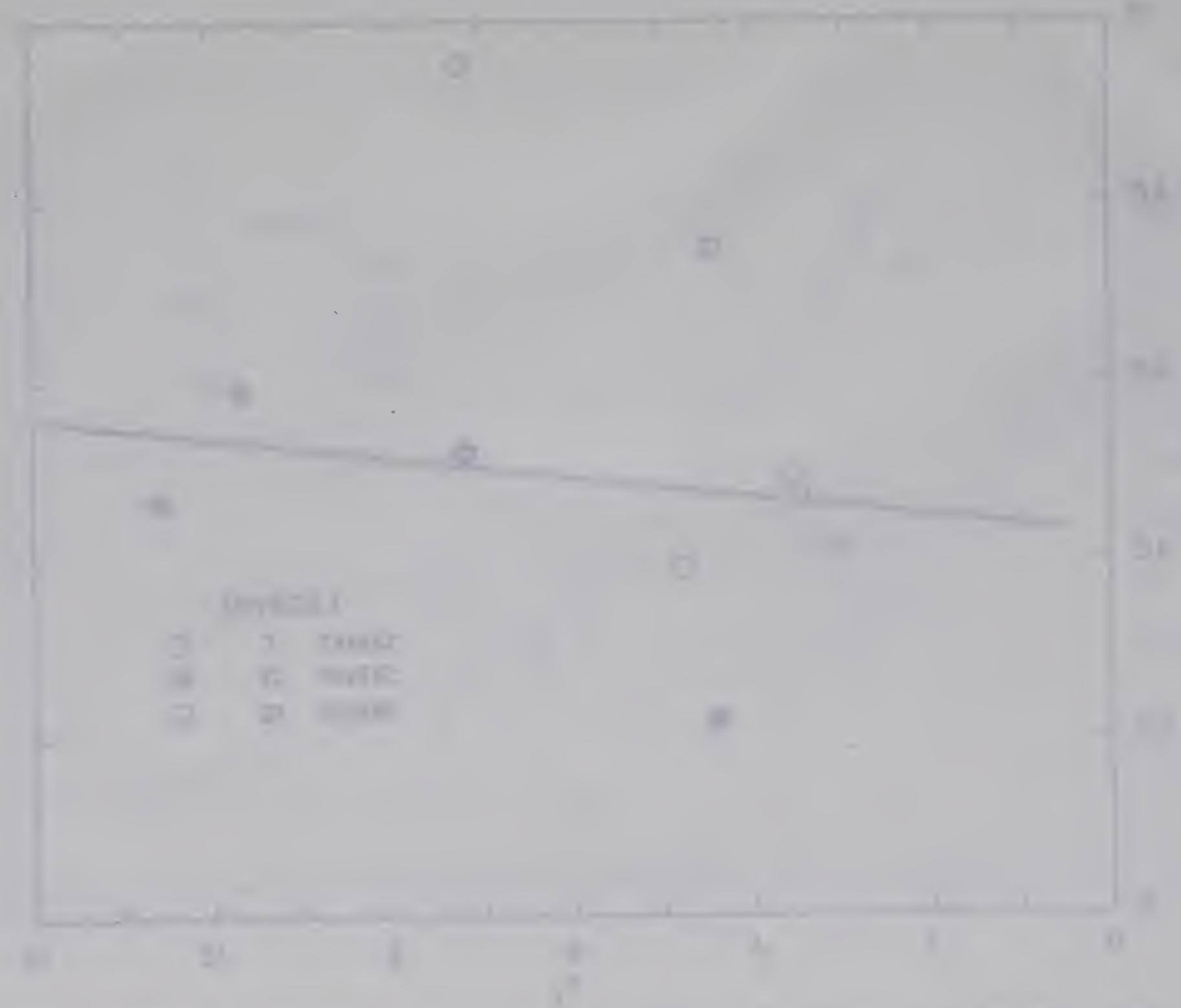

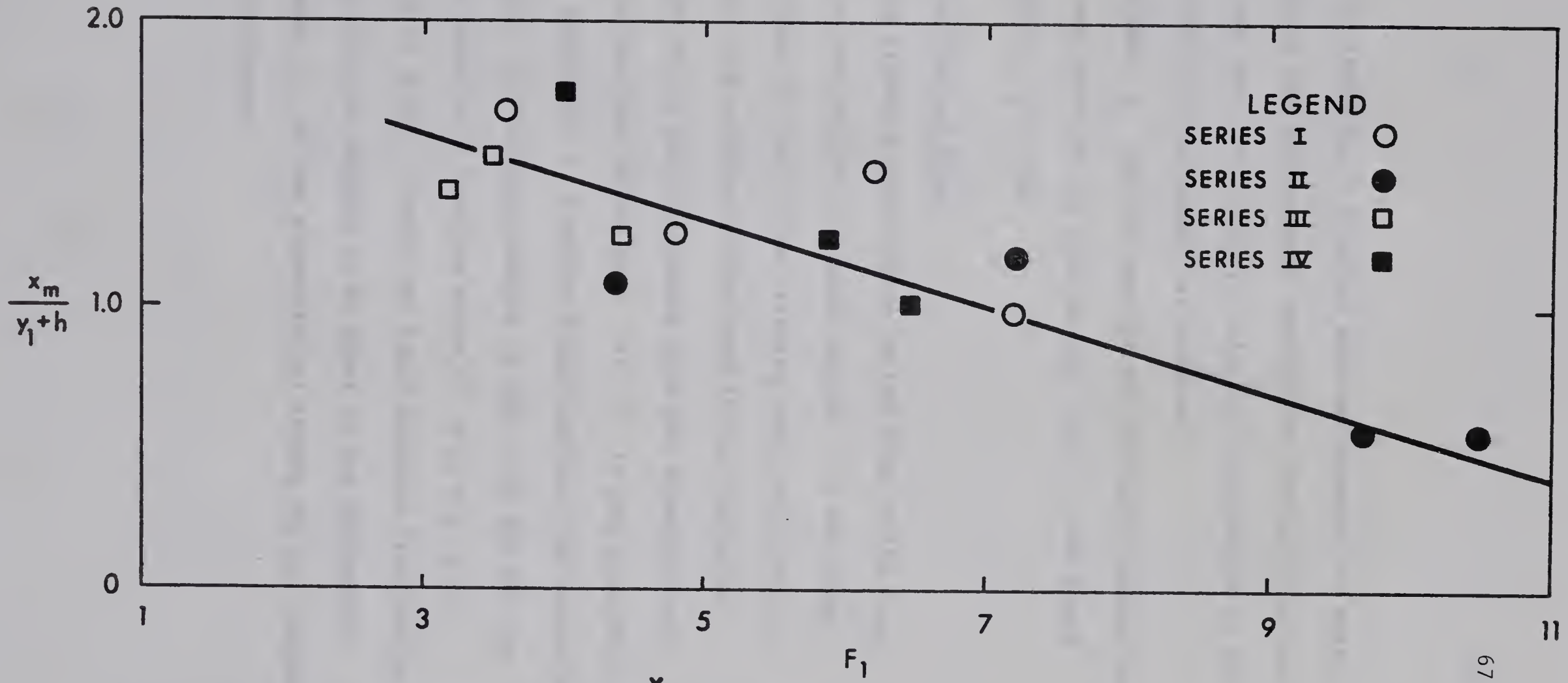

FIG. 3-22 Variation of $\frac{x_m}{y_1+h}$ with F_1

The Standing Eddy

At the foot of the drop, a standing eddy was observed to exist and the end of the eddy is the reattachment section for the wall jet considered earlier. In this work, the backward velocity distribution in the eddy was not measured and only its length was observed.

It was found that L_e did not vary in any systematic manner with either F_1 or h/y_1 and based on the plot in Fig. 3-23, it was found that in the range studied, $L_e \approx 3.0h$.

Pressure Distribution on Face of Drop

To measure the pressure distribution on the face of the drop, 10 holes were drilled on the drop as discussed earlier. It was found that because of the pattern of flow in the standing eddy, which was in some cases quite violent, the pressure on the face is not static but static and dynamic equal to the static pressure plus the velocity head of the impinging flow on the face of the drop. If h' is the piezometric head for any hole at a height of z from the downstream bed, the variation of $h'/h + y_1$ with $z/h + y_1$ is shown plotted in Fig. 3-24 for all the runs. The average line appears to have the value of $h'/h + y_1 = 1.0$ with a maximum variation of $\pm$ 0.2 . Hence the total pressure distribution on the face of the drop could be assumed to be equal to the hydrostatic variation due to the depth y_1 of the supercritical stream for the maximum B-Jump, for preliminary purposes.

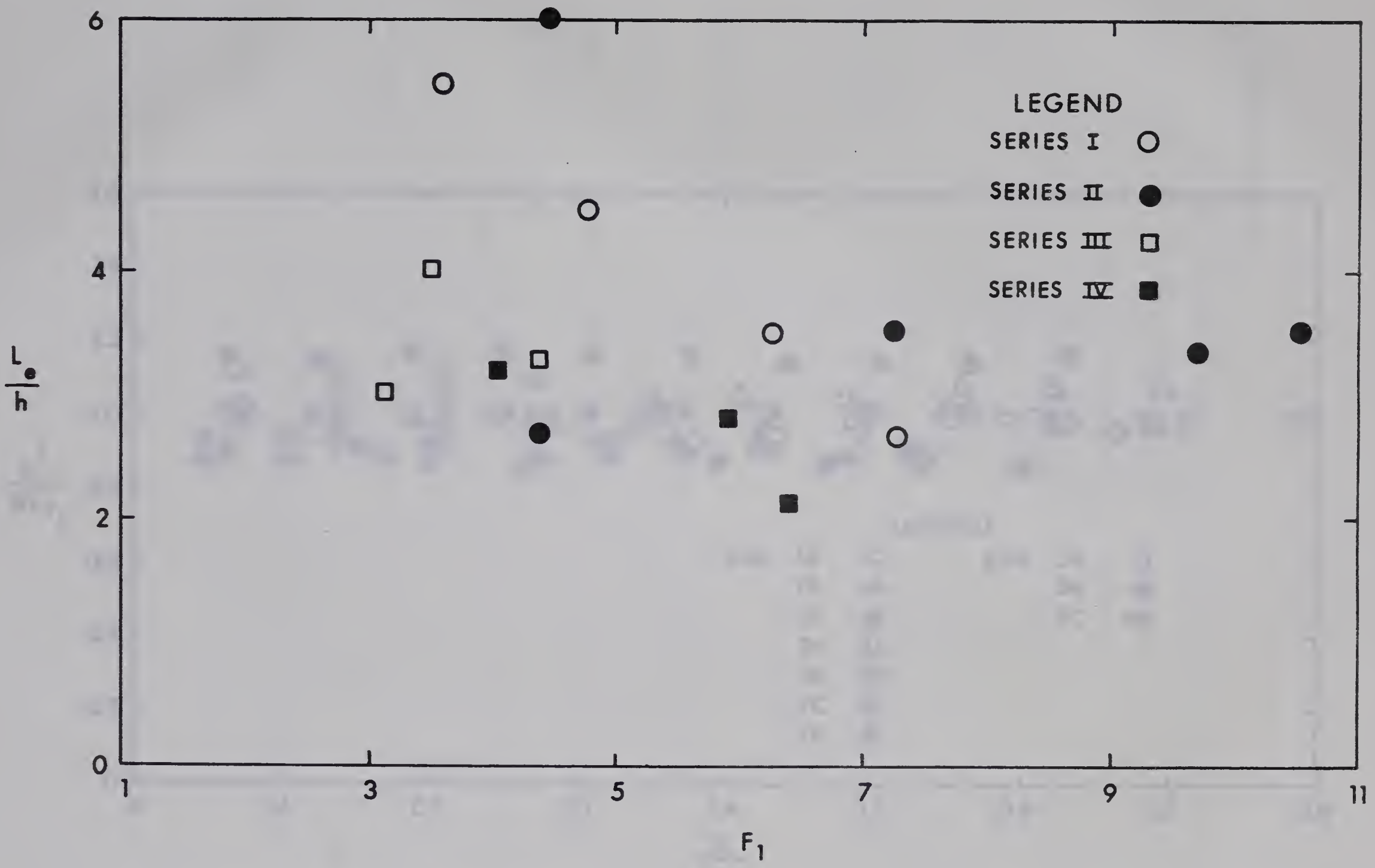

FIG. 3-23 Length of Standing Eddy.

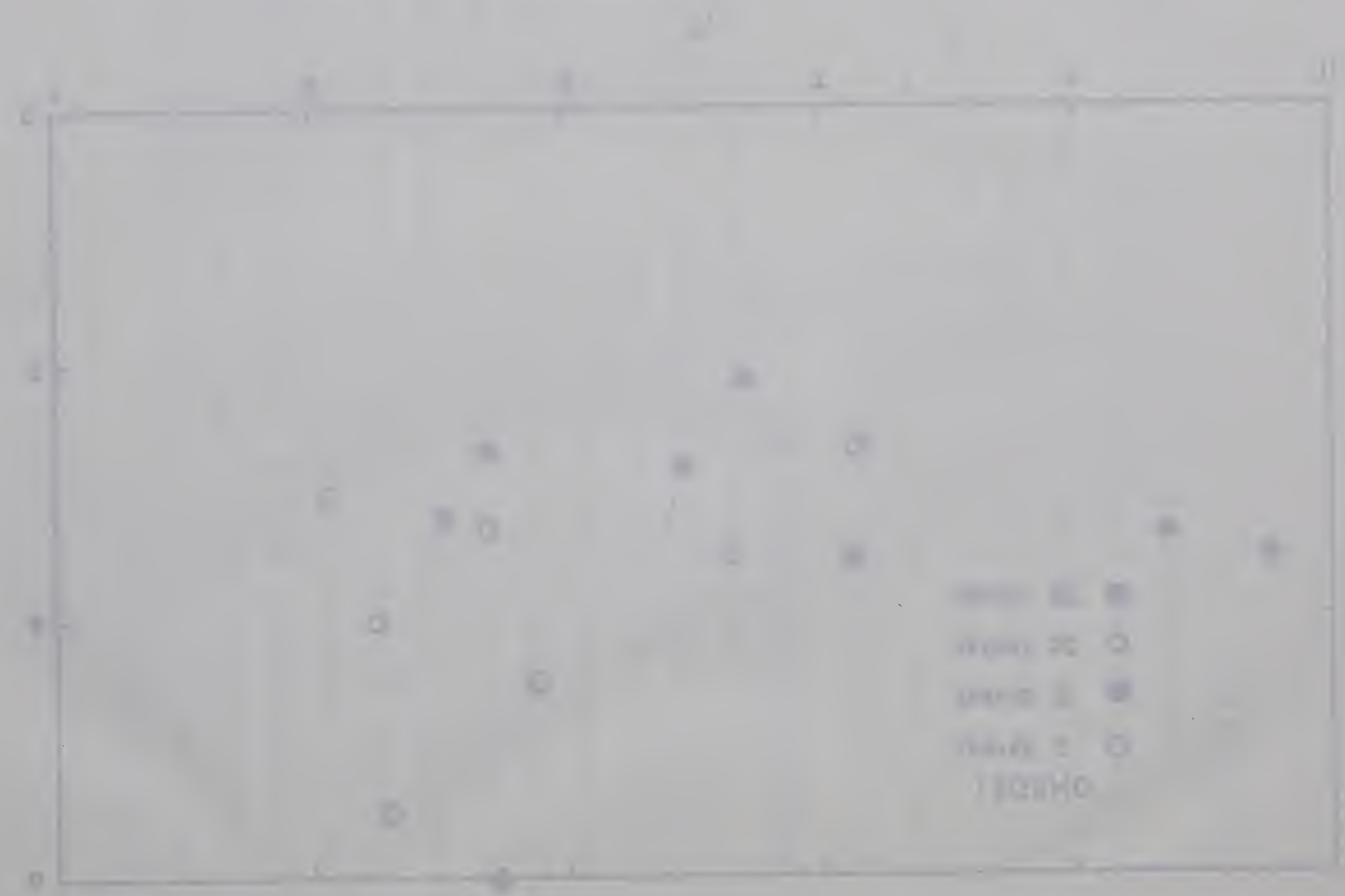

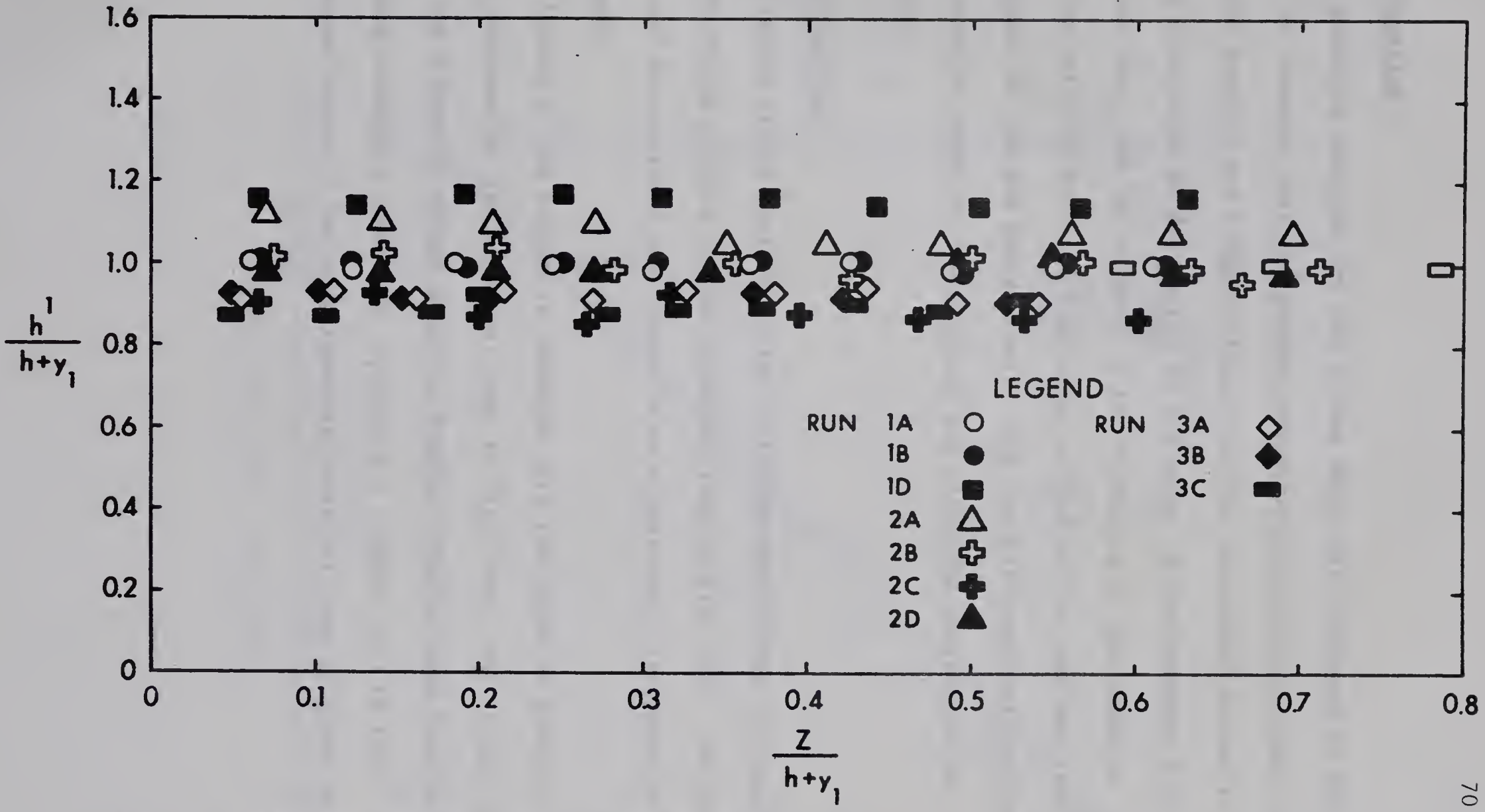

FIG. 3-24 Pressure Distribution on Drop

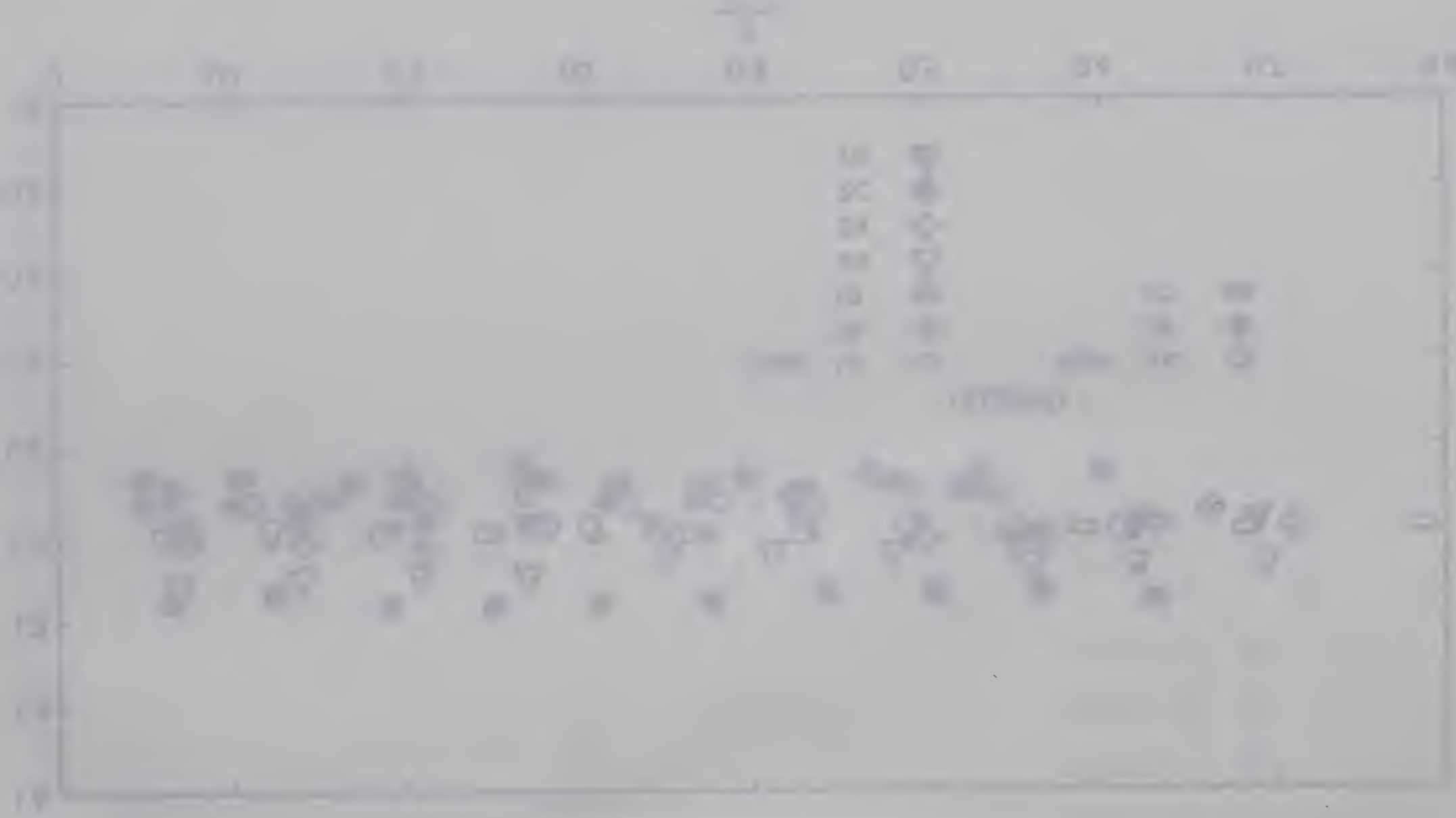

The Momentum Equation

The momentum equation for the B-Jump which was discussed in the first chapter is compared with the present experimental results in Fig. 3-25. The experimental results are slightly lower than the calculated values in some cases and this could be due partly to the error in the pressure distribution on the drop, and the neglect of the variation of the momentum coefficient from unity at both the beginning and end of the jump and also due to the neglect of the bed shear stress. But for all practical purposes, the momentum equation could be used without any elaborate correction for the above factors.

Length Characteristics

The length of the surface roller of the maximum B-Jump is compared with the corresponding results of the classical jump in Fig. 3-26. On the average, it could be concluded that there is no significant difference in the roller length.

The length of the B-Jump is compared with the curve of Bradley-Peterka and Rajaratnam for the classical jump in Fig. 3-26. For $F_1 \gtrapprox 5$, the length of the B-Jump at abrupt drops is somewhat shorter than that of the corresponding classical jumps and $L_j/y_2 \approx 5.2$, where y_2 is the subcritical sequent depth of the corresponding classical jump as given by Eq. 1-02.

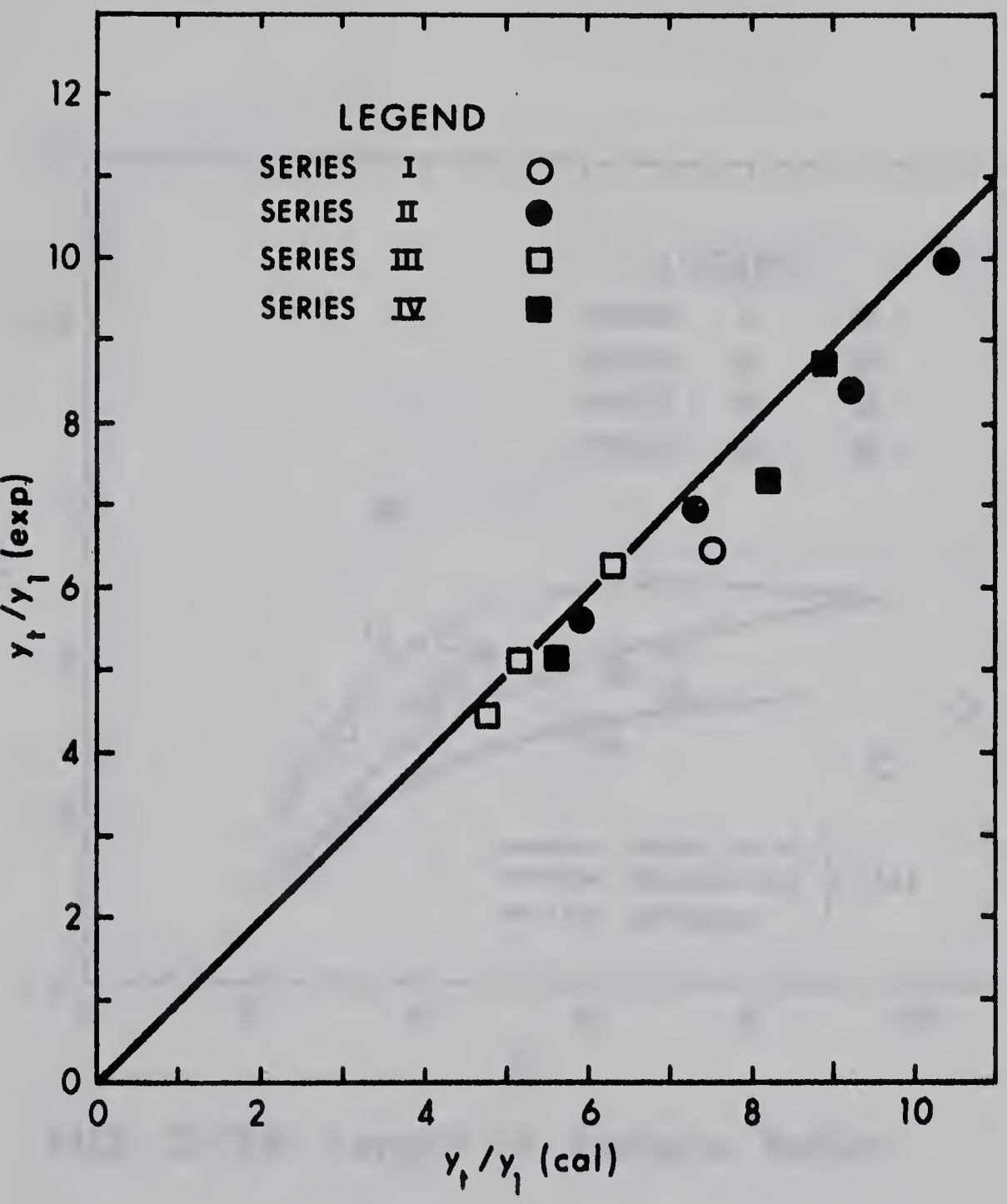

FIG. 3-25 Experimental Verification of the Momentum Equation

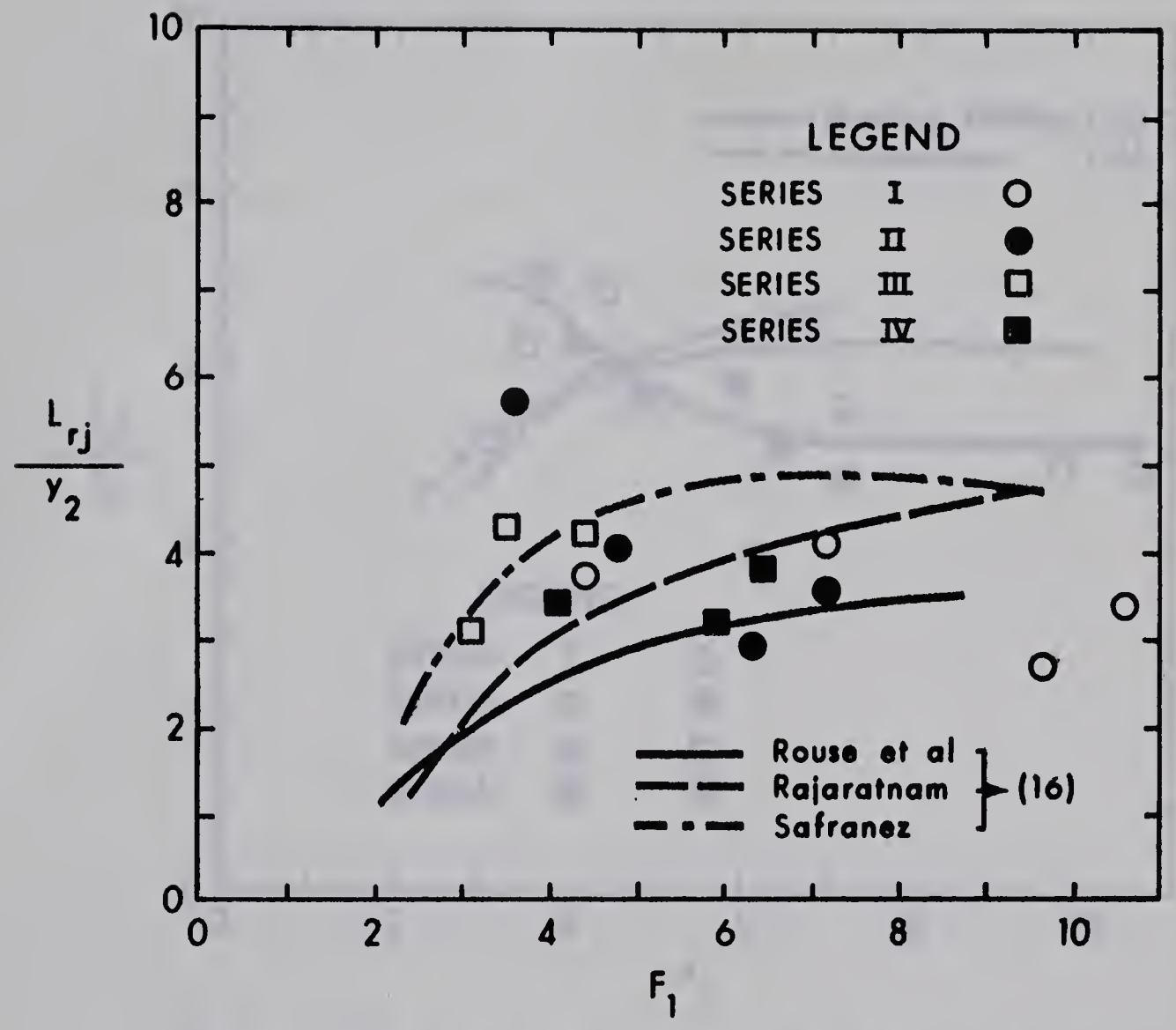

FIG. 3-26 Length of Surface Roller

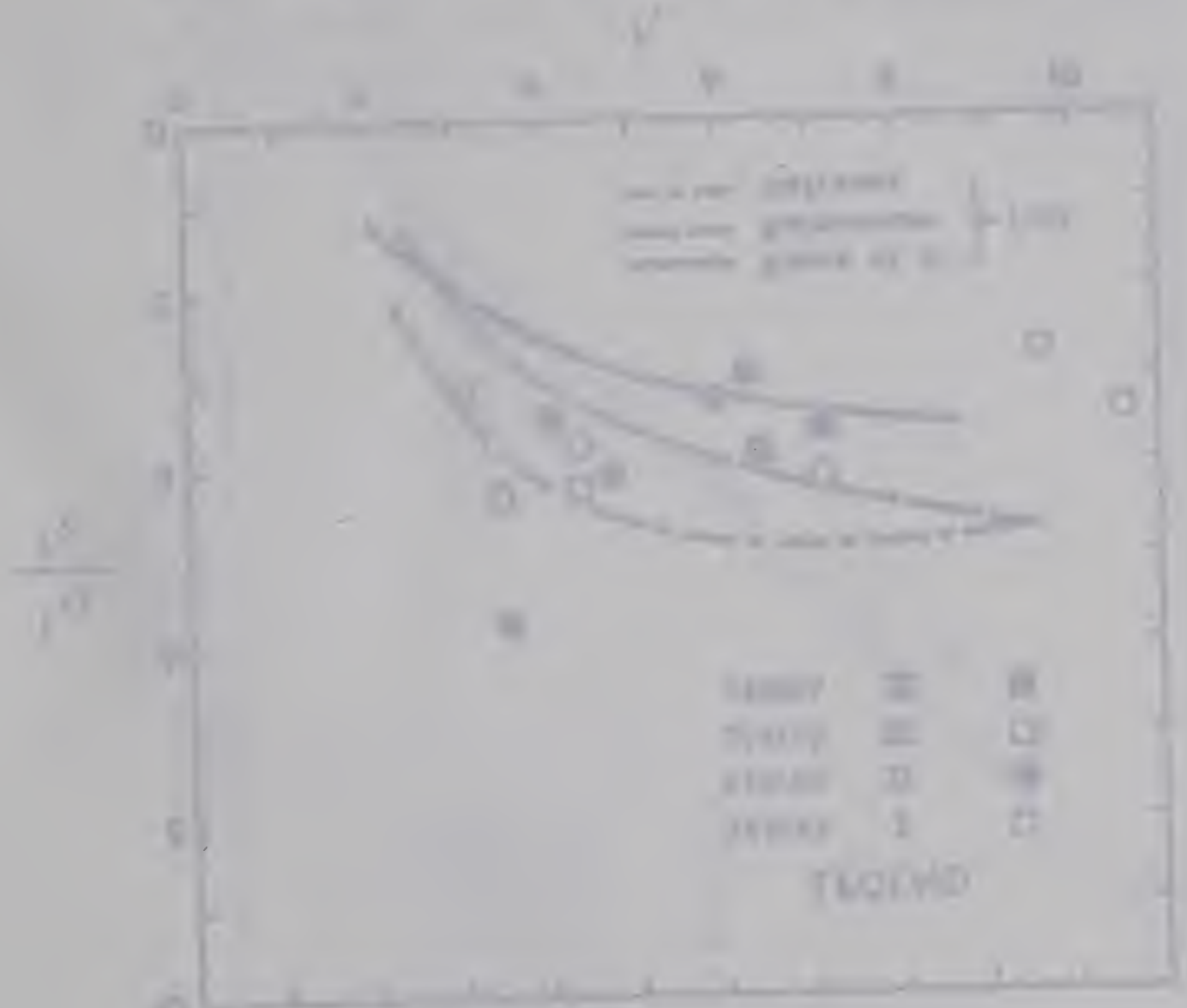

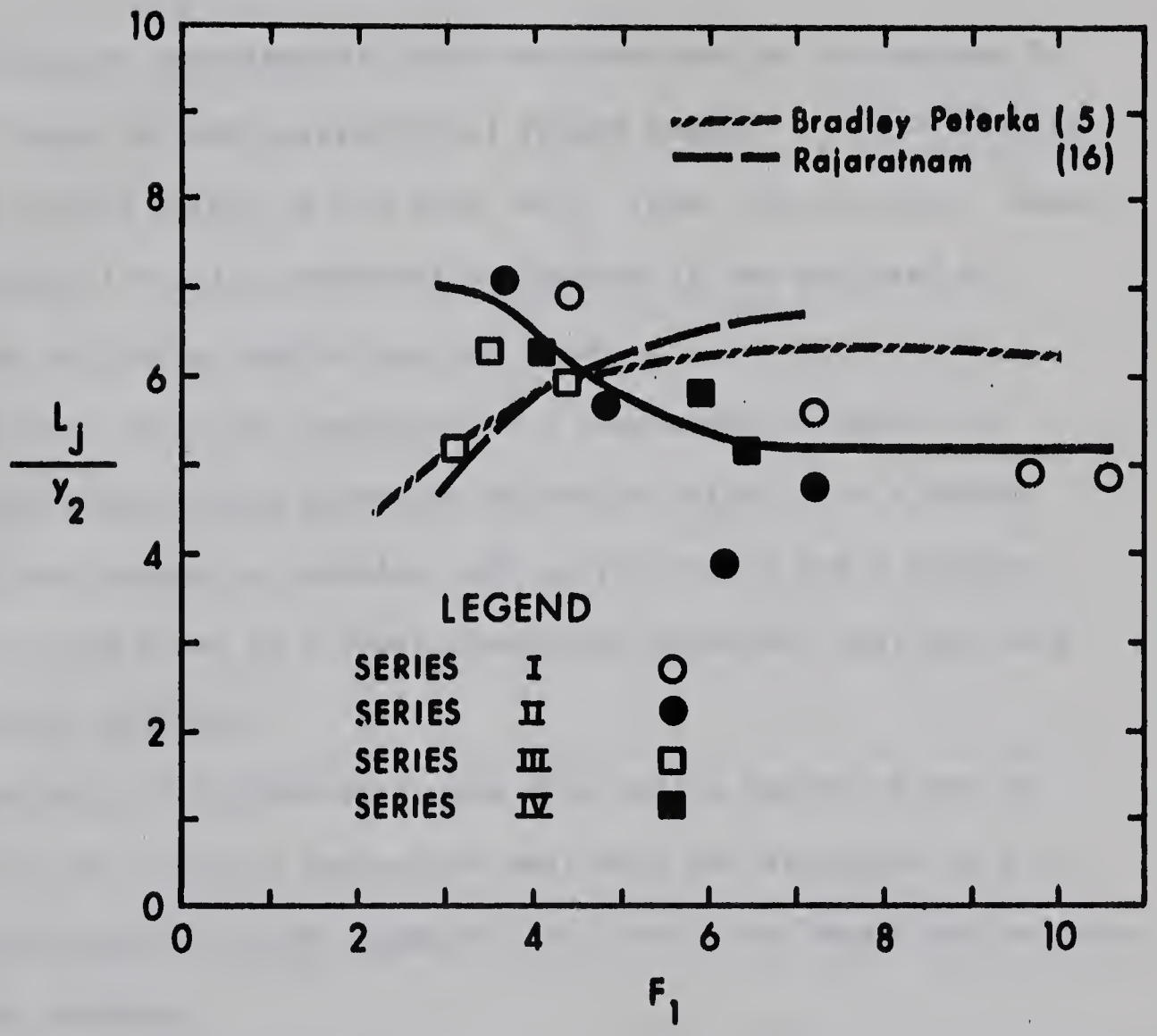

FIG. 3-27 Length of Jump

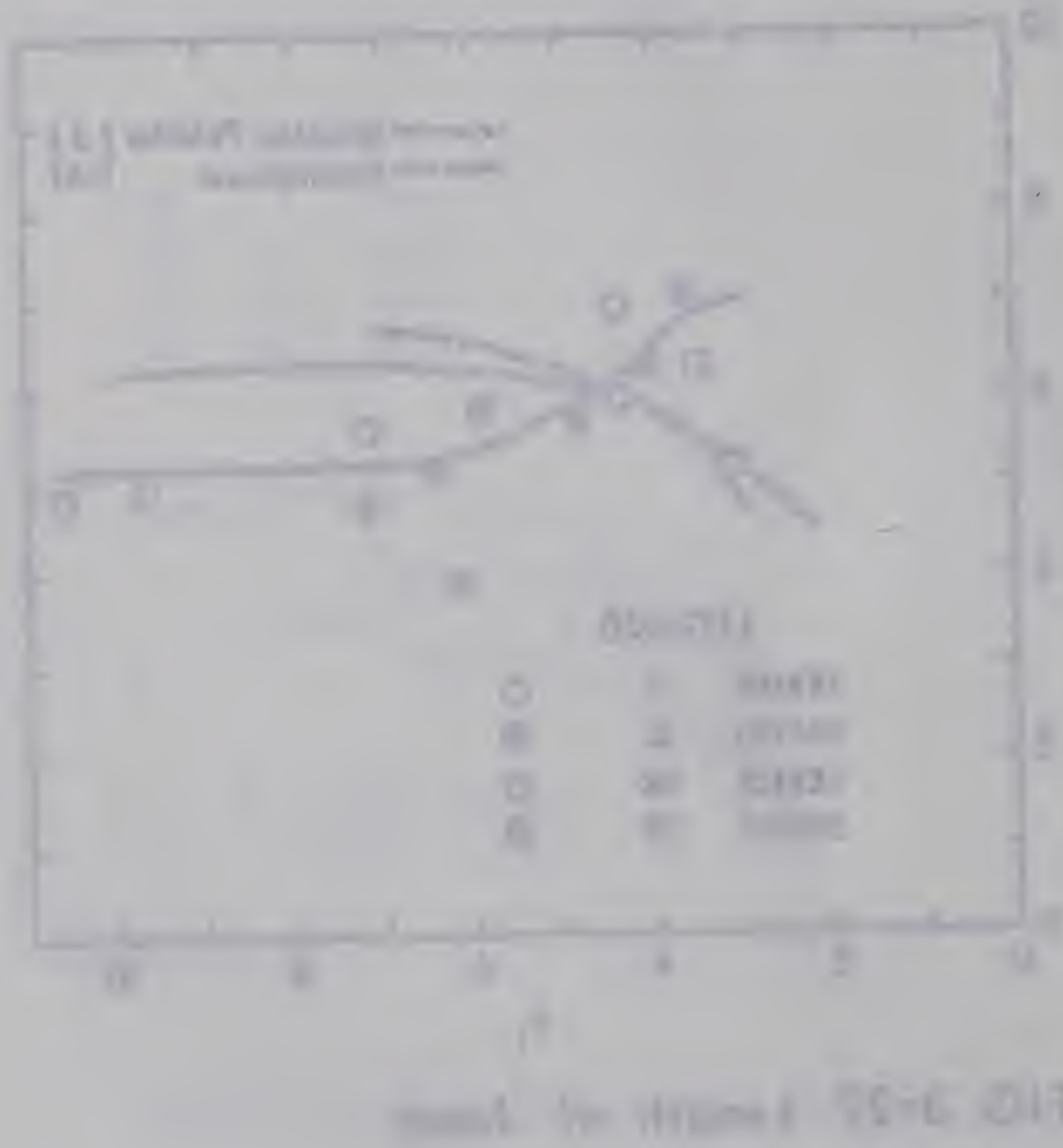

CHAPTER IV

CONCLUSIONS

An extensive experimental study has been made on the maximum B-Jump at abrupt drops for the supercritical Froude number F_1 from 3.14 to 10.55 and the relative height of the drop h/y_1 from 1.26 to 5.68 . Based on these experimental results presented in Chapter II and analysed in Chapter III, the following conclusions are drawn.

1. The B-Jump could be considered as a phenomenon in which the supercritical turbulent stream undergoes diffusion; firstly as a curved free jet sandwiched between a standing eddy on the bottom and a surface roller on the top and later as a reattached plane turbulent wall jet with an adverse pressure gradient.

2. The velocity distribution in the free mixing region of the re-attached wall jet is "similar" and agrees well with the distribution for the corresponding portion of the classical wall jet. The length and velocity scales have been studied.

3. In the boundary layer portion of the jet, the velocity distribution follows the power law with the exponent equal to 1/8.5. The rate of growth of the boundary layer has been studied.

4. It has been indicated that in the early portion of the B-Jump, the supercritical stream diffuses as a curved free jet. Considering only the small length in which the radius of curvature of the jet is large, the

velocity distribution agrees fairly well with the theoretical distribution of the straight free jet.

5. The distribution of the bed shear stress on the reattached wall jet was obtained using the Preston technique and a generalised shear stress distribution has been developed for practical purposes.

6. The path of the maximum velocity filament in the B-Jump has been studied and a practically useful curve has been developed for predicting the maximum velocity at any section.

7. The junction velocity has been studied in great detail and a generalised distribution has been established for it. The length and velocity scales have also been studied.

8. In the experimental range studied, the length of the standing eddy was found to be roughly equal to three times the height of the drop.

9. The effective pressure distribution on the face of the drop could be taken as that controlled by the depth of the supercritical stream under hydrostatic conditions.

10. The prediction of the variation of the ratio of the tailwater depth to the supercritical depth with the supercritical Froude number as given by the simple momentum equation (i.e. Eq. 1-04) agrees fairly well with the experimental results, with the experimental ratio in some cases being somewhat lower.

11. The length characteristics of the maximum B-Jump are essentially the same as that of the corresponding classical jump.

The present method of analysis could advantageously be used for understanding the mechanism of the entire range of jump formation at abrupt drops.

LIST OF REFERENCES

1. Elevatorski, E.A., "Hydraulic Energy Dissipators", McGraw-Hill Book Company Inc., N.Y. 1959.

2. Chow, V.T., "Open Channel Hydraulics", McGraw Hill Book Company Inc., N.Y. 1959.

3. Govinda Rao, N.S. and Rajaratnam, N., "The Submerged Hydraulic Jump", Proc. American Soc. of Civil Engrs., J. Hyd. Div., Vol. 89, No. HY 1 pp 139-161, Jan. 1963.

4. Forster, J.W. and Skrinde, R.A., "Control of the Hydraulic Jump by Sills", Trans. American Soc. of Civil Engrs., Vol. 115, pp 973-987, 1950.

5. Bradley, J.N. and Peterka, A.J.,"Hydraulic Design of Stilling Basins", Proc. American Soc. of Civil Engrs., J. Hyd. Div., Vol. 83, No. HY5, paper 1401-1406, Oct. 1957.

6. Rajaratnam, N., "The Forced Hydraulic Jump", Water Power London, Vol. 16, Part I, pp 14-19, Jan. 1964 and Vol. 16, Part II, pp 61-65, Feb. 1964.

7. Rouse, H., Bhoota, B.V. and Hsu, E.Y., "Design of Channel Expansion", Trans. American Society of Civil Engrs., Vol. 116, pp. 360, 1951.

8. Moore, W.L. and Morgan, C.W., "Hydraulic Jump at an Abrupt Drop", Trans. American Soc. of Civil Engrs., Vol. 124, pp. 507-516, 1959.

9. Ingram, L.F., Oltman, R.E. and Tracy, N.J., "Surface Profiles at a Submerged Overfall", Proc. American Soc. of Civil Engrs., J. Hyd. Div., Vol. 82, No. HY4, pp 1038-12 to 1038-16, Aug. 1956.

10. McPherson, M.B. and Dittig, R.G., Discussion of Ref. 9, Proc. American Soc. of Civil Engrs., J. Hyd. Div., Vol. 83, No. HY2, pp. 1230-41 to 1230-45, April 1957.

11. Prandtl, L. and Tietjens, O.G., "Applied Hydro-and Aero-Mechanics", English Translation, Dover Publication Inc., N.Y., p. 231, 1934.

12. Preston, J.H., "The Determination of Turbulent Skin Friction by Means of Pitot Tubes", J. Royal Aero. Soc., London, Vol. 58, pp. 109-121, 1954.

13. Patel, V.C., "Calibration of the Preston Tube and Limitations on its use in Pressure Gradients", J. Fluid Mech., Great Britain, Vol. 23, Part I, pp. 185-208, 1965.

14. Sigalla, A., "Measurements of Skin Friction in a Plane Turbulent Wall Jet", J. Royal Aero. Soc., London, Vol. 62, No. 12, pp. 873-877, 1958.

15. Schwarz, W.H. and Cosart, W.P., "The Two Dimensional Turbulent Wall Jet", J. Fluid Mech., London, Vol. 10, p. 481, 1961.

16. Rajaratnam, N., "The Hydraulic Jump as a Wall Jet", Proc. American Soc. of Civil Engrs., J. Hyd. Div., Vol. 91, No. HY5, pp. 107-131, Sept. 1965.

17. Rajaratnam, N., "Plane Turbulent Wall Jets on Rough Boundaries", Water Power, London (In Press).

18. Schauer, J.J., and Eustis, R.S., "The Flow Development and Heat Transfer Characteristics of Plane Turbulent Impinging Jets", Tech. Report No. 3, Dept. of Mech. Engrg., Standford Univ., Standford, Calif. 1963.

19. Albertson, M.L., Dai, Y.B., Jensen, R.A., and Rouse, H., "Diffusion of Submerged Jets", Trans. American Soc. of Civil Engrs., Vol. 115, pp. 639-664, 1950.

20. Schlichting, H., "Boundary Layer Theory", McGraw-Hill Book Company Inc., N.Y., 1955.

21. Tracy, H.J. and Lester, C.M., "Resistance Coefficients and Velocity Distribution - Smooth Rectangular Channel", U.S.G.S. Water Supply Paper, 1592.A, 1961.